Effect of Formaldehyde on Selective Catalytic Reduction of Nitrogen Oxides by Ammonia on V_2O_5-WO_3/TiO_2 catalysts

Dissertation

Zur Erlangung des akademischen Grades
doctor rerum naturalium (Dr. rer. Nat.)
an der Mathematisch-Naturwissenschaftlichen Fakultät
der Universität Rostock

Vorgelegt von
Anh Binh Ngo, geboren am 12.08.1993 in Nghe An
aus Vietnam
Rostock, 12.02.2021

https://doi.org/10.18453/rosdok_id00003764

Gutachter:

1. Prof. Dr. Angelika Brückner, Universität Rostock, Leibniz Institute für Katalyse
2. Prof. Dr. Sven Kureti, Technische Universität Bergakademie Freiberg, Institut für Energieverfahrenstechnik und Chemieingenieurwesen

Jahr der Einreichung: 2021

Jahr der Verteidigung: 2021

Erklärung

Hiermit erkläre ich, dass ich die vorliegende Arbeit selbstständig verfasst und keine anderen als die angegebenen Quellen und Hilfsmittel benutzt zu habe.

Rostock, 12.02.2021

Anh Binh Ngo

Acknowledgment

First, I would like to express my gratitude to Prof. Dr. Angelika Brückner for giving me an opportunity to be her PhD student. The three years of studying in the Department of Catalytic *in situ* Studies are great for improving my knowledge and working ability. I have received a fascinating topic that will be the premise for developing my future work. In addition, Prof. Brückner has also facilitated me to join many scientific conferences. It is beneficial for me to increase understanding and expand the relationship in the scientific world.

I would like to thank Dr. Vuong Thanh Huyen for her very kindly and thoughtful support of my experimental research and guiding me to use the software to analyze the data. I also want to express my gratitude to Assoc. Prof. Nguyen Hong Lien, my first supervisor in Vietnam. The guideline and support of Assoc. Prof. Lien are the premise for me to step on the academia. I would like to thank Dr. Dirk Hollmann, Prof. Dr. Le Minh Thang, and Dr. Esteban Meja for their kind support to help me get the scholarship from Rohan project and join the scientific conferences and the German language courses as well.

I also want to express my grateful to Dr. Hanan Atia and Mr. Reinhard Erkert for their help for the experiment set up and the H_2-TPR results. I would like to thank Dr. Jabor Rabeah for his support for the *in situ* EPR experiment and his contributions during the discussion. I also want to thank Dr. Ursula Bentrup for her support for the IR data analysis and her corrections for the papers. I want to thank Dr. Udo Armbruster for allowing me to experiment in his laboratory and his corrections for my scientific reports.

I also want to thank Christine Rautenberg for the Pyridine adsorption experiments and Dr. Sonja Keller to support the experiment set up. I would like to thank Dr. Jana Weiß for the Raman spectra measurement, Dr. Henrick Lund for contributing to the XRD results, and Dr. Stephan Bartling for the XPS results. I also want to thank Dr.Nils Rockstroh and Dr. Reni Grauke for their help with the difficulties I have met in a strange country.

I would like to thank the Vietnamese community for the great period of time in Rostock, helping me feel less lonely and homesick.

Finally, I would like the thank my family and my friends for the best I have had.

Zusammenfassung

Die Selektive katalytisch Reduktion von Stickoxiden (NO_x) ist die Standardmethode für die Nachbehandlung von Verbrennungsabgasen, um umweltschädliche Substanzen zu entfernen. Die Herausforderungen dieser Technologie liegen darin, die NO_x-Umsätze bei niedriger Temperatur zu erhöhen und gleichzeitig die negativen Effekte von anderen Komponenten im Abgas wie beispielsweise H_2O, SO_2, Phosphor oder Schwermetalle zu beschränken. Es ist jedoch zu beachten, dass durch unvollständige Verbrennung Formaldehyd entsteht, dessen Einfluss auf die Reaktion bisher weitestgehend unerforscht ist. Daher ist das Ziel dieser Arbeit die Untersuchung des Mechanismus der Formaldehydreaktion in der NH_3-SCR von NO_x an unterschiedlichen V_2O_5-WO_3/TiO_2- Katalysatoren, in Abhängigkeit von dessen Zusammensetzung und Oberflächeneigenschaften durch den kombinierten Einsatz von katalytischen Ausprüfungen und *in situ* FTIR und EPR Experimenten.

Unsere Untersuchungen wurden zunächt an kommerziellen $V_2O_5WO_3/TiO_2$ Katalysatoren (1 wt.% V, 6 wt.% W) durchgeführt. Die Resultate zeigten mehrere negative Effekte des Formaldehyds. HCHO reagierte mit NH_3 und bildete dabei HCN als Hauptprodukt. Diese unerwünschte Nebenreaktion führte zu geringerem NO_x-Umsatz und verringerter N_2-Selektivität. Durch *in situ* FTIR Spektroskopie war es möglich zu zeigen, dass HCHO und NH_3 an der Katalysatoroberfläche zum Intermediat $HCONH_2$ reagieren, aus dem HCN entsteht. In einem zweiten Schritt wurden andere Katalysatoren unterschiedlicher Zusammensetzung untersucht, WO_3/TiO_2 (W-Ti), V_2O_5/TiO_2 (V-Ti) und V_2O_5-WO_3/TiO_2 (V-W-Ti). Auf diese Weise sollte der Einfluss der unterschiedlichen Katalysatorkomponenten auf die Reaktion mit HCHO studiert werden. An dem aktivsten Katalysator V-W-Ti führte HCHO zu dem stärksten Rückgang an NO_x-Umsatz über den gesamten Temperaturbereich, während gleichzeitig große Mengen an HCN freigesetzt wurden. *In situ* FTIR Messungen zeigten eine verstärkte NH_3-Adsorption an Säurezentren auf der Oberfläche des V-W-Ti Katalysators und damit die Bildung von $HCONH_2$. Im Vergleich dazu adsorbierte NH_3 auf den W-Ti und V-Ti Katalysatoren weniger stark, sodass HCHO mit Gittersauerstoff des Katalysators $HCOO^-$ bildete, welches wiederum zerfiel oder zu CO und CO_2 oxidiert wurde. Zusätzlich zeigten *in situ* EPR Experimente, dass die hohe Redoxaktivität von V-W-Ti die Umsatzgeschwindigkeit von HCHO und $HCONH_2$ erhöhte und

so die Bildung von HCN begünstigte, sodass dadurch die Menge des für die SCR zur Verfügung stehenden NH_3 sank. Diese Resultate der Arbeit können Grundlage für weitere Studien zur Untersuchung des negativen Effekts von HCHO in der NH_3-SCR Technologie sein.

Abstract

Selective catalytic reduction of nitrogen oxides (NO_x) by ammonia (NH_3-SCR) is the state-of-the-art technology for the abatement of these harmful substances to the environment. The challenges of this technology are to improve the conversion of NO_x at low temperature and restrict the negative effects from other components in the flue gas such as H_2O, SO_2, phosphorous and heavy metals.[1] However, from the uncompleted combustion of the fuel, formaldehyde is also formed, the effect of which has been widely neglected so far. Therefore, it was the aim of this work to investigate the mechanism of formaldehyde conversion in NH_3-SCR of NO_x on different V_2O_5-WO_3/TiO_2 catalysts, depending on their composition and surface properties by combining catalytic tests with in situ FTIR and EPR experiments.

Our study was first carried out on a commercial V_2O_5-WO_3/TiO_2 catalyst (1 wt. % V, 6 wt. % W). These results showed many adverse effects of formaldehyde.[2] HCHO reacts with NH_3 and forms HCN as the main product. This undesired reaction lowers NO_x conversion and N_2 selectivity. By *in situ* FTIR spectroscopy, it was found that HCHO and NH_3 react on the surface of the catalyst to intermediate $HCONH_2$, which liberates HCN. Subsequently, catalysts of different compositions, WO_3/TiO_2 (W-Ti), V_2O_5/TiO_2 (V-Ti), and V_2O_5-WO_3/TiO_2 (V-W-Ti), were analyzed to explore the effect of the different catalyst components on the reaction of HCHO. On the most active V-W-Ti catalyst, HCHO caused the highest decline of NO_x conversion in the whole temperature range and released the highest amount of HCN. *In situ* FTIR results indicated that the high surface acidity of V-W-Ti promotes NH_3 adsorption and formation of $HCONH_2$. In contrast, on W-Ti and V-Ti catalysts, the amount of adsorbed NH_3 is not large enough, HCHO rather interacts with lattice oxygen of the catalysts to form $HCOO^-$ which then decomposed or was oxidized to CO and CO_2. Besides, results from *in situ* EPR experiments revealed that V-W-Ti's high redox activity also accelerates the conversion rate of HCHO to $HCONH_2$, facilitating the formation of HCN and simultaneously reducing the amount of NH_3 for the SCR reaction. These results may support further studies to restrict the negative effect of HCHO in NH_3-SCR technology.

Table of Contents

Acknowledgment ..... **i**

Zusammenfassung ..... **ii**

Abstract ..... **iv**

Table of Contents ..... **v**

List of abbreviations ..... **vii**

Aims of Study ..... **viii**

1. State of The Art **1**

1.1 Sources of NO_x and effect on the environment and human health *1*

1.1.1 The emission of NO_x *1*

1.1.2 Effect of NO_x on human health and environment 3

1.2 NH_3-SCR technologies for NO_x abatement *4*

1.2.1 Overviews of the NH_3-SCR technologies 4

1.2.2 Active sites, intermediates, and reaction pathways 6

1.2.3 Effect of other components in flue gas 8

1.3 Sources of HCHO emission and impact on NH_3-SCR *11*

1.3.1 The formation of HCHO 11

1.3.2 Reaction of HCHO with the components of standard SCR feed gas 13

2. Experimental methods **16**

2.1 Catalyst preparation *16*

2.2 Characterization methods *17*

2.2.1 Inductively coupled plasma - optical emission spectrometry (ICP-OES) 17

2.2.2 The X-ray diffraction spectroscopy 17

2.2.3 Brunauer – Emmett – Teller (BET) surface area analysis 18

2.2.4 Hydrogen Temperature-Programmed Reduction (H_2-TPR) 20

2.2.5 Raman spectroscopy 21

2.2.6 UV-Vis Diffuse Reflection Spectroscopy 22

2.2.7 Pyridine adsorption analyzed by FT-IR spectroscopy 23
2.2.8 In situ FT-IR 24
2.2.9 In situ EPR 26

2.3 Catalytic test *30*
2.3.1 The standard SCR reaction 30
2.3.2 Reaction of HCHO in NH_3-SCR 31
2.3.3 The presence of H_2O in NH_3-SCR reaction 33
2.3.4 Oxidation of HCN under transient conditions 35

3. Results and discussion **36**

3.1 Effects of HCHO on a commercial V_2O_5-WO_3/TiO_2 catalyst *36*
3.1.1 Catalytic test 36
3.1.2 In situ FT-IR experiments 40
3.1.3 Reaction of $HCONH_2$ on the commercial V_2O_5-WO_3/TiO_2 catalyst 43
3.1.4 The oxidation of HCN 45

3.2 Effects of HCHO on different V_2O_5-WO_3/TiO_2 catalysts *47*
3.2.1 Catalyst characterizations 47
3.2.2 Catalytic test 53
3.2.3 In situ FT-IR experiments 59
3.2.4 In situ EPR experiments 64
3.2.5 Effect of H_2O 70

4. Conclusions and outlook **73**

References **76**

Appendix **85**

List of abbreviations

SCR	Selective Catalytic Reduction
FT-IR	Fourier Transformance Infrared Radiation
UV-Vis DRS	Ultraviolet-Visible Diffuse Reflection Spectroscopy
XRD	X-Ray Diffraction
ICP-OES	Inductively Coupled Plasma Optical Emission Spectrometry
H_2-TPR	Hydrogen Temperature-Programmed Reduction
EPR	Electron Paramagnetic Resonance
EU	European Union
E-R	Eley - Rideal mechanism
L-H	Langmuir - Hinshelwood mechanism
ZSM-5	Zeolite Socony Mobil 5
SAPO	Silicoaluminophosphate
ppbV	Part per billion Volume
DOCs	Diesel Oxidation Catalysts
DPF	Diesel Particulate Filter
ACS	Ammonia Catalyst Slip
NIR	Near-Infrared Region
cw	Continuous microwave
GHSV	Gas hour space velocity
TAP	Temporal analysis products
AMU	Atomic mass units
HMT	Hexamethylenetetramine
E_g	Edge energy

Aims of Study

Nowadays, in parallel with the development of the industries and transportations, air pollution is becoming a persistent problem. The emission of the greenhouse gases such as CO_2, NO_x, etc., is causing global warming and affecting the Earth's survival day by day. For a long time, removing the greenhouse gases has been studied to facilitate a highly effective and productive, inexpensive, and practical application approach. The reduction of NO_x (most known as NO and NO_2) is one of the most concerned topics so far due to its negative effects on the environment and human health. Nitrogen oxides are generated from the reaction of N_2 and O_2 at high temperatures. Its formation during the combustion of fuel is inevitable because the air (80 % N_2, 20 % O_2) is always used as the oxygen source.

Among various methods and technologies to reduce NOx emission, selective catalytic reduction of nitrogen oxides by ammonia (NH_3-SCR of NO_x) is the state-of-the-art method for the abatement of NO_x so far. The requirements of this technology are high activity and high N_2 selectivity in an extensive temperature range. However, to approach the practical application, the NH_3-SCR catalyst needs to show high effectivity at low temperature and restrict the adverse effects of other components in the flue gas such as H_2O, SO_2, phosphorous, alkali, heavy metals, and HCl.[1] In the flue gas, an amount of HCHO generated from the partial oxidation of fuels could affect the NH_3-SCR. Interestingly, there are almost no detailed studies on the effect of HCHO in NH_3-SCR up to now, and this is the aim of this work.

Because V_2O_5-WO_3/TiO_2 catalysts have been widely studied and applied for NH_3-SCR, we firstly studied the effect of HCHO in a commercial V_2O_5-WO_3/TiO_2 catalyst under different concentrations of HCHO. Besides looking at the change of the main factors of the SCR reaction such as the NO_x conversion, NH_3 conversion, and the N_2 selectivity, the conversion of HCHO and the formation of products from HCHO have been analyzed. After that, *in situ* FT-IR experiments have been carried out to study the formation of intermediate species formed from the interaction of HCHO. This could be the key to explain the effect of HCHO in the NH_3-SCR on the commercial V_2O_5-WO_3/TiO_2 catalyst.

In the second part of the thesis, the reaction of the effect of HCHO was studied on catalysts of different composition, such as V_2O_5/TiO_2 (V-Ti), WO_3/TiO_2 (W-Ti), and V_2O_5-WO_3/TiO_2 (V-

W-Ti) to explore explicitly the role of V, Ti, and W, preferentially by using *in situ* FT-IR and *in situ* EPR to obtain information on formed intermediates and redox properties.

The main aims of this thesis comprised investigation of:

- the effect of HCHO for the performance of NH_3-SCR on V_2O_5-WO_3/TiO_2 catalysts: NO_x conversion, NH_3 conversion, and N_2 selectivity
- the conversion of HCHO, the formation of the intermediate species on the surface of catalysts, and the formation of products from its reaction in NH_3-SCR of NO_x
- the role of surface acidity and redox property for HCHO reactions in NH_3-SCR and the relation between the effect of HCHO and the SCR activity on different catalysts

This information will be the basis for further studies to restrict the negative effect of HCHO and find out the new direction to improve the activity of catalysts for the abatement of NO_x.

1. State of The Art

1.1 Sources of NO_x and effect on the environment and human health

1.1.1 The emission of NO_x

NO_x is the genetic term of the nitrogen oxides with different valence states of nitrogen from +1 to +5 (N_2O, NO, N_2O_2, N_2O_3, NO_2, N_2O_4, N_2O_5).[3] In atmospheric chemistry, due to the stability and the effects on the environment, NO_x is generally known as the genetic term of nitrogen oxide (NO) and dinitrogen oxide (NO_2).[4] Both of these oxides are toxic, and their emission is becoming a serious problem for the environment.

Generally, the NO_x emission mainly comes from three main sources: transportations, the energy supply processes, and daily commercial activities. Lorenz et al. has described the distribution of NO_x emission sources from different sector groups (Figure 1).[5] The road transportation provides the highest part of NO_x emission (40 %), and the non-road transportation contributes 7 % in total NO_x emission. The contribution of the industrial processes and agriculture are insignificant, only 3 % and 2 % respectively. The energy production and energy use in the industry contribute 21 % and 13 % of the NO_x emission, respectively. In addition, the commercial institutional and households release a significant amount of NO_x (14 %).

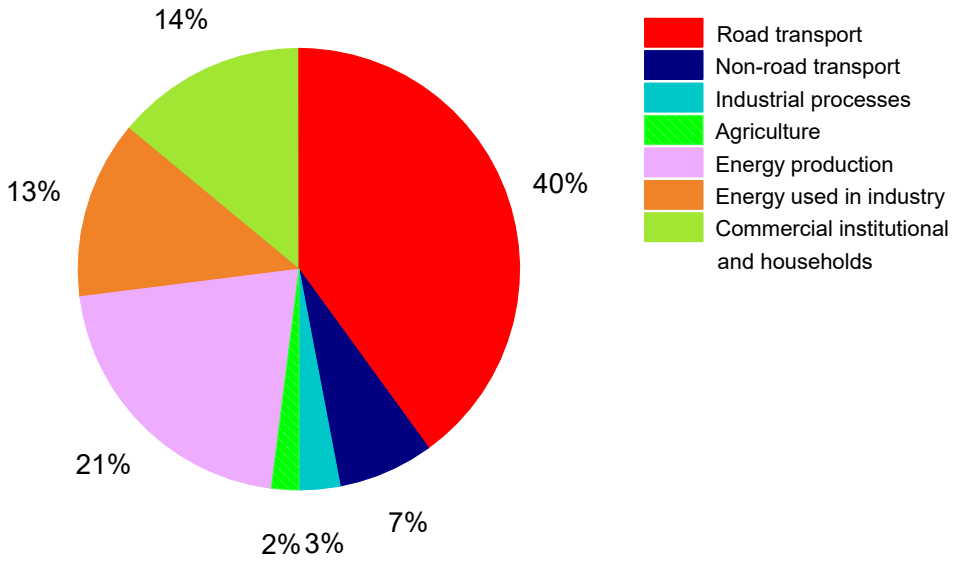

Figure 1. The emission of NO_x in the European Union from different sector groups. Data collected from UNECE Convention on Long-range Trans-boundary Air Pollution (LRTAP)[5]

Nitrogen oxides are formed from the reaction of oxygen and nitrogen at temperatures higher than 1300 °C. The formation of NO depends on the ratio of the fuel and the air, and it is accelerated in the stoichiometric ratio on the fuel-lean side.[6] Meanwhile, at temperatures below 760 °C, the NO formation is negligible. It can be described according to the Zeldovich equations below (Equations 1-3):

$$N_2 + O \rightarrow NO + N \quad (1)$$

$$N + O_2 \rightarrow NO + O \quad (2)$$

$$N + OH \rightarrow NO + H \quad (3)$$

$$NO + ½\ O_2 \rightarrow NO_2 \quad (4)$$

Because of the characteristics of the emission sources, the distribution of the NO_x emission is not uniform. It mainly accumulates in the large industrial zones and the big cities where many vehicles are circulated. A report from the European Environmental Agency showed the NO_2 map over the whole of Europe in 2018 (Figure 2).[7] Because of the easy conversion of NO to NO_2 in the atmosphere (Equation 4), the NO_2 emission map is the representatives of the NO_x emission. As the information in Figure 2, the emission of NO_x mainly accumulates in the west of Germany, Belgium, Netherlands, North Italy, and England. In addition, some other big cities such as Moscow, Paris, Madrid, Istanbul, etc., also release a significant amount of NO_x. Therefore, the key areas of the economy where the population is concentrated are most affected by NOx emissions.

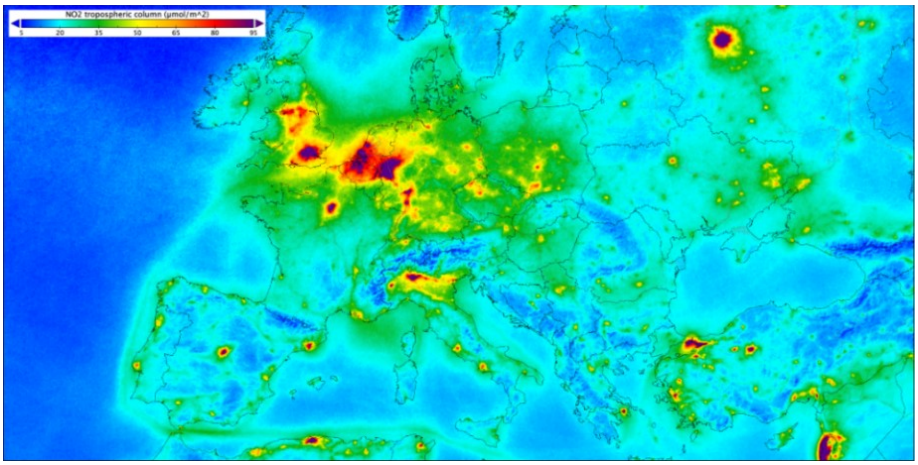

Figure 2. The emission map of NO_2 in Europe between April and September 2018. Source from the European Environmental Agency[7]

Due to NO_x's negative effects on the environment and human health, many organizations have earnestly requested a reduction of NO_x emissions. For a long time, many efforts have tried to reduce the NO_x emission in parallel with the economy's rise and transportation. According to the data from Eurostat, based on the emission in 1990, the NO_x emission is decreasing every year (Figure 3).[8]

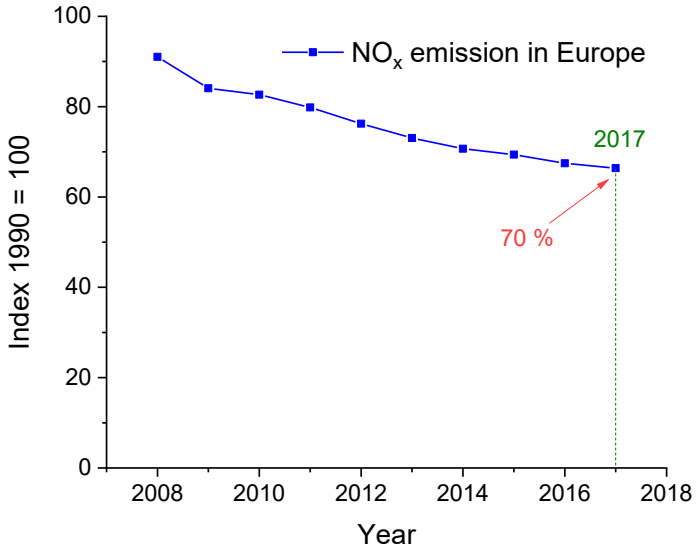

Figure 3. Timeline of NO_x emission in Europe, data based on the emission in 1990. Data collected from Eurostat[8]

However, the abatement rate of NO_x emission in the EU is relatively slow. In 2017, the emission of NO_x equaled 70 % of the value in 1990. Therefore, despite the outstanding efforts of NO_x reduction, the air's NOx emission is still high, and the development of new technologies to remove NO_x remains a topic of interest.

1.1.2 Effect of NO_x on human health and environment

NO_x causes several negative effects on human health and the environment. It can directly affect human health by directly contacting the respiratory system or indirectly by forming other harmful compounds. Exposure of NO_x can lead to asthma symptoms. It also can associate with other health problems such as heart disease, birth outcome, and all case mortality.[9] In addition,

NO_x can also react with the volatile organic compounds under solar irradiation to form O_3, leading to lung damage. NO_x can also react with other chemicals to form various toxic compounds such as nitroarenes, nitrosamines, and nitrate radicals, which can cause DNA mutation.[10]

One of the most pronounced effects of NO_x on the environment is acid rain. As mentioned above, in the ambient condition, NO can easily be converted to NO_2. In the presence of water, NO_2 will react to generate HNO_3 (Equation 5).

$$2\ NO_2 + ½\ O_2 + H_2O \rightarrow 2\ HNO_3 \qquad (5)$$

HNO_3 a strong acid and can destroy outdoor constructions. In addition, NO_x can deposit on the surface of materials in the absence of moisture. When it rains, the chemical reactions take place and produce nitric acid, which is then flushed by the water flow and through the ground, harm to the plants and the survivals such as insects and fishes.[11]

Because of their high chemical activity, NO and NO_2 will react with the other compounds in the air (O_2, H_2O, volatile organics, etc., as mentioned above) and will not last long in the atmosphere. Hence, although NO and NO_2 can absorb the infrared ray, the greenhouse effect of NO and NO_2 is not considered. However, the contribution of nitrous oxide N_2O to the greenhouse effect is significant. According to the United States Environmental Protection Agency data in 2018, N_2O occupies 7 % in total contribution of greenhouse gases.[12] Therefore, the reduction of NO_x should produce N_2 as the final product.

1.2 NH_3-SCR technologies for NO_x abatement

1.2.1 Overviews of the NH_3-SCR technologies

Selective catalytic reduction of NO_x to N_2 is the most common method to remove NO_x. The used reducing agents are usually ammonia (NH_3-SCR), hydrogen (H_2-SCR), and hydrocarbons (HCs-SCR). However, HCs and H_2 have some drawbacks which prevent their practical application. At high temperatures ($T > 500$ °C), HCs are oxidized, and their efficiency in NO_x reduction is reduced. H_2-SCR can reduce NO_x at low temperatures ($T < 200$ °C) on supported noble metals (Pd, Pt), but these catalysts are expensive and not sufficiently resistant against H_2O, and SO_2.[13-14] NH_3-SCR is the most applied technology for the NO_x abatement. In vehicles, the reducing agent NH_3 is produced by the decomposition of urea $CO(NH_2)_2$ (Equation 6). The

generated NH_3 further reacts with NO to form N_2, known as standard SCR (Equation 7), or NO_2 and NO, known as the fast SCR (Equations 8-9).

$$CO(NH_2)_2 + H_2O \rightarrow 2\ NH_3 + CO_2 \quad (6)$$

$$4\ NH_3 + 4\ NO + 3\ O_2 \rightarrow 4\ N_2 + 6\ H_2O \quad (7)$$

$$8\ NH_3 + 6\ NO_2 \rightarrow 7\ N_2 + 12\ H_2O \quad (8)$$

$$2\ NH_3 + NO + NO_2 \rightarrow 2\ N_2 + 3\ H_2O \quad (9)$$

NH_3-SCR is mainly applied in the range of 250 – 450 °C in a heterogeneous catalytic bed reactor. The reducing agent NH_3 is sprayed into the flue gas and its reaction with NO_x takes place on the surface of the catalyst (Figure 4).

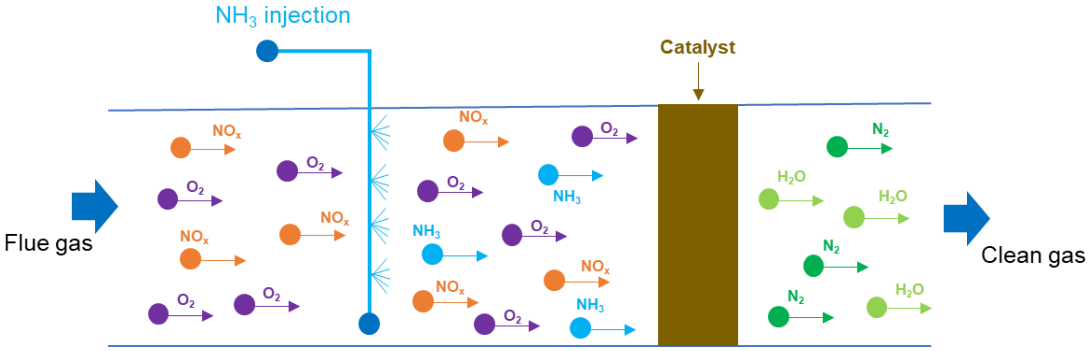

Figure 4. Scheme of selective catalytic reduction by ammonia

Depending on the operating temperatures, the efficiency of NO_x removal, and the catalyst regeneration pathway, various catalysts have been applied for NH_3-SCR. Zeolites-based materials can perform high NO_x conversion at high temperatures (345 – 590 °C) and low NH_3 slip. However, this type of catalyst can destruct NH_3 and only can restrict SO_2 above 425 °C. The metal oxides (vanadium, titanium, tungsten, molybdenum, etc.) operate at medium temperatures (260 – 425 °C) and tolerate sulfur quite well. At low-temperature range (150 – 300 °C), the noble metals on support can perform high NO_x conversion but very low sulfur tolerance.[15] Vanadium pentoxide V_2O_5 supported catalysts are the most applied for NH_3-SCR of NO_x. The big advantages of vanadium supported catalysts are high NO_x conversion, high N_2 selectivity, affordability, and high SO_2 tolerance. Due to the unstable activity at the high temperature of V_2O_5/TiO_2 catalysts, WO_3 has been widely used as the promoter, which can inhibit the transforming of anatase TiO_2 to rutile and the loss of surface area.[16-17] In addition,

WO_3 also enhances the surface acidity and stabilizes the dispersion of vanadium on the support, which is further beneficial for the SCR performance.[18]

1.2.2 Active sites, intermediates, and reaction pathways

In general, the heterogeneous catalytic reaction of NH_3 and NO_x comprises four main steps:

- the adsorption of NH_3 on the surface of the catalyst to form either $NH_4^+{}_{ads}$ on the Brønsted acid sites or $NH_{3\ ads}$ on the Lewis cites.
- the reaction of NH_3/NH_4^+ with either NO/O_2 gases according to the Eley-Rideal (E-R) mechanism or with nitrites/nitrates according to the Langmuir-Hinshelwood (L-H) mechanism to form the intermediate species NH_x-NO_y.
- the decomposition of NH_x-NO_y to form N_2 and H_2O.
- the oxidation of metal from low valence state to high valence state by oxygen.

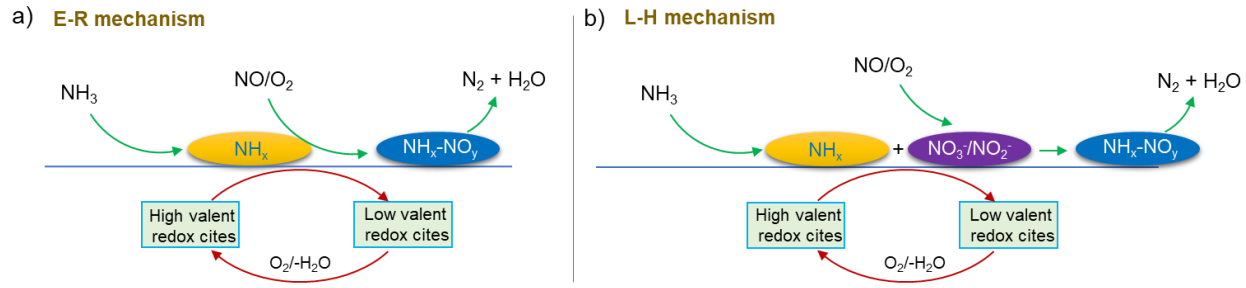

Figure 5. A schematic diagram of SCR reaction following a) Eley-Rideal (E-R) mechanism b) Langmuir-Hinshelwood (L-H) mechanism

However, up to now, the reaction mechanism of NH_3-SCR remains controversial. One of the most controversial issues is the Brønsted and Lewis acid sites' role in the SCR reaction. Topsøe et al. has proposed the SCR mechanism on Brønsted acid sites, including two cycles: the acid circle and the redox circle.[19-20] First, NH_3 adsorb on the active cite V^{5+}-OH to form NH_4^+ and activates V^{5+}=O in the vicinity to form V^{4+}-OH. The NH_3 adsorbate then reacts with NO to form intermediate species, which then decomposes to form N_2 and H_2O. Ramis et al. has proposed the SCR reaction on the Lewis cites. The reaction of $NH_{3\ ads}$ with NO forms NH_2-NO as the intermediate, which further decomposes to N_2 and H_2O.[21] In principle, depending on the type of

catalysts and the reaction conditions, the involvement of the Lewis and Brønsted sites is different and still under debate.

The reaction of NH_x (NH_3/NH_4^+) with NO is also a matter of discussion in NH_3-SCR studies. NH_x can react with gaseous NO according to the E-R mechanism or with the adsorbates of NO on the surface (nitrites/nitrates) according to the L-H mechanism to form the intermediate species NH_x-NO_y (Figure 5). However, some studies have reached the consensus that this reaction's pathway depends on the temperature. At low temperatures, the SCR reaction follows the E-R mechanism, while the L-H mechanism dominates at high temperatures.[1, 22] Ramis et al. has indicated that the nitrosamine NH_2-NO is the intermediate species of the SCR reaction. Meanwhile, in the presence of abundant NH_4^+, the surface complex NH_3-NO is be formed. However, there is no evidence for the existence of the complex NH_4^+-NO by IR spectroscopy because of either the low concentration or the fast decomposition.[18, 21, 23]

To approach the practical application, the SCR catalysts need to perform the high activity at low temperatures and tolerate the negative effects of the other components in the flue gas. The enhancement of the redox property and the surface acidity are the targets for preparing the SCR catalysts. The high surface acidity will be favorable for the formation of NH_4^+/NH_3 adsorbates, increasing the amount of the reactants. Hence, the SCR supports always have a high surface area and high thermal stability (TiO_2, ZSM-5, SAPO 34, etc.). The nature of the metal oxides and their dispersion on support are the determinant factors for the catalysts' surface acidity. In principle, increasing the content of the metal oxides will increase the surface acidity. However, the overload of the metal oxides on the support can lead to the aggregation and forming the crystalline. The sintering of the metal oxides can reduce the redox property of the catalysts, which is also an important factor of the SCR reaction.[18]

The oxidation of the low valence states to the higher valence states by oxygen has been agreed by many studies that it will follow the Mars–van Krevelen mechanism. The lattice oxygen interacts with the adsorbents before being recovered by the oxygen in the gas phase. The oxidation rate is the determinate factor for the SCR reaction.[24] Therefore, enhancing the redox property of catalyst will improve the SCR activity. However, the high redox property will also oxidize NH_3 and reduce this reducing agent for SCR reaction. Besides, the improvement of the redox property should also accompany the high selectivity of the N_2. Some of the catalysts

contain Mn show very high redox property at low temperature but liberates quite a lot of N_2O which is also not a friendly compound for the environment.[25-26]

Furthermore, it was tested that in the presence of NO_2 (fast SCR), the conversion of NO_x at low temperature is higher than the standard SCR (without NO_2 in the feed).[27] Therefore, accelerating the formation of NO_2 by the oxidation of NO during the SCR reaction could also enhance the SCR activity. Many studies have tried to enhance the oxidation of NO to NO_2 to achieve a higher NO_x conversion at low temperatures.[28-30] Furthermore, the formation of the nitrites/nitrate species can also affect the effectiveness of catalyst since it performs different reactivity. The nitrites/nitrate species with lower thermal stability will react with the NH_4^+ at low temperature, and the high thermal stability will reduce the SCR activity. Kijlstra et al. has shown the order of the thermal stability of the nitrites/nitrates: monodentate nitrites, bridged nitrites, linear nitrites < bridged nitrates < bidentate nitrates.[31]

Therefore, the SCR catalysts must satisfy the balance of both surface acidity and the redox property. It is fundamental for any catalytic preparations to optimize the SCR application. In addition, fossil fuel is a complex mixture of many mineral compounds. Therefore, the combustion of fuel will generate many unexpected combinations in the flue gas. Although these compounds are generally not that much, they can strongly affect the exhaust gas treatment systems. Hence, besides the improvement of NO_x conversion, the study on the restriction of the other components in the exhaust gas such as SO_2, P/HCl, alkali, and heavy metals has also been considered, and it will be described in part below.

1.2.3 Effect of other components in flue gas

SO_2 poisoning. Fossil fuels always contain some sulfur compounds that generate SO_2 upon combustion. Three steps can describe the effect of SO_2: i) the SO_2 adsorption, ii) the SO_2 oxidation to SO_3, and iii) the deposition of $(NH_4)_2SO_4/NH_4HO_4$ on the surface of the catalyst. The latter blocks the active sites for SCR reaction, enormously decreasing the catalytic activity. The pathways of restricting SO_2 poisoning are based on the sulfate formation mechanism and its effects on the active sites of the catalyst (Figure 6).

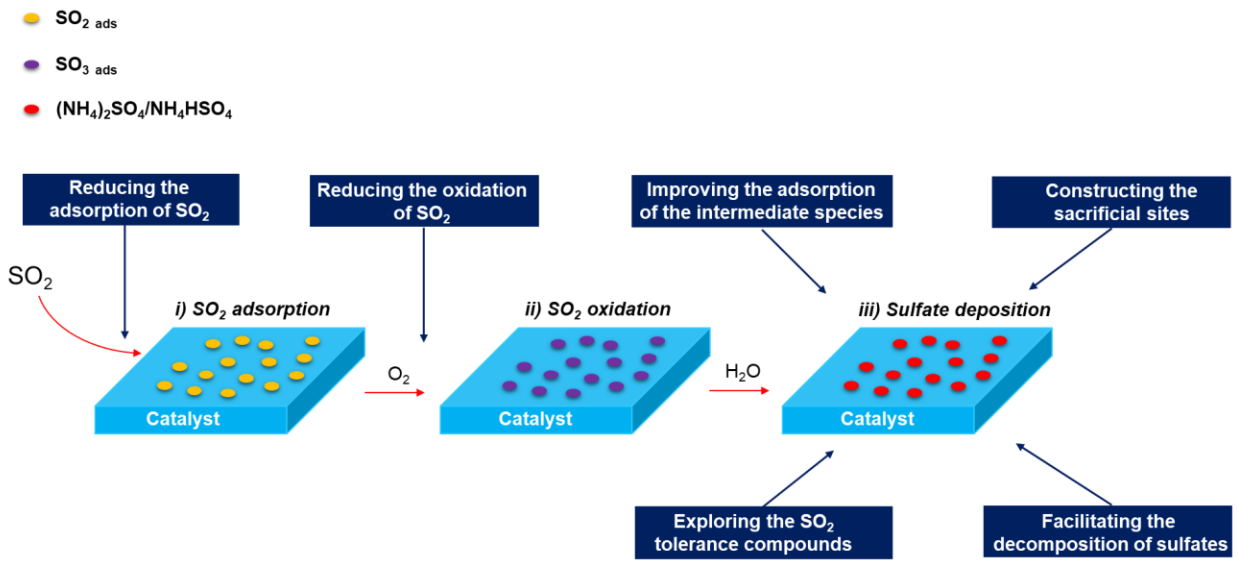

Figure 6. Three steps of the sulfate deposition and the corresponding methods for the restriction of the negative effects of the SO_2 poisoning

In principle, they can be divided into five major directions:[1]

- *Inhibition of the adsorption and/or the oxidation of SO_2*: Introducing a strong surface acidity can inhibit the adsorption of SO_2 since this acidic component prefers to interact rather with base sites. However, the oxidation capacity is an essential aspect of enhancing the SCR activity, as discussed above, and it is easy to oxidize SO_2 to SO_3. Therefore, this pathway has not been so attractive.

- *Improving the adsorption of the intermediate species*: Since the deposition of sulfates will block the active sites, enhancing the adsorption of the active intermediate species (NH_4^+, NH_3, nitrates, nitrites) could be an option to keep the amount of reactant large enough for SCR reaction.

- *Introducing sacrificial sites*: The coverage of sulfates on the active sites could be avoided by introducing additional sites that help in the deposition of sulfates. CeO_2 is mostly used as the sacrificial sites since it is easy to form $CeSO_4$ and $Ce_2(SO_4)_3$, then protecting the other active sites for the SCR reaction.[32-33]

- *Preventing the decomposition of sulfates:* The decomposition of NH_4HO_4 and $(NH_4)_2SO_4$ on the active sites can be prevented by water washing and thermal treatment after the SCR reaction.[34-35] However, sulfates usually are high thermal stability. The suppression of sulfates in

harsh conditions can lead to the deactivation of catalysts.[36] Therefore, this method has not been considered that much.

- *Using SO_2 tolerant compounds:* Some studies have shown that sulfate catalysts can inhibit ammonium sulfates' formation since the surface is sulfated already. In some works, the SCR reaction was performed on $CuSO_4/TiO_2$,[37] $CuSO_4/CeO_2$-TiO_2 catalysts of these catalysts showed a high SO_2 tolerance.

Alkali poisoning. Many works have indicated the negative effects of alkali on NH_3-SCR, mostly known as the effect of KCl. The presence of alkali can decrease the reducibility, reduce the surface acidity, and accelerate the catalysts' sintering. The mechanism of the alkali effect comprises the reaction of KCl with V-OH groups (Equations 10-12). This reaction will strongly decrease the amount of Brønsted sites V-OH for the SCR reaction. Furthermore, the formed HCl reacts with VO_x will destroy the active vanadium sites and change the valence states.[39]

$$\text{-V-OH} + \text{KCl} \rightarrow \text{-V-OK} + \text{HCl} \qquad (10)$$

$$\text{-}VO_2 + 2\text{HCl} \rightarrow \text{-}V(OH)_2Cl_2 \qquad (11)$$

$$V(OH)_2Cl_2 \rightarrow VOCl_2 + H_2O \qquad (12)$$

The construction of sacrificial sites on the catalysts or highly acidic supports could be a way to improve alkali resistance. It was performed on V_2O_5/sulfated-TiO_2[41] and V_2O_5/sulfated-ZrO_2[43] catalysts. The other direction for the restriction of alkali is constructing the alkali trapping system in front of the SCR.[44] The studies on the effect of alkali were mostly carried out by impregnation of alkali on the surface of catalysts prior to the SCR testing. However, in experimental conditions, the effect of alkali comes from the flue gas, and the actual effect of alkali could be very different compared to the tests under model conditions. Therefore, up to now, the alkali resistance is still the challenge for approaching the functional requirement.[1]

Heavy metal poisoning. Fossil fuels always contain a trace amount of heavy metals resulting from the mineral salts. The deactivation of SCR catalysts by the effect of heavy metals such as Pb, As, and Zn has been widely investigated so far. The heavy metals deposit on the surface of the catalyst and block the active sites, inhibiting the adsorption of NH_3 and NO and the reaction of the intermediate species via.

For example, the presence of Pb also can restrain the formation of active poly-tungstate species, leading to the formation of inactive bridge nitrate species. The same results were also

obtained for Ce/TiO_2 catalysts. The Pb poisoning suppresses the adsorption and activation of NH_3 and NO on the surface, accompanied by the decrease of Brønsted acid sites.[45]

The As-poisoning on V_2O_5-WO_3/TiO_2 catalyst has been reported by Lu et al.[46] It was shown that As presents in the form of $H_2AsO_4^-$ and $HAsO_4^{2-}$, leading to the decrease both Lewis and Brønsted sites of the catalyst. In addition, As also promote the N_2O formation above 300 °C, destroying the V-OH sites and then leading to the deactivation. The co-poison of As-Ca can decrease the surface area, accelerate the WO_3 crystalline, and irreversible loss of oxygen defect sites.[47] Since the strong interaction of catalysts with the heavy metals poisoning and it is hard to remove it effectively, enhancing the quality of fuels could be the good direction to reduce the negative effect of the heavy metals for the NH_3-SCR catalysts.

P/HCl poisoning. The combustion of fossil fuels can generate a small amount of phosphorous, which will affect the SCR catalysts. P-compounds can impair the redox property of V_2O_5-WO_3/TiO_2 catalyst then inhibit the oxidation of NO. On CeO_2-MoO_3 catalyst, the low amount of P-poisoning can be superior the NO oxidation and improve the activity. But increase the content of P up to 3.9 wt % will decline the NO_x conversion.[48]

HCl formation from the combustion of halogenated organic in the flue gas can also deactivate the catalyst. Due to the strong acidic property, HCl can destroy the metal oxides (V_2O_5) and form the salts that are inactivated for SCR reaction. The negative effects of HCl in NH_3-SCR on CeMo/Ti and VW/Ti catalysts have also been reported.[49-50] For the restriction of the effects of phosphorous and HCl, constructing the sacrificial sites or the protective shell could be the interesting pathway.

1.3 Sources of HCHO emission and impact on NH_3-SCR

1.3.1 The formation of HCHO

The exothermic fuel combustion is the energy supply for the engines. CO_2 is the final product of the oxidation, but the uncompleted combustion can generate some other products in the flue gas, among them HCHO.[51] A report from International Council on Combustion Engines has indicated that HCHO formation from methane is invertible from the port injection or homogenous charge supply.[52]

In the exhaust gas, the concentration of HCHO varies depending on the type of fuels, the combustion regimes, and the type of engines. Depending on the purpose and the condition of each study, the units for measuring HCHO concentration are not the same. Rodrigues et al. has studied the concentration of formaldehyde from sites impact of heavy-duty vehicles using diesel and biodiesel fuels. It was found that formaldehyde, acetaldehyde, and propanone are the most abundant quantified compounds. The emission of formaldehyde ranges from 28.45 to 287.3 ppbV (part per billion by volume), depending on the working time of the bus in a day.[53] Suarez-Bertoa et al. has measured the formation of ethanol, formaldehyde, and acetaldehyde from flex-fuel vehicle exhaust. The emission of formaldehyde from their tests rises from 0.4 to 0.7 $mg.km^{-1}$ depending on the points inside the exhaust gas system of the measurement.[54]

Since this work aims to study the effect of HCHO on the NH_3-SCR of NO_x, it would be better to compare the concentration of HCHO with the concentration of NO_x in the flue gas. Mitchell et al. has indicated no good correlations between HCHO concentration and NO_x concentration due to their different formation mechanisms. As mentioned above, NO_x is formed by the reaction of N_2 and O_2 at very high temperatures. Meanwhile, HCHO will be completely converted at this condition and mainly comes from the partial oxidation of hydrocarbons in the processes of gas flow insight the engine.[51] A document from the United States Environmental Protection Agency has studied the emission of HCHO and NO_x from the light-duty vehicles and light-duty trucks; depending on the specific conditions, the ratio of HCHO and NO_x concentration is different, ranging from 1.83 % to 7.50 %.[55] Clairotte et al. has studied the emission of HCHO from light-duty vehicles using ethanol – blend gasoline at low ambient temperatures. The ratio of HCHO:NO_x can up to approximately 18 % at high blend content of ethanol in the fuel.[56]

Role of DOC. The presence of Diesel Oxidation Catalysts (DOCs) in the exhaust gas treatment system is an important factor need to be considered. It is inserted in front of the SCR to oxidize the unburned organic compounds of the flue gas (Figure 7). HCHO can be converted to CO and CO_2 in the DOCs, and its concentration in the SCR will be no longer significant. However, in some specific conditions, a considerable amount of HCHO after the DOCs still exists. P.C. Shukla et al. has studied the role of DOCs for the unregulated emissions from the

biodiesel fuels on the transportation engine. Despite the DOCs can reduce the HCHO concentration, a significant amount of HCHO still presents at low engine load (0 – 50 % loading condition).[57] Furthermore, the concentration of HCHO even increase after the DOCs, resulting from the partial oxidation of the other organic compounds. Wei et al. has studied the role of DOCs in the emission of volatile organic compounds from the combustion of blended methanol fuels. The concentration of HCHO increases from 2.5 – 7 g/kWh to 8 – 11 g/kWh at the speed of 1660 rpm at the 25 % engine load.[58]

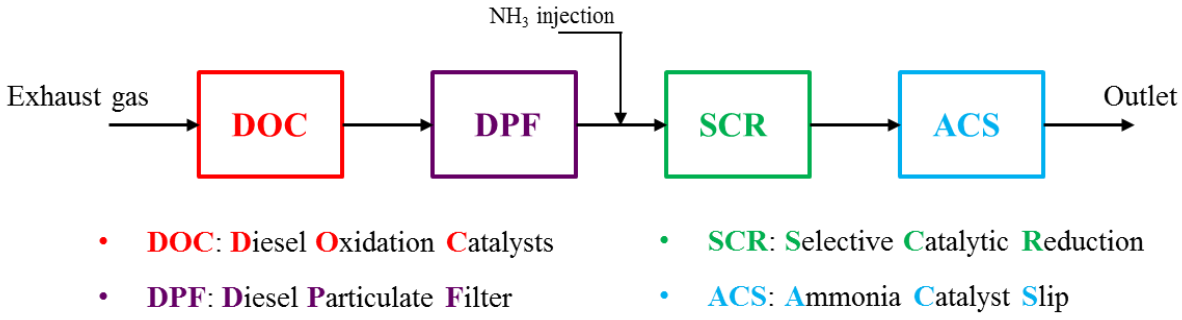

Figure 7. The exhaust gas treatment systems of the diesel engine

In summary, the concentration of HCHO in the exhaust gas and its ratio with NO_x varies depending on the work conditions of the engines. In principle, it does not exceed 20 % of the NO_x emission. Therefore, in this study, to ensure the concentration of HCHO is large enough to observe the change of the SCR activity and also not too far to the practical condition, the concentration of HCHO will be set equal to 10 – 18 % (100 – 180 ppm) of the NO_x concentration in the feed gas.

1.3.2 Reaction of HCHO with the components of standard SCR feed gas

A study on the reaction of HCHO with the components of the SCR feed gas (O_2, NH_3, NO) is the basic to explain the effect of HCHO in NH_3-SCR. First, regarding to O_2, which is always present a considerable amount in the feed gas, HCHO can be oxidized by O_2 to form CO and CO_2 (Equations 13-14).

$$HCHO + ½\ O_2 \rightarrow CO + H_2O \qquad (13)$$

$$HCHO + O_2 \rightarrow CO_2 + H_2O \quad (14)$$

Vanadium catalysts can accelerate the oxidation of HCHO via the formation of the intermediate species on the surface. E. V. Danilevich et al. has studied the oxidation of HCHO on Vanadia-Titania catalyst at 120 – 140 °C. CO_2, HCOOH, and CO are the main products and their selectivity depends on the time of reaction due to the further decomposition and oxidation of HCOOH.[59] Many studies have indicated that the oxidation of HCHO on the heterogenous catalysts will form formate species ($HCOO^-$) on the surface as the intermediates, which further form CO or CO_2 depending on the specific conditions.[60-62] Because the concentration of O_2 in the feed gas (5 vol %) is much higher than the initial concentration of HCHO (100 – 180 ppm), the reaction of HCHO will not affect the amount of O_2. However, the oxidation of HCHO, especially the formation of formates on the surface, is an essential factor to explain the formation of gaseous products of the reaction of HCHO in NH_3-SCR.

There is no significant reaction between NO and HCHO that occurs in the ambient condition. However, HCHO can react with NO_2 and nitrates on the surface of a catalyst, which can be formed during the SCR reaction (Equations 15-17):[63]

$$HCHO + NO_2 \rightarrow CO + NO + H_2O \quad (15)$$

$$HCHO + 2\ NO_2 \rightarrow CO_2 + 2\ NO + H_2O \quad (16)$$

$$HCHO + 4\ NO_3^- + 4\ H^+ \rightarrow CO_2 + 4\ NO_2 + H_2O \quad (17)$$

Therefore, HCHO does not reduce NO to the lower oxidation states, but its reaction can decrease amounts of nitrates on the catalyst's surface, reform NO to the gas phase, and decrease the NO_x conversion.

In the gas phase, HCHO reacts with NH_3 to form hexamethylenetetramine and water (Equation 18).[64] On the surface of the catalyst, the adsorbates of NH_3 ($NH_4^+{}_{ads}$, $NH_{3\ ads}$) and HCHO (formates) can react with each other (L-H mechanism) or with the gaseous (E-R mechanism) to form ammonium formate and formamide, which will further decompose to liberate the harmful products such as HCN and CO (Equations 18-22).[65-66]

$$6\ HCHO + 4\ NH_3 \rightarrow (CH_2)_6N_4 + 6\ H_2O \quad (18)$$

$$NH_3 + HCOOH \rightarrow HCOONH_4 \quad (19)$$

$$HCOONH_4 \rightarrow HCONH_2 + H_2O \quad (20)$$

$$HCONH_2 \rightarrow HCN + H_2O \quad (21)$$

$$HCONH_2 \rightarrow CO + NH_3 \quad (22)$$

The reactions of HCHO with NH_3 will reduce the amount of NH_3, and no more NH_3 available for the SCR reaction. These undesired reactions lead to the decrease of NO_x conversion and the N_2 selectivity. Furthermore, the liberation of the toxic products (HCN, CO) from these reactions is also a serious problem and should be limited.

2. Experimental methods

2.1 Catalyst preparation

For the beginning of the study, a fresh pellet of a commercial V_2O_5-WO_3/TiO_2 (1 wt. % V, 6 wt. % W) catalyst from Argillon GmbH was ground and screened by a sieve to filter particles of a size suitable for the catalytic tests (250 – 315 µm). After that, three different catalysts WO_3/TiO_2 (W-Ti), V_2O_5/TiO_2 (V-Ti), and V_2O_5-WO_3/TiO_2 (V-W-Ti) were prepared by the wetness impregnation method. The content of vanadium and tungsten were chosen to be the same as in the commercial catalyst V_2O_5-WO_3/TiO_2 (1 wt. % V, 6 wt. % W). The commercial TiO_2 (P25 nano powder, Aldrich) was used as the support.

For the synthesis of the W-Ti catalyst, 0.5404 g of ammonium para tungstate hydrate $(NH_4)_{10}H_2(W_2O_7)_8.xH_2O$ (99.99%, Aldrich) was added to 58.00 mL deionized water at 35 °C, then stirred until the solution becomes transparent. After that, 6.00 g TiO_2 P25 was slowly added to the solution. The suspension was heated up to 55 °C and continuously stirred in 12 h to let the molecules of tungsten salt deposits on the surface of TiO_2. Finally, the mixture was dried overnight at 100 °C, crushed into powder, and calcinated at 400 °C (5 K/min) in 2 h in synthetic air (Figure 8a).

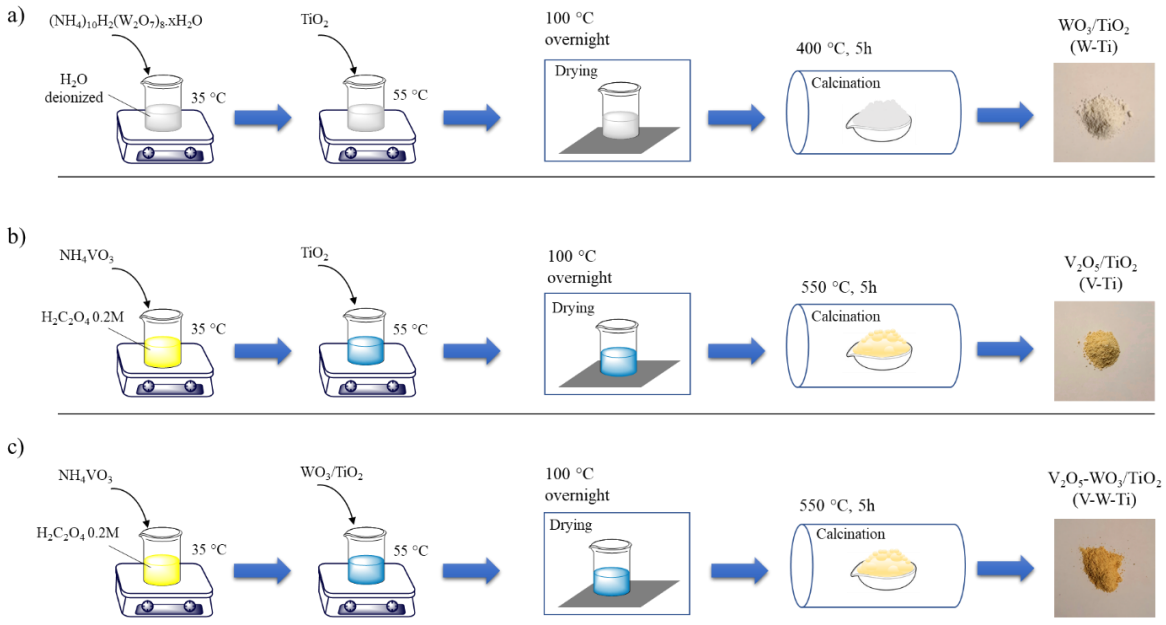

Figure 8. The preparation of a) W-Ti, b) V-Ti, c) V-W-Ti catalysts by the wetness impregnation method

For the preparation of V-Ti catalyst, 0.1378 mg of ammonium metavanadate NH_4VO_3 (99 %, Sigma-Aldrich) was dissolved in 30 mL oxalic acid 0.2 M. The solution was stirred until it turned to turquoise color when vanadium forms an oxalate complex. After that, 6.00 g TiO_2 was added to the solution and continuously stirred at 55 °C for 12 h for the deposition of vanadium salt on the TiO_2 surface. Finally, it was dried overnight at 100 °C, crushed into powder, and calcinated at 550 °C (5 K/min) in 2 h in synthetic air (Figure 8b). The V-W-Ti catalyst was prepared in the same way the V-Ti catalyst, but instead of adding TiO_2, 6.00 g powder of the W-Ti catalyst was added to the vanadium oxalate complex solution. The suspension was also dried at 100 °C overnight then calcinated at 550 °C (5 K/min) in 2 h (Figure 8c).

2.2 Characterization methods

2.2.1 Inductively coupled plasma - optical emission spectrometry (ICP-OES)

The chemical composition of catalysts is measured by inductively coupled plasma optical emission spectrometry (ICP-OES). In the ICP-OES measurement, a sample was excited to take place the electrons ionization. The electrons will take the thermic energy and reach the higher excited states. When it drops back to the ground level, the energy will be released by a diverse emission spectrum, depending on the type of elements. The wavelength and intensity of the emission spectrum are the basis for detecting the elements and their composition on the catalyst.

In this study, for each measurement, 10.00 mg of sample was dissolved in 8.00 mL aqua regia and 2 mL hydrofluoric acid and was treated by the microwave-assisted sample preparation system “MULTI WAVE Pro” (Anton Paar) at 200 °C and 60 bars. After that, the solution was diluted by water up to 100 mL then was analyzed by a Varian 715-ES ICP-emission spectrometer and the ICP Expert software.

2.2.2 The X-ray diffraction spectroscopy

The X-ray powder diffraction (XRD) is commonly used to investigate the structural crystalline of the catalysts. When an X-ray beam was irradiated to the crystal, the planes play a role as the diffraction grating. The space between planes is d, and θ is the incident angle of the X-ray beam (Figure 9a). Therefore, the distance between two diffraction rays is d.sinθ. To satisfy the interference condition of the light, the incident angle must satisfy the Bragg’s Law (Equation 23) since the wavelength λ, and the planes space d are constant.

$$n.\lambda = 2d.\sin\theta \qquad (23)$$

Hear n is any integer, λ is the wavelength of the incident light, d is the spacing between two adjacent planes, and θ is the laser beam's incident angle. For the measurement, the sample is rotated in the path of the collimated X-ray beam at an angle θ, and the detector for collecting the diffraction is rotated at an angle of 2θ. Various crystalline will show the characteristic peaks, which will be the fingerprint to detect their presence (Figure 9b).

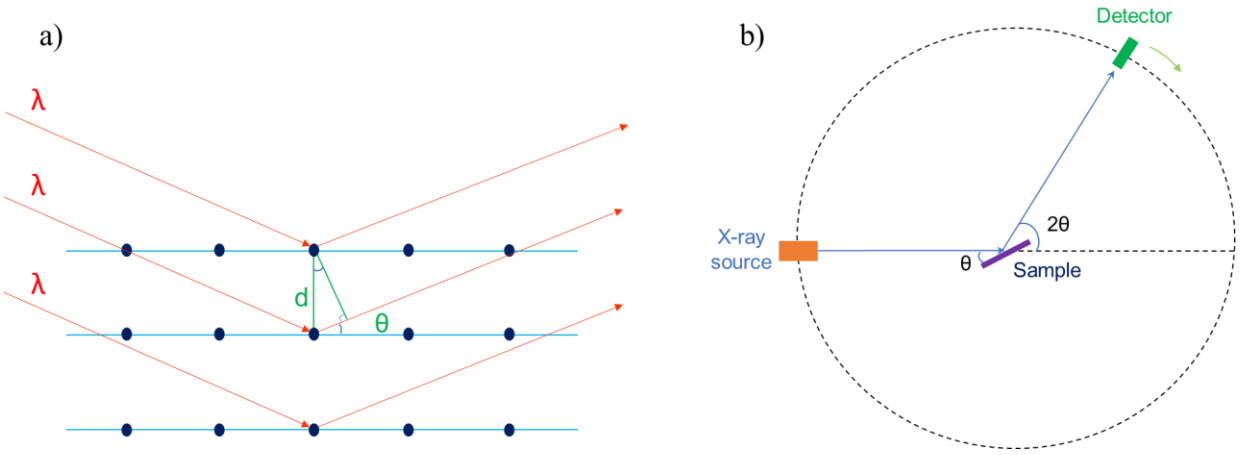

Figure 9. a) The diffraction of the X-ray beam on the planes of the crystalline of the solid, b) the principle of the X-ray powder diffraction

In this study, the reflection spectra were recorded by a *θ/θ* diffractometer (X'Pert Pro, Panalytical, Almelo, The Netherlands) using a X'Celerator RTMS detector with the Cu Kα radiation. The phase composition of catalysts was determined by the program suite WinXPOW (Stoe&Cie), including the diffraction file PDF2 of the International Centre of Diffraction Data (ICDD).

2.2.3 Brunauer – Emmett – Teller (BET) surface area analysis

The BET methodology is used to measure the specific area and the pore volume of the catalysts. The theory of this method is based on applying the multilayer adsorption system and assuming that there is no chemical reaction between the gas and the solid material. Therefore, N_2 is principally employed as the gaseous adsorbate. The concept of BET theory is an extension of the Langmuir theory, from monolayer to multilayer adsorption. The equation of BET is following Equation 24.

$$\frac{1}{\upsilon[(p_0-p)-1]} = \frac{c-1}{\upsilon_m.c} \cdot \left(\frac{p}{p_0}\right) + \frac{1}{\upsilon_m.c} \qquad (24)$$

p is the equilibrium pressure of the adsorbate at a temperature of the experiment (atm)

p_0 is the saturation pressure of the adsorbate at a temperature of the experiment (atm)

υ is the adsorbed gas quantity

υ_m is the monolayer adsorbate quantity

c is the BET constant, following Equation 25:

$$c = \exp\cdot\left(\frac{E_1 - E_L}{RT}\right) \qquad (25)$$

E_1 is the heat of adsorption for the first layer

E_L is the heat of adsorption for the second and higher layers and is equal to the heat of liquefaction or heat of vaporization

Equation 24 is an adsorption isotherm and can be plotted as the straight line with the value $1/[\upsilon(p_0/p) - 1]$ is the y-axis, p_0/p value is the x-axis, which is called BET plot. The linear relationship of the plot was maintained in the range of $0.05 < p_0/p < 0.35$. The value of slope A and the intercept I is used to calculating the monolayer adsorbed gas quantity υ_m and the BET constant c, following Equations 26 and 27 below.

$$\upsilon_m = \frac{1}{A+I} \qquad (26) \qquad\qquad c = 1 + \frac{A}{I} \qquad (27)$$

The total surface area S_{total} and the specific area of the material are calculated according to the equations below:

$$S_{total} = \frac{\upsilon_m.N.s}{V} \qquad (28) \qquad\qquad S_{BET} = \frac{S_{total}}{a} \qquad (29)$$

υ_m is the units of the monolayer volume of the adsorbate gas

N is the Avogadro number

S is the adsorption cross-section of the adsorbate species

V is the molar volume of the adsorbate gas

a is the mass of the solid sample or adsorbent

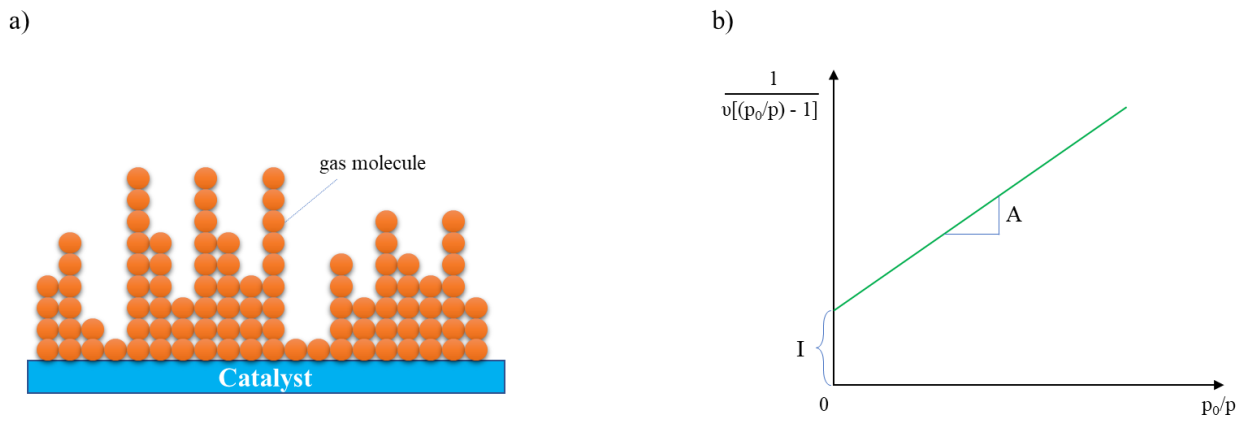

Figure 10. a) the BET model of multilayer adsorption on the surface of the catalyst, b) BET plot result

For each experimental measurement, the sample was firstly degassed at 200 ºC at 0.01 mmbar for 3 h. The specific surface areas were determined by nitrogen adsorption at −196 °C using the single-point BET procedure (Gemini III 2375, Micromeritics).

2.2.4 Hydrogen Temperature-Programmed Reduction (H_2-TPR)

The temperature-programmed reduction is used to investigate the reducibility of catalysts. Since the different species of vanadium oxides and tungsten oxides perform different reducibility, the H_2-TPR results could provide information on the dispersion of metal oxides on bare support. The catalyst was set up in a fixed bed reactor, a flow of reductant (hydrogen) was pumped across the reactor simultaneously with the gradual increase of the temperature. The TPR reactor outlet was connected to a Mass Spectrometer to determine the amount of H_2 leaving the reactor, from which H_2 consumption was calculated (Figure 11).

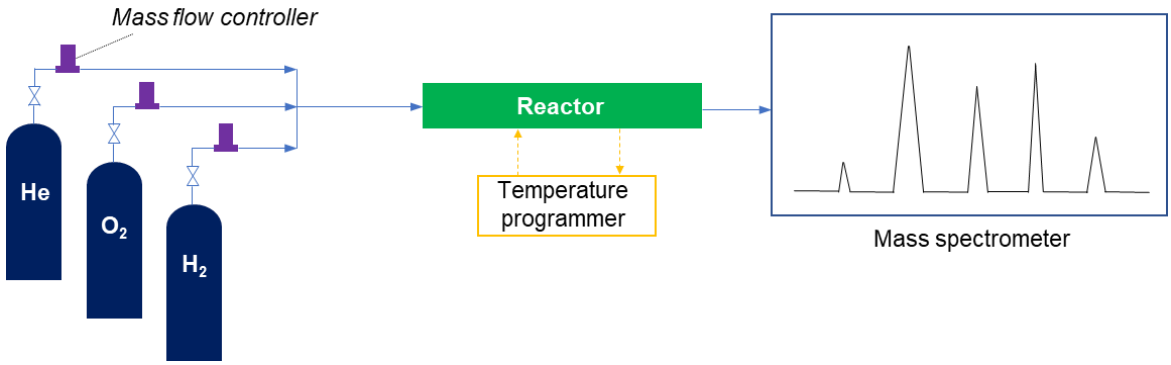

Figure 11. Scheme of the H_2-TPR set up

In this study, H_2-TPR measurements were performed using a Micromeritics Autochem II 2920 instrument. For each experiment, 200 mg of catalyst particles (250-350 µm) was loaded into a U-shaped quartz reactor and pre-treated in 5 vol % O_2/He (30 mL.min^{-1}) at 400 °C for 30 min. After that, it was cooled down to room temperature by flushing the Ar flow. The TPR experiments were carried out from room temperature to 800 °C in 50.00 mL.min^{-1} of 5 vol % H_2/Ar flow (10 °C.min^{-1}), and the hydrogen consumption was monitor by a TCD detector.

2.2.5 Raman spectroscopy

Raman spectroscopy was used to investigate the molecular structure of the supported catalysts. Raman spectra can identify different types of vanadium and tungsten oxides scattering on the surface of a support. It is based on the Raman effect of the light's scattering when it was irradiated to the sample (Figure 12).

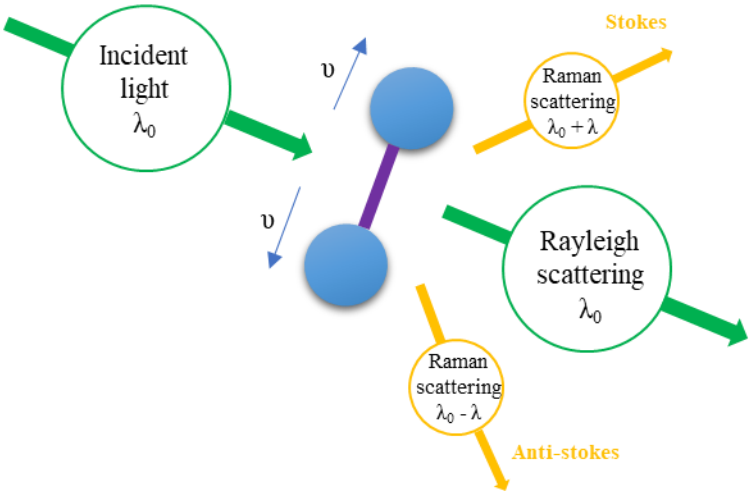

Figure 12. The scattering of the light from the irradiation and the molecule vibrations

When a sample was excited by a high-intensity laser beam, three light scattering types can be observed. The elastic scattering (Rayleigh) is the main part and occurs with the same wavelength as the incident light. Due to the excitation of vibration in the molecules, inelastic (Raman) scattering is observed at a different wavelength, and it is used to determine the structure of the molecules. Typically, the Raman scattering stokes lines are used for the analysis, but sometimes

the anti-stokes can also be used. The Raman shift is the energy difference between the incident light and the scattered light (Equation 30).

$$\text{Raman shift} = \frac{1}{\lambda_0 - \lambda} - \frac{1}{\lambda_0} \ (\text{cm}^{-1}) \qquad (30)$$

In the resulting spectrum, the vertical axis is the intensity of the scattered light. The horizontal axis is the Raman shift value, which can identify the structure of metal oxide species loaded on the surface of a support.

In this study, the Raman spectra of catalysts were recorded in the range of 300 – 2000 cm^{-1} by a Renishaw inVia Raman microscope, using a laser at 633 nm with a power of 1.7 mW. For each experiment, 50.00 mg of catalyst powder was first pretreated in synthetic air at 300 °C for 1 h then cooled down to room temperature. The measurements were carried out in 10 seconds accumulation in a Linkam reaction cell. Due to the induced fluorescence of tungsten, Raman spectra of W-Ti were collected at 300 °C.

2.2.6 UV-Vis Diffuse Reflection Spectroscopy

In situ UV-Vis diffuse reflection spectroscopy (UV-Vis DRS) is used to study the dispersion of vanadium oxides and tungsten oxides on the support. The UV-Vis DRS spectrum can provide information on the oxidation states and the coordination geometry of the vanadium and tungsten oxides on the surface of a support. It probes the electronic charge transfer transitions and the d-d transition of the loaded oxides strongly related to the polymerization level and the oxidation states of the metal oxides. However, this technic also has some disadvantages since the bands are frequently very broad, and the individual absorption bands are overlapped with each other and complicate the analysis.

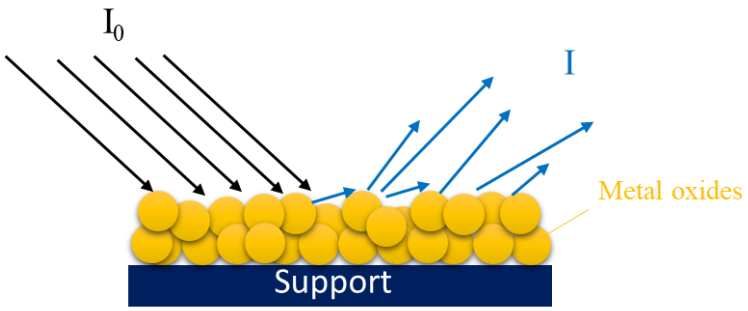

Figure 13. The diffuse reflection of the light on the surface of metal oxides loading on support

The diffuse reflection of the light at the phase boundaries of supported catalysts is described in Figure 13. An equivalent to the well-known Lambert-Beer law, which represents a linear correlation between light absorption and concentration of a species in a liquid solution, is the Kubelka-Munk function $F(R_\infty)$ for diffuse reflectance on solids (Equation 31), in which R_∞ is the reflectance at infinite layer thickness. Under specific boundary conditions $F(R_\infty)$ is proportional to the concentration of a species.

$$F(R_\infty) = \frac{(1 - R_\infty)^2}{2R_\infty} \qquad (31)$$

However, this is only true for low $F(R_\infty)$ values. Love et al. found that the dependence of the $F(R_\infty)$ function is nonlinear with the concentration of vanadium (the main active site of the SCR reaction) even at moderate values (Equation 32).[67] Therefore, the edge energy E_g is used to determine the local coordination of metal oxides on the support. The edge energy (E_g) of catalysts was calculated using the Tauc's plot.[68-69]

$$[F(R_\infty)\cdot h\upsilon]^2 \propto (h\upsilon - \varepsilon_0) \qquad (32)$$

In this study, UV-Vis DRS experiments were performed by a Carry 5000 UV-Vis-NIR Spectrometer equipped with a diffuse reflectance accessory (praying mantis, Harrick). $BaSO_4$ was used as the standard baseline. The catalyst particles were placed inside a heat-able reaction chamber (Harrick) connected to a temperature programmer (Eurotherm) and mass flow controllers (Bronkhorst) for gas-dosing. All catalysts were pretreated by a flow of 5 vol % O_2/He at 300 °C for 60 min to remove moisture before cooling down to the ambient temperature for the measurement.

2.2.7 Pyridine adsorption analyzed by FT-IR spectroscopy

Pyridine adsorption infrared spectroscopy is widely used to discriminate and calculate the amount of Brønsted and Lewis sites on the surface of solid catalysts since it is more selective and stable than the NH_3 adsorption. When Pyridine was introduced to the surface of the catalyst, it will either interact with the metal atoms (Lewis sites) or OH groups (Brønsted sites). The peak area of the adsorption bands will be calculated by integration to determine the amount of Lewis (band at 1445 cm^{-1}) and Brønsted sites (band at 1538 cm^{-1}) on the surface of catalyst (Figure 14).[70]

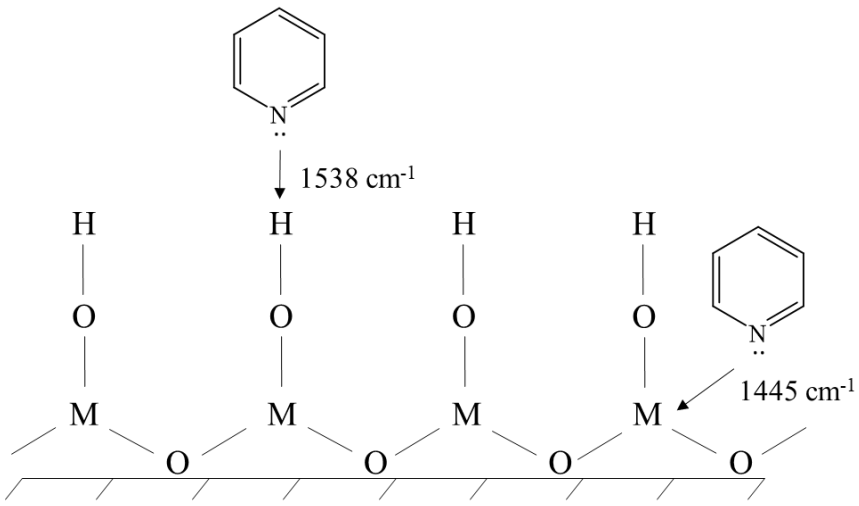

Figure 14. The surface interaction of Pyridine with the acidic sites of the catalyst

In this study, the surface acidity of the catalysts was analyzed by a Tensor 27 spectrometer (Bruker) equipped with a heat-able and evacuate-able IR cell, connecting to a gas dosing and evacuation system. For each experiment, 50 mg of catalyst powder was pressed into self-supporting wafers (Φ = 20 mm), pretreated by the evacuation at 400 °C for 1 h then cooled to room temperature for recording a background spectrum. The adsorption of Pyridine was carried out at room temperature until saturation. The spectra were recorded after the evacuation of the gas phase remain in the cell and subsequently every 50 °C during the heating in vacuum up to 400 °C.

2.2.8 In situ FT-IR

Infrared spectroscopy (IR) is the most comprehensive application method of identifying and analyzing chemical compounds. Each functional group (such as C-H, C=O, COO^-, etc.) adsorb the IR rays in different wavelengths and intensities, depending on the nature of the vibration and the compounds' concentration. Therefore, tracking the IR bands' changes during the interaction of the reactants on the surface of the catalyst will provide information on the formation and reaction of the intermediate species. Nowadays, the Fourier-Transformation Infrared Spectrometer (FTIR), which records the data collected and transforms it to the spectrum, is predominately used.

In this study, *in situ* FTIR experiments were carried out on a Thermo Scientific Nicolet 6700 spectrometer in transmission mode to study the formation of the intermediate species on the catalyst surface. For each experiment, 60 mg catalyst was pressed into a thin wafer ($\Phi = 20$ mm) and was placed inside a heat-able IR quartz reaction cell using a CaF_2 window connected to a gas dosing system. Before each experiment, the catalyst was pretreated at 350 °C in 5 vol % O_2/He flow (50 mL.min^{-1}) for 1 h, then cooled down to 150 °C for the *in situ* experiment.

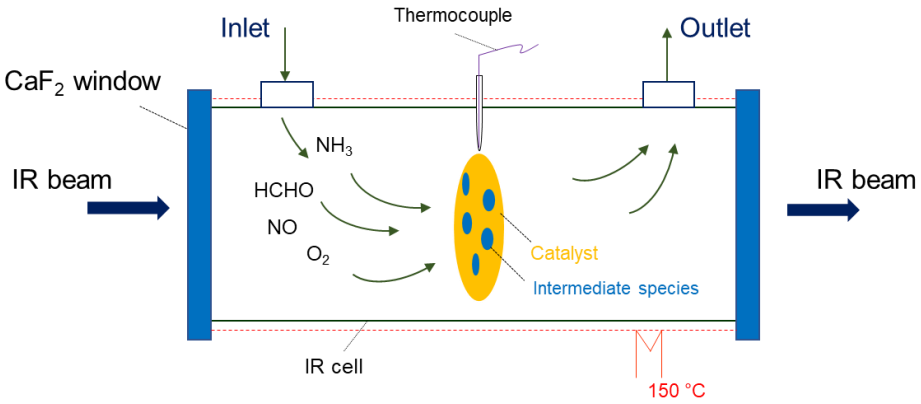

Figure 15. The scheme of *in situ* FT-IR experiments set up

The interaction of HCHO/O_2 with NH_3 on the surface of catalysts was first conducted by the adsorption of 0.1 vol % NH3 (50 mL.min-1) for 1 h followed by flushing He flow for 30 min to remove the unstable species on the surface of the catalyst. Subsequently, the outlet was closed, and the catalyst was exposed to a flow of 400 ppm HCHO, 5 vol % O_2 (25 mL.min^{-1}) for 10 min. Finally, the cell was closed for 50 min to observe the formation of the intermediate species. The various experiment was carried out by the first adsorption of 200 ppm HCHO, 5 vol % O_2/He in 60 min (50.00 mL.min^{-1}). After that, a flow of He was flushed to the catalyst to remove the unstable species. Finally, the cell was closed, and a flow of 0.2 vol % NH_3/He (20.00 mL.min^{-1}) was dosed in 10 min, and the cell was kept in 50 min to observe the formation of the intermediate species.

The simultaneous interaction of HCHO and NH_3 was carried out by the flushing a flow of 200 ppm HCHO, 0.1 vol % NH_3, 5 vol % O_2/He over the catalyst at 150 °C in 1 h. After that, the cell was closed and heated up to 350 °C to observe the decomposition of the intermediate species.

The formation and reaction of the intermediate species of the SCR reaction were firstly studied by the adsorption of 0.1 vol % NH_3/He (50.00 mL.min^{-1}) on the catalyst in 1 h at 150 °C. After flushing by He in 30 min to remove the unstable species, a flow of 0.2 vol % NO, 5 vol % O_2/He (20.00 mL.min^{-1}) was injected into the IR cell in 10 min, then keeping the cell closed in 50 min to observe the reaction. The same process was carried out for the simultaneous interaction of HCHO/NO/O_2 with the adsorbate of NH_3 by dosing a flow of 400 ppm HCHO, 0.2 vol % NO, 5 vol % O_2/He (20.00 mL.min^{-1}) to the IR cell.

2.2.9 In situ EPR

Electron paramagnetic resonance (EPR) spectroscopy is a unique and selective method to study the nature of species containing unpaired electrons. As mentioned above, vanadium is the leading active site for the SCR reaction, and the redox pair V^{5+}/V^{4+} plays a crucial role in the catalytic activity. V^{4+} contains an unpaired electron and, therefore, can be well detected by EPR spectroscopy.

A single electron has an electron spin S and a magnetic moment $\bar{\mu}$ which are both vectors. When brought into an external magnetic field B_0, S and $\bar{\mu}$ are aligned with the magnetic field direction, leading to two states of different energy (Figure 16a). This is called the Zeeman interaction. The two states of the unpaired electron are labeled by the energies $E_{1/2}$ and $E_{1/2}$ with the corresponding spin quantum numbers $m_s = +½$ and $m_s = -½$, respectively (Equations 33-34). β is the Bohr magneton, and g_e is the spectroscopic g-factor of the free electron (≈ 2.0023).

$$E_{1/2} = ½\, g_e.\beta.B_0 \qquad (33)$$

$$E_{1/2} = -½\, g_e.\beta.B_0 \qquad (34)$$

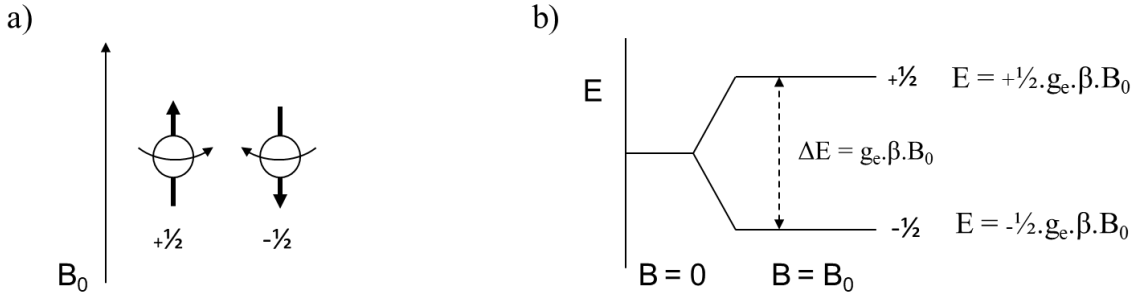

Figure 16. a) The orientations of the electron moment $\bar{\mu}$ in the magnetic field B_0, b) corresponding the spin state energies

In a molecule, the electron resides in an orbital where spin-orbit coupling can take place. This leads to deviations of the g value from g_e and will be used to detect the existence of the species containing a single electron of the molecules. It is calculated from the frequency of the wavelength υ (MHz) and the value of the magnetic B_0 (Gauss) (Equation 35).

$$g = \frac{\Delta E}{\beta . B_0} = \frac{h . \upsilon}{\beta . B_0} = 0.7145 \cdot \frac{\upsilon (MHz)}{B_0 (Gauss)} \qquad (35)$$

h is the Planck constant ($h = 6.626 \cdot 10^{-34}$ J·s)

υ is the value of the frequency (MHz)

β is the Bohr magneton constant ($\beta = 9.274 \cdot 10^{-28}$ J.G^{-1})

There are two common methods for the EPR spectra record experiment: the continuous wave EPR (cw) and the pulse EPR. In this study, the cw method is applied in the microwave range from 9-10 GHz in X-band frequency. In the case of V^{4+}, which has the electron spin S = 1/2 and nuclear spin I = 7/2, the interaction of the nuclear magnetic moment with the unpaired electron will turn to the perturbation, known as the nuclear hyperfine structure (Figure 17).

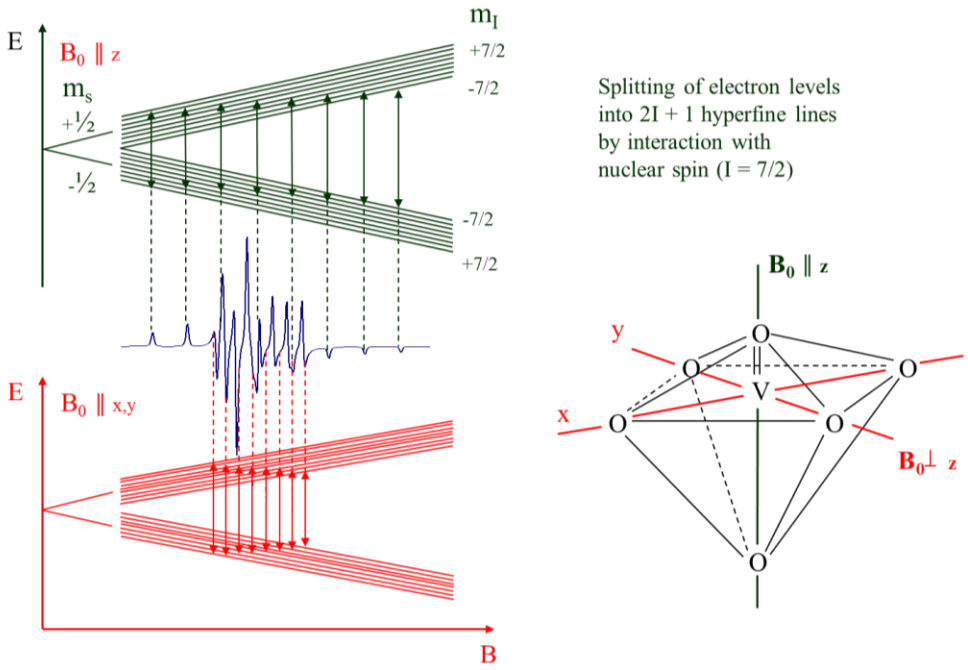

Figure 17. The energy splitting levels and the corresponded EPR spectra of VO^{2+} species. Reproduced from ref. A. Brückner.[71]

The resonance condition now becomes:[72]

$$\Delta E = h \cdot \upsilon = g \cdot \beta \cdot B_0 + h \cdot A \cdot m_I \qquad (36)$$

A is the anisotropic hyperfine tensor called the hyperfine coupling constant (cm^{-1})

m_I is the magnetic quantum number of nuclear ($m_I = I, I - 1, \ldots, 0, \ldots, -I + 1, -I$)

In addition, the structure of VO^{2+} species is usually a square pyramid or an octahedron. V atom places in the center and is surrounded by oxygen atoms in the corner. It leads to axial distortion and the rise to an anisotropic spin distribution. Therefore, the g-tensor and A-tensor value will be divided into three principle components:

$$g = \begin{pmatrix} g_{xx} & 0 & 0 \\ 0 & g_{yy} & 0 \\ 0 & 0 & g_{zz} \end{pmatrix} \qquad (37) \qquad A = \begin{pmatrix} A_{xx} & 0 & 0 \\ 0 & A_{yy} & 0 \\ 0 & 0 & A_{zz} \end{pmatrix} \qquad (38)$$

In the perpendicular orientation of the external magnetic field and the z-axis of the VO_6 octahedron, the g-tensor values as $g_\perp = g_{xx} = g_{yy}$. In the parallel orientation of the external magnetic with the z-axis, the g-tensor values as $g_\parallel = g_{zz}$ (Figure 17). The hyperfine coupling effect of V^{51} nuclear leads to the splitting energy level of the unpaired electron. The axial geometry of VO^{2+} turns the g-tensor into two components $g_\perp$ and $g_\parallel$ with the corresponding value of the hyperfine coupling constants $A_\perp$ and $A_\parallel$, respectively.

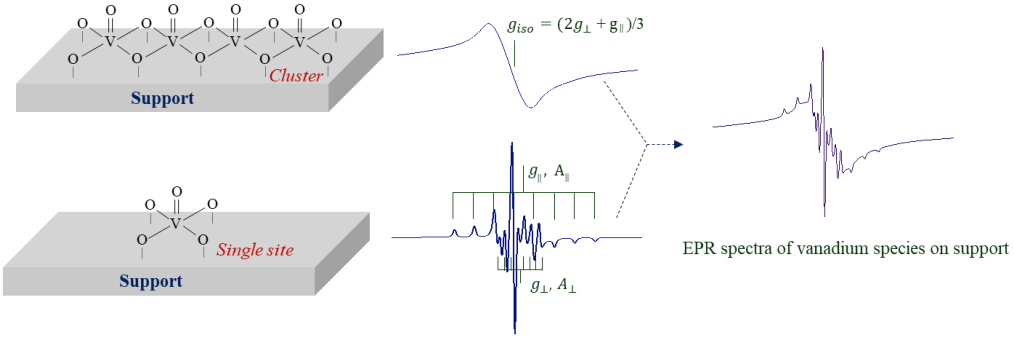

Figure 18. The contribution of vanadium species on support for EPR spectra. Reproduced from ref. A. Brückner.[73]

The EPR signals of V^{4+} also depend on the dispersion of vanadium on the support. In the cluster forming case, the anisotropic g and A splitting are averaged out and turn to the isotropic

signal. Since the dispersion of vanadium on the support's surface is not uniform, the EPR spectra normally contain two components: the cluster specie and the isolated species. As mentioned above, the axial geometry of VO^{2+} will turn the g-tensor into 2 values ($g_{\perp}$ and $g_{\parallel}$) and these values will be affected by the components surrounding the V atom. Therefore, the EPR spectra with the corresponding values (g, A) will provide information on the dispersion of the vanadium species on the surface of the catalyst and its contribution to the reaction (Figure 18). The determination of the contribution of vanadium species for the EPR spectra will be carried out by the simulation.[73]

In this study, EPR spectra were collected by an ELEXSYS 500-10/12 X-band cw spectrometer (Bruker) using 6.3 mW microwave power, 100 kHz modulation frequency, and 5 G amplitude. For each experiment, 100 mg catalyst of particles (250 – 315 µm) was placed inside a homemade quartz plug-flow reactor equipped with mass flow controllers (Bronkhorst) at the inlet for gas dosing (Figure 19).

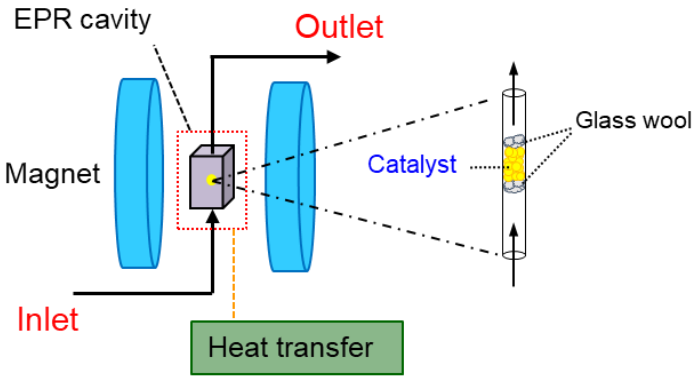

Figure 19. Scheme of the *in situ* EPR experiment set up

Before each experiment, the catalyst was pretreated in a flow of 5 % vol O_2/He at 300 °C for 1 h, then cooled down to 150 °C under Ar flow for the measurement. The catalyst was first exposed to a flow of 50 mL.min^{-1} 0.2 vol % NH_3/He for 1 h, and subsequently to Ar flow for 30 min to remove all the unstable species on the surface of the catalyst. After that, a flow of 50 mL.min^{-1} of 400 ppm HCHO, 5 vol % O_2/He or 0.2 vol % NO, 5 vol % O_2/He was flushed over catalyst for 1 h. Spectra were collected every 3 minutes to observe the change of V^{4+} species during interaction of HCHO/O_2 or NO/O_2 with the adsorbates of NH_3 on the surface of the

catalyst. The EPR spectra of the catalysts were simulated by the software package Easyspin implemented in the MATLAB program.[74]

2.3 Catalytic test

2.3.1 The standard SCR reaction

In this study, the SCR reaction was carried out using a feed of 0.1 vol % NH_3, 0.1 vol % NO, 5 vol % O_2, balance He. A fixed-bed quartz plug-flow reactor was used. For each experiment, 100 mg catalyst of particles of size 250-315 µm diluted with 500 mg α-Al_2O_3 was used. The total flow rate of the feed was set at 100 mL.min^{-1}, corresponding to a GHSV of 70 000 h^{-1} (Figure 20). Before the experiment, the SCR catalyst was pretreated by a flow of 20 vol % O_2/He at 500 °C for 1 h for the removal of all the contaminants on the surface of the catalyst. In addition, this catalytic pretreatment also oxidized all the active sites to the highest valance state, which would be beneficial to achieve the maximum catalytic activity. The reaction was carried out in the temperature range of 150 – 500 °C (50 °C/step). In each step of temperature, the reaction was kept for 1 h to achieve the stable catalytic performance.

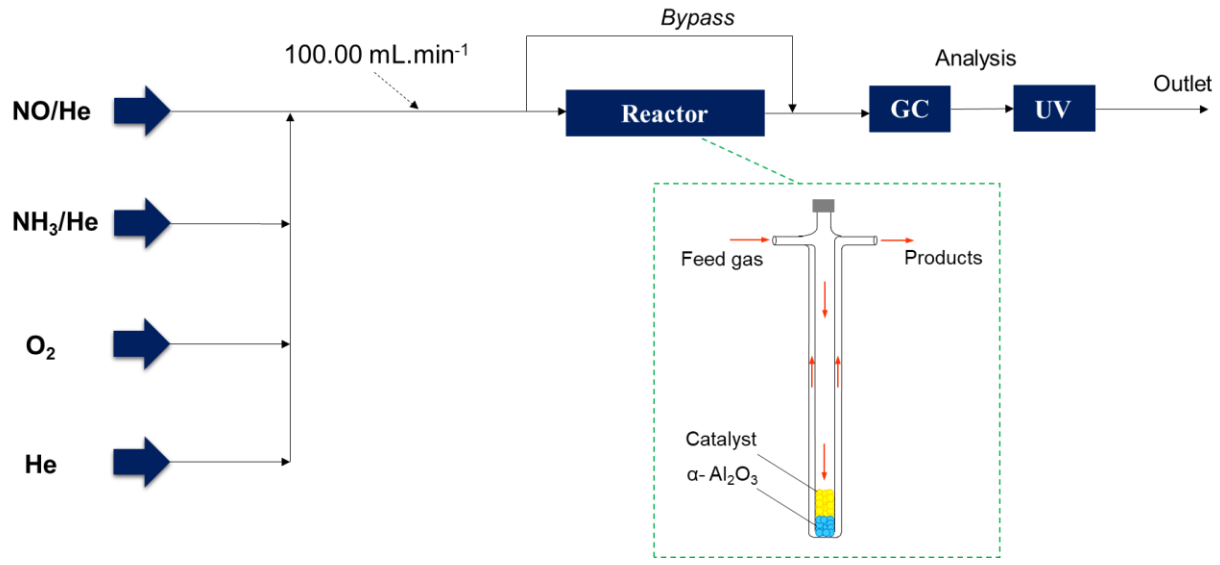

Figure 20. The scheme of the experimental set up of the NH_3-SCR reaction

Because NO readily reacts with O_2 to form NO_2 under ambient conditions, a small amount of NO_2 is present in the feed gas, and it is counted as a reactant. The reactants (NO, NO_2, NH_3) was

detected by a UV multi-gas sensor detector (ABB Gas Analyzer models AO2020, Limas 11HW, Manheim, Germany). The SCR reaction's products (N_2 and N_2O) were detected by an Agilent HP 6890 GC using a molecular sieve 5A and a Porapak Q capillary column. The conversion of NO_x (NO and NO_2) and NH_3 was calculated according to the reacted amount over its concentration in the feed gas (Equations 39-40). The selectivity of N_2 was calculated according to the quotient of N_2 and the reacted amount of NO_x and NH_3 (Equation 41).

$$X_{NO_x} = \frac{[NO_x]_{in} - [NO_x]_{out}}{[NO_x]_{in}} \cdot 100\% \quad (39)$$

$$X_{NH_3} = \frac{[NH_3]_{in} - [NH_3]_{out}}{[NH_3]_{in}} \cdot 100\% \quad (40)$$

$$S_{N_2} = \frac{2[N_2]}{[NO_x]_{in} + [NH_3]_{in} - [NO_x]_{out} - [NH_3]_{out}} \cdot 100\% \quad (41)$$

2.3.2 Reaction of HCHO in NH_3-SCR

HCHO generation. The formation of HCHO was conducted by the thermal decomposition of trioxane.[2] Trioxane vapor was generated by its sublimation in a diffusion cell. The diffusion cell was put inside an aluminum block to keep the temperature stable at room temperature. A He flow was set up to flush trioxane vapor to a converter made by 3.0 m Restek silicon steel tube (outer and inner diameter: 1/16 and 0.04 inch). The converter was heated up to 290 °C for the decomposition of trioxane to form HCHO (Equation 42). All the lines containing HCHO were heated up to 120 °C to avoid the polymerization and accumulation of HCHO inside (Figure 21). The HCHO concentration leaving the converter was taken as stable when the concentration of trioxane entering the converter reached a stable level. This is only possible when the sublimation of solid trioxane reaches equilibrium with the amount of trioxane flushed out by Helium flow. It took at least 5 h from the beginning of the Helium flushing to the diffusion cell.

$$(CH_2O)_3 \rightarrow 3\ HCHO \quad (42)$$

The concentration of HCHO and the formation of products from its reaction was measured by an online FT-IR spectrometer (ThermoFisher Scientific) (Figure 21). The total flow rate of the feed gas was always kept constant in each SCR experiment at 100 $mL.min^{-1}$. The

concentration of HCHO in the feed gas entering the SCR reactor was controlled by the flow rate of He passed through the diffusion cell.

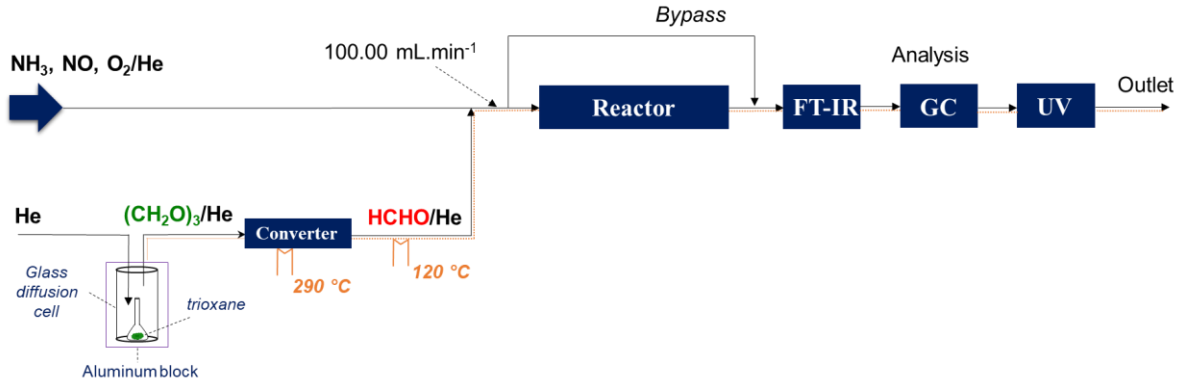

Figure 21. The experimental set up of the HCHO formation from the thermal decomposition of trioxane, connecting with the normal SCR experiment set up

HCHO calibration. To set up the suitable concentration of HCHO, different rates of the He flushing trioxane flow were added to the feed, which was always kept constant at 100.00 mL.min^{-1} and containing an excess amount of O_2 (5 vol % O_2/He). It took at least 5 h from the beginning of trioxane flushing to achieve a stable concentration of HCHO in the feed. HCHO will be oxidized by the catalyst to form CO and CO_2 and the concentration of CO and CO_2 will be used to calculate the concentration of HCHO in the feed. In this case, the conversion of HCHO (X_{HCHO}) was calculated from its IR peak area before and after the reaction. Therefore, the concentration of HCHO was calculated by dividing the total concentration of CO_2 and CO by the conversion of HCHO (Equation 43).

$$X_{HCHO} = \frac{[CO_2]_{out} + [CO]_{out}}{[HCHO]_{in}} \quad \Rightarrow \quad [HCHO]_{in} = \frac{[CO_2]_{out} + [CO]_{out}}{X_{HCHO}} \qquad (43)$$

Table 1. The corresponding concentration of HCHO in the total feed gas (100 mL.min^{-1}) as a function of He flow rate through trioxane diffusion cell

Flow rate (mL.min^{-1})	1.0	1.5	2.0	2.5
C_{HCHO} (ppm)	100	125	150	180

The concentration of HCHO in the feed gas resulting from the different flow rates of He through the diffusion cell is shown in Table 1. In principle, it increases following the increase of He flow rate but not linearly. As mentioned above, the stable concentration of HCHO will be achieved when the sublimation of solid trioxane balances with the flushing of He flow to the converter.

Effect of HCHO on NH_3-SCR. These tests were carried out by adding 100 – 180 ppm HCHO, 0.1 vol % NH_3, 0.1 vol % NO, 5 vol % O_2 balance He. The injection point of HCHO with the standard SCR feed gas was set up close to the reactor to restrict the side reaction of HCHO with the other components in the line. The reaction conditions (temperature, time of each step, gas detection) were kept the same as the normal SCR reaction. In addition, the conversion of HCHO and the formation of gas products from its reaction were measured by FT-IR spectrometer. The selectivity of products (CO, CO_2, HCN, and $(CH_2)_6N_4$) was calculated based on the reacted concentration of HCHO (Equations 44-47). The calibration of the concentration of HCHO, CO, CO_2, HCN, and $(CH_2)_6N_4$ by FT-IR measurement is shown in Figure A1.

$$S_{CO_2} = \frac{[CO_2]_{out}}{[HCHO]_{in} - [HCHO]_{out}} \cdot 100\% \quad (44)$$

$$S_{CO} = \frac{[CO]_{out}}{[HCHO]_{in} - [HCHO]_{out}} \cdot 100\% \quad (45)$$

$$S_{HCN} = \frac{[HCN]_{out}}{[HCHO]_{in} - [HCHO]_{out}} \cdot 100\% \quad (46)$$

$$S_{(CH_2)_6N_4} = \frac{6[(CH_2)_6N_4]_{out}}{[HCHO]_{in} - [HCHO]_{out}} \cdot 100\% \quad (47)$$

2.3.3 The presence of H_2O in NH_3-SCR reaction

Water vapor is always presenting in the exhaust gas since it is a fuel combustion product (Equation 48). Therefore, the SCR studies should always be taken in the presence of steam to approach the practical condition.

$$C_xH_yO_z + (x + \frac{y}{4} - \frac{z}{2})\ O_2 \rightarrow x\ CO_2 + \frac{y}{2} H_2O \qquad (48)$$

For dosing H_2O, a flask containing distilled water was surrounded by a water jacket heated up to 54 °C in which the saturated steam pressure at 54 °C is 112.5 mm Hg. The He flow for balance (Figure 22) was bubbled into the flask before mixing with the other flows. The volume percentage of water vapor in the feed gas was calculated by the equation below:

$$C_{H_2O} = \frac{f_1}{f_2} \cdot \frac{P_{H_2O}}{P_{atm}} \cdot 100\ \%$$

$$= \frac{55}{100} \cdot \frac{112.5}{758} \cdot 100\ \%$$

$$= 8.2\ (\%)$$

f_1 is the flow rate of the Helium flow flushing water vapor (55.00 mL.min^{-1})

f_2 is the flow rate of the feed gas (100.00 mL.min^{-1})

P_{H_2O} is the saturated steam pressure (112.5 mm Hg)

P_{atm} is the atmospheric pressure (758 mm Hg)

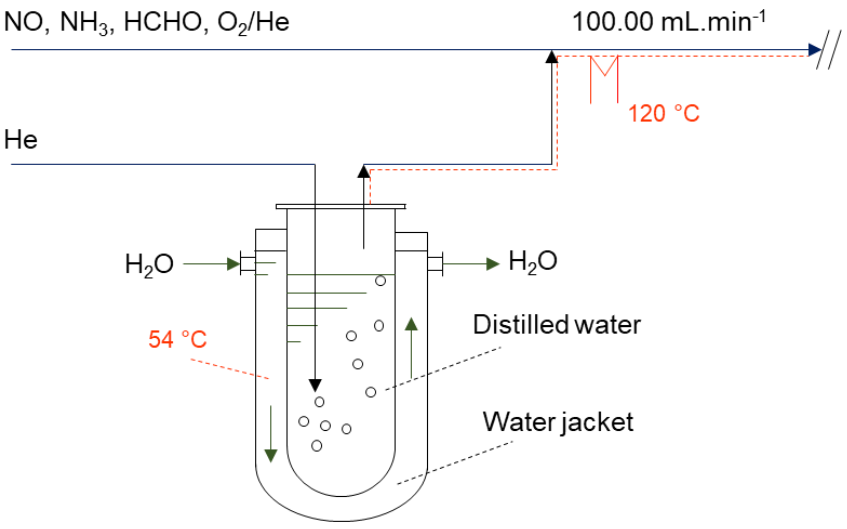

Figure 22. A scheme set up of the water evaporation for the experiments of the effect of the water

2.3.4 Oxidation of HCN under transient conditions

The oxidation of HCN over V_2O_5-WO_3/TiO_2 catalyst was carried out in temporal analysis of products (TAP-2) reactor. A resolution of about 100 µs was used for the time-resolved technique. A quadruple mass spectrometer (HAL RD 301 Hiden Analytical) at atomic mass units (AMU) was used to analyze the reaction products in the outlet. For each experiment, 41 mg of catalyst (particle size of 250-315 µm) was added between two layers of quartz particles within the isothermal zone of the quartz microreactor. The sample was pretreated by a flow 3 mL.min^{-1} of 100 % vol O_2 at 500 °C for 30 min. After that, two types of pulse experiments were carried out from 350 to 500 °C (50 °C/step).

The oxidation of HCN was first tested in the ability of lattice by pulsing a mixture of 10 vol % HCN/N_2. The test of HCN oxidation by adsorbed oxygen species was carried out by pulsing a flow of 30 vol % $^{18}O_2$/Ar then with 10 vol % HCN/N_2, a time delay of 0.5 s between two pulses. After that, the catalyst was treated in a flow of 3 mL.min^{-1} 100 % vol O_2 for 5 min to remove the ^{18}O species on the surface.

3. Results and discussion

3.1 Effects of HCHO on a commercial V_2O_5-WO_3/TiO_2 catalyst

3.1.1 Catalytic test

The elemental composition of the used commercial V_2O_5-WO_3/TiO_2 catalyst is shown in Table 2. The content of V and W is 1 wt. % and 6 wt. %, respectively. In addition, some other elements such as Na, Al, Si, etc., are also present, mainly for improving the surface area and thermal stability.

Table 2. Elemental composition of the commercial V_2O_5-WO_3/TiO_2 catalyst measured by ICP-OES

Element	V	W	Ti	Na	Al	Si	O & others
Content (wt. %)	1.01 %	6.22 %	44.46 %	0.06 %	1.52 %	3.85 %	42.88 %

The conversion of NO_x and NH_3 as well as, N_2 selectivity in the absence and in the presence of HCHO are shown in Figure 23. In the absence of HCHO, the commercial V_2O_5-WO_3/TiO_2 catalyst shows the highest activity above 250 °C (90 – 96 %), which declines again above 400 °C (Figure 23a, blue line). The decrease of NO_x conversion at high temperatures is due to the partial oxidation of NH_3 (Equations 49-50). Furthermore, the formation of N_2O from the oxidation of NH_3 at high temperature also leads to decreased N_2 selectivity above 400 °C (Figure 23c, blue line). This has also been confirmed by the reaction of 0.1 vol % NH_3, 5 vol % O_2/He over the commercial catalyst (Figure A2).

$$2\ NH_3 + 3/2\ O_2 \rightarrow N_2 + 3\ H_2O \qquad (49)$$

$$2\ NH_3 + 2\ O_2 \rightarrow N_2O + 3\ H_2O \qquad (50)$$

In the presence of 100 – 180 ppm HCHO, the conversion of NO_x drops (~ 10 – 18 %) in the whole temperature range (Figure 23a). Meanwhile, the NH_3 conversion is almost unchanged except for the slight decrease at 200 °C (Figure 23b). The selectivity of N_2 decreases in the whole temperature range, especially at low temperatures (Figure 23c). This suggests that HCHO prefers to react with NH_3, reducing the amount of NH_3 for SCR reaction and reducing NO_x conversion and N_2 selectivity. Besides, the strong decrease of N_2 selectivity from 150 to 200 °C suggests that the reaction of HCHO and NH_3 can even be strong at low temperatures.

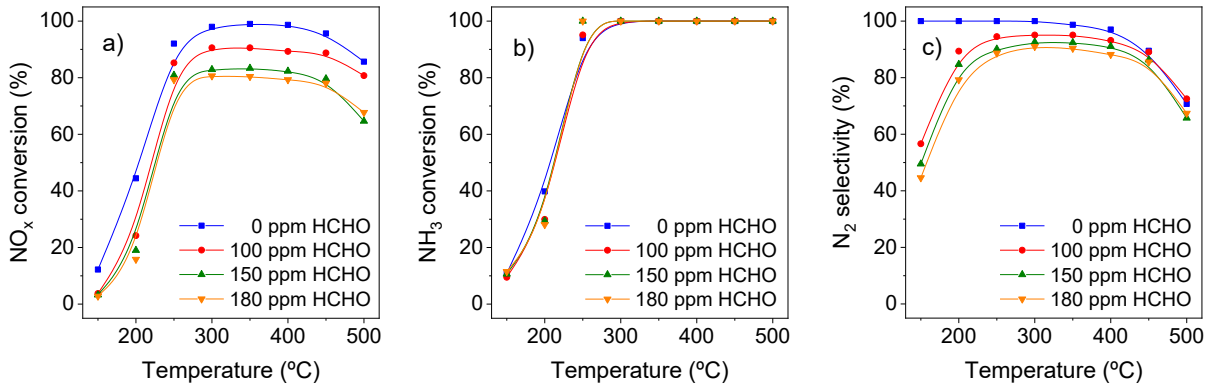

Figure 23. Conversion of NO_x, NH_3 and the selectivity of N_2 from the reaction of 0 – 180 ppm HCHO, 0.1 vol % NO, 0.1 vol % NH_3, 5 vol % O_2/He on commercial V_2O_5-WO_3/TiO_2 (1 wt, % V, 6 wt. % W) catalyst. Reproduced from ref. Ngo et al.[2]

HCHO is completely converted in all cases. Therefore its conversion curves are not added. The formation of products from the HCHO reaction in NH_3-SCR is shown in Figure 24. There are four main products detected from the HCHO reaction: HCN, CO_2, CO, and $(CH_2)_6N_4$. The selectivity of products depends on the temperature and does not change much when the concentration of HCHO increases from 100 to 180 ppm. In principle, HCN is the main product; its formation reaches the maximum in the range of 250 – 400 °C. CO_2 is significantly formed at temperatures higher than 400 °C, corresponding with the decline of HCN formation. Interestingly, a small maximum of CO_2 formation is found at 200 °C, which matches with the slight decrease of NH_3 conversion at 200 °C. It could be explained by the formation of $HCOONH_4$ on the surface of a catalyst, which further decomposes to CO_2 and NH_3. This will be discussed in the *in situ* FT-IR part later. CO is significantly formed in the range 250 – 400 °C in all cases of HCHO concentration. At temperatures below 200 °C, a small amount of hexamethylenetetramine (HMT) is formed. As mentioned above, this product comes from the gas phase reaction of HCHO and NH_3 (Equation 18, part 1.3.2). Surprisingly, the total selectivity of products below 250 °C does not add to 100 % in all cases, although no HCHO was detected in the outlet. This suggests that the interaction of HCHO forms an intermediate species on the surface of the catalyst, which does not decompose at low temperatures. This could be another negative effect of HCHO since such intermediate species may block the active sites of catalyst and could be the reason for the strong decrease of N_2 selectivity at low temperature (Figure 23c).

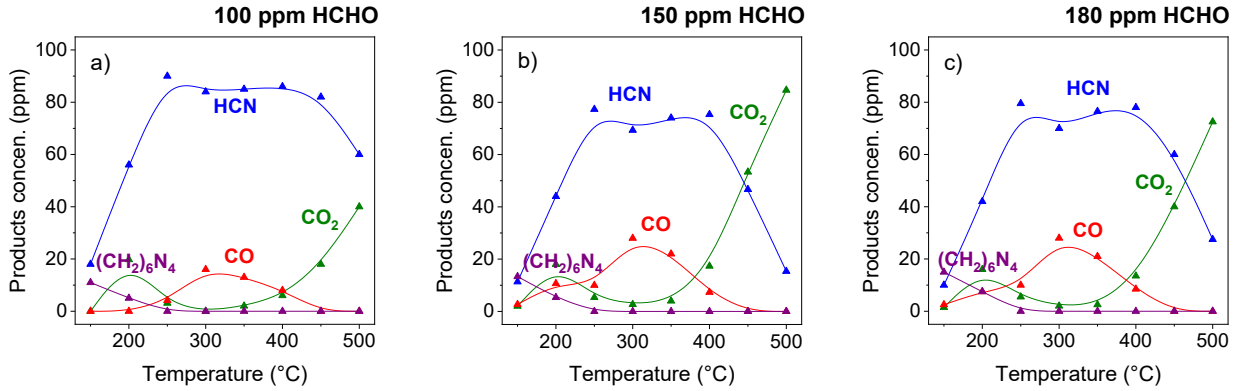

Figure 24. Conversion of HCHO (dash line) and the selectivity of products based on HCHO from reaction of 0 – 180 ppm HCHO, 0.1 vol % NO, 0.1 vol % NH_3, 5 vol % O_2/He on commercial V_2O_5-WO_3/TiO_2 catalyst. Reproduced from ref. Ngo et al.[2]

In the following, the role of each component of the SCR feed gas will be clarified by their separate reaction with HCHO. The oxidation of HCHO by O_2 was carried out by the reaction of 100 ppm HCHO in 5 vol % O_2/He. HCHO is completely oxidized by O_2 above 250 °C and forms CO as the main product (Figure 25). CO_2 is significantly formed above 350 °C due to the oxidation of CO.

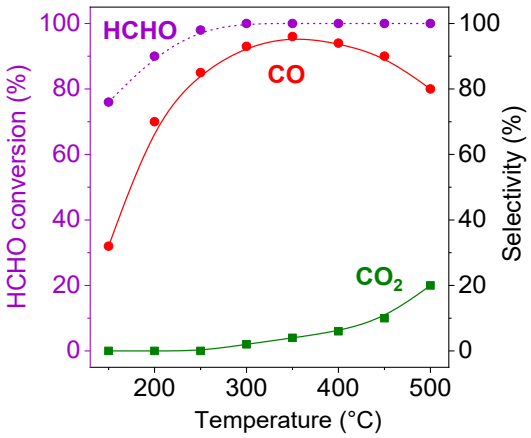

Figure 25. Conversion of HCHO and the formation of products from the reaction of 100 ppm HCHO, 5 vol % O_2/He on commercial catalyst V_2O_5-WO_3/TiO_2. Reproduced from ref. Ngo et al.[2]

Below 250 °C, only 75 – 90 % HCHO is converted, and interestingly, only 30 – 70 ppm CO is formed, lower than the reacted concentration of HCHO. It could be explained by the

uncompleted decomposition of formates formed on the surface of a catalyst, which will be shown in the *in situ* FT-IR part below (Figure 28). The reaction of HCHO in the full feed of NH_3-SCR (Figure 24) produces much less CO and much more CO_2 at high temperatures in comparison to its reaction with only O_2 (Figure 25). Therefore, the oxidation by O_2 is not the main pathway of the HCHO reaction in NH_3-SCR.

Conversion and formation of products from the reaction of 100 ppm HCHO, 0.1 vol % NO, 5 vol % O_2/He is shown in Figure 26. CO is still the main product, and its curve of selectivity is the same as in the reaction of HCHO/O_2. Meanwhile, no conversion of NO could be detected during the reaction. However, interestingly, different from the reaction with only O_2, a significant amount of CO_2 was formed below 250 °C, with the complete conversion of HCHO. This could be explained by the reaction of HCHO with NO_2 or nitrates which are created by the oxidation of NO, as mentioned in the part 1.3.2 (Equations 15-17). It has been confirmed by the experiments of 100 ppm HCHO, 100 ppm NO_2, 0.1 vol % O_2/He on the commercial V_2O_5-WO_3/TiO_2 catalyst at 150 °C (Figure A3a). NO_2 reacts with HCHO to form CO and CO_2, being itself reduced to NO. Meanwhile, when the feed of 100 ppm HCHO, 100 ppm NO, 0.1 vol % O_2/He was flushed over the catalyst, no direct reaction of HCHO and NO was found (Figure A3b).

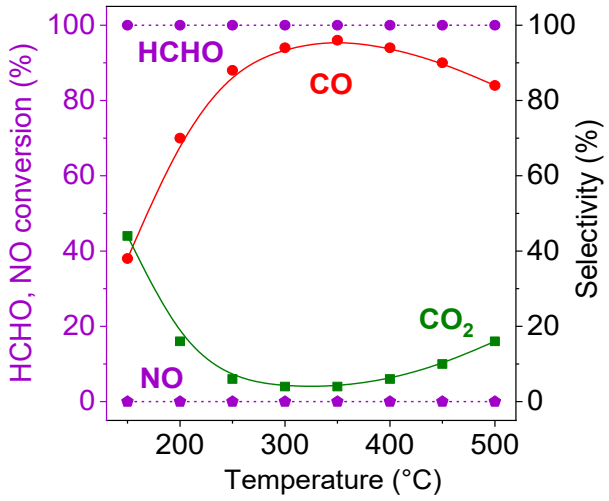

Figure 26. Conversion of HCHO and the formation of products from the reaction of 100 ppm HCHO, 0.1 vol % NO, 5 vol % O_2/He on commercial catalyst V_2O_5-WO_3/TiO_2. Reproduced from ref. Ngo et al.[2]

Even though HCHO completely reacted with NO/O_2, the formation of products from this reaction differs from the formation of products from HCHO reaction in NH_3-SCR (Figure 24). Besides, HCHO does not directly affect the total concentration of NO. Therefore, the interaction of HCHO with NO/O_2 is also not the main pathway of its reaction in NH_3-SCR.

Significant changes were found by the reaction of 100 ppm HCHO, 0.1 vol % NH_3, 5 vol % O_2/He. HCHO is completely converted in the whole temperature range, and the formation of gas products is the same as during its reaction in the full SCR feed gas (Figure 27). The conversion of NH_3 is approximately 10 % in the temperature range of 150 – 300 °C and strongly increases at higher temperature due to its oxidation by O_2 (Figure A2). In principle, HCN is the main product, accompanied by a significant formation of CO_2 above 400 °C and a small amount of $(CH_2)_6N_4$ below 200 °C. Interestingly, the small maximum in the formation of CO_2 at 200 °C is also found. These results strongly confirm the suggestion above that HCHO preferably reacts with NH_3 in the SCR reaction.

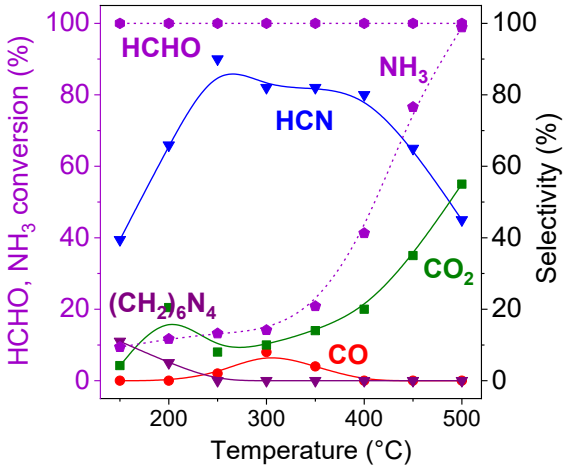

Figure 27. Conversion of HCHO and the formation of products from the reaction of 100 ppm HCHO, 0.1 vol % NH_3, 5 vol % O_2/He on commercial catalyst V_2O_5-WO_3/TiO_2. Reproduced from ref. Ngo et al.[2]

3.1.2 In situ FT-IR experiments

As discussed above, HCHO prefers to react with NH_3 in the NH_3-SCR. Therefore, analysis of the formation of intermediate species from the interaction of HCHO and NH_3 on the surface of

the catalyst is the key to explain its negative effects. The interaction of adsorbates resulting from the reaction of $HCHO/O_2$ with gaseous NH_3 on the commercial V_2O_5-WO_3/TiO_2 catalyst is shown in Figure 28. The catalyst was first exposed to 200 ppm HCHO and 5 vol % O_2/He in 60 min, followed by 30 min flushing in He to remove unstable species from the catalyst surface. An intense broad band around 1575 cm^{-1} of $\nu_{as}(COO^-)$ and a slightly weaker band at 1410 - 1350 cm^{-1} of $\nu_s(COO^-)$ + δ(CH) vibrations of formate species are found.[75] The formation of a large amount of formate on the surface of the catalyst explains the lower concentration of CO compared to the reacted concentration of HCHO in Figure 25. At low temperatures, HCHO is not totally converted to CO, but it partly retains on the surface of the catalyst in the form of adsorbed formates as the intermediate.

Subsequently, the catalyst was exposed to 0.1 vol % NH_3/He; the formate bands disappeared completely after 5 min (Figure 28). Simultaneously, the bands at 1686, 1600, and 1393 cm^{-1} raised, which could be assigned to the vibrations of ν(C=O), δ(NH_2), and δ(CH) of $HCONH_2$, respectively. The excess NH_3 adsorbed on Brønsted sites is reflected by the band at 1432 cm^{-1}.[76-77] A shoulder at 1721 cm^{-1} also raises during the exposure of NH_3. It could be assigned to the splitting from transverse optical symmetry of ν(C=O) to a longitudinal optical symmetry band of adsorbed formamide.[78-79]

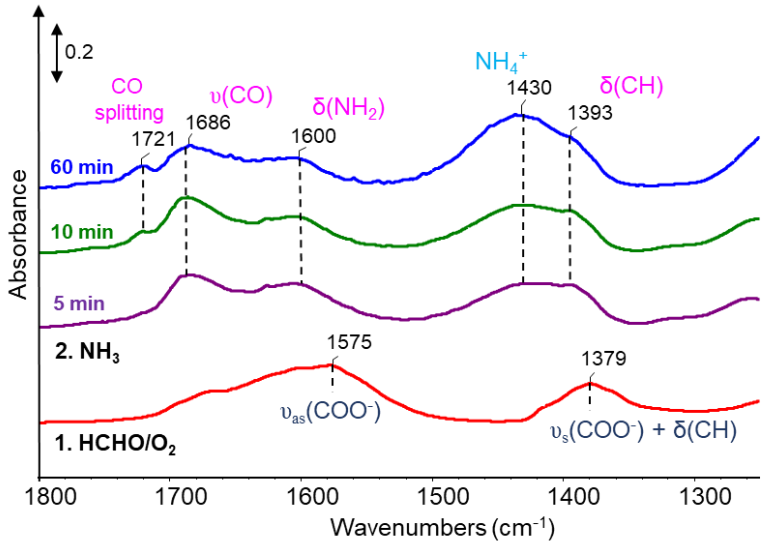

Figure 28. FTIR spectra of the commercial V_2O_5-WO_3/TiO_2 catalyst obtained after the pre-adsorption of $HCHO/O_2$ and subsequent exposure to NH_3 in a closed cell for 60 min. Reproduced from ref. Ngo et al.[2]

The FTIR spectra of the interaction of adsorbed NH_3 with gaseous $HCHO/O_2$ is shown in Figure 29. After 60 min exposure to 0.1 vol % NH_3/He, a strong band of NH_3 adsorbs on Brønsted sites at 1430 cm^{-1} is found (Figure 29).[76-77] The exposure to 200 ppm HCHO and 5 vol % O_2/He for 60 min leads to the decrease of the NH_4^+ band and the rise of the typical bands of $HCONH_2$ at 1676 cm^{-1}, 1588 cm^{-1}, 1390 cm^{-1}, and 1721 cm^{-1}.[80-81]

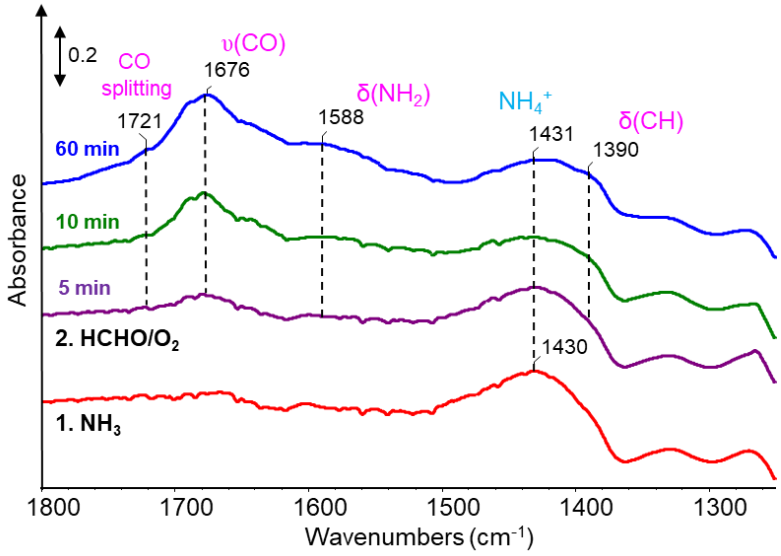

Figure 29. FTIR spectra of the commercial V_2O_5-WO_3/TiO_2 catalyst after pre-adsorption of NH_3 and subsequent exposure to $HCHO/O_2$ for 60 min in the closed cell. Reproduced from ref. Ngo et al.[2]

This shows that in any case, the interaction of HCHO and NH_3 forms $HCONH_2$ as the intermediate species, and this does not depend on the sequence of their adsorption, 1. $HCHO/O_2$, 2. NH_3 or vice versa. The formation of $HCONH_2$ matches with the work of Kröcher et al. and could be the explanation for the formation of HCN shown above.[65-66]

To prove the role of $HCONH_2$ for the reaction of HCHO in NH_3-SCR, the interaction of HCHO and NH_3 was performed in the presence of NO. The catalyst was first exposed to a flow of 0.1 vol % NH_3/He in 60 min and subsequently to a flow of 400 ppm HCHO, 0.2 vol % NO, 5 vol % O_2/He. Different from the exposure to $HCHO/O_2$, the band of NH_4^+ at 1429 cm^{-1} completely disappears after 60 min interaction with $NO/HCHO/O_2$ (Figure 30). This is due to the

reaction of NO with adsorbed NH_4^+ as in the standard SCR reaction. Typical bands of $HCONH_2$ were also found at 1673 cm^{-1}, 1600 cm^{-1}, and 1379 cm^{-1}. Bands at 1617 cm^{-1} and 1470 cm^{-1} can be assigned to the bridged nitrate and monodentate nitrate from the adsorption of excess NO, respectively.[82]

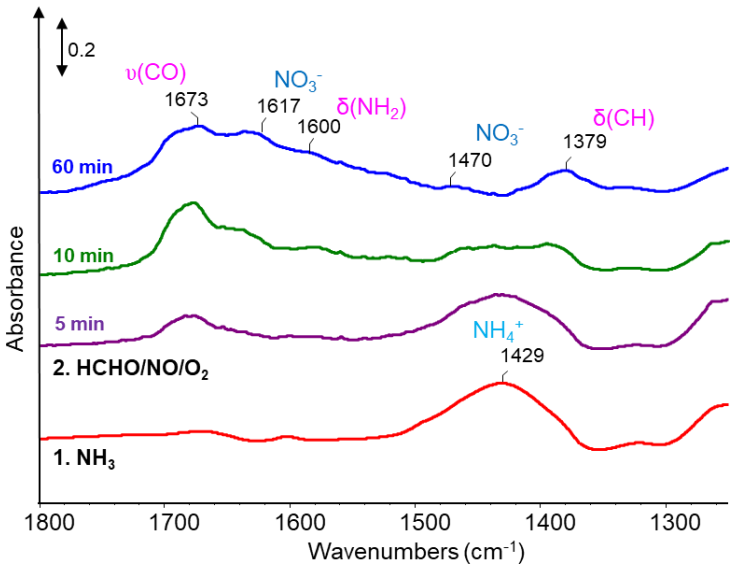

Figure 30. FTIR spectra of the commercial V_2O_5-WO_3/TiO_2 catalyst obtained after pre-adsorption of NH_3 and subsequent exposure to HCHO/NO/O_2 in the closed-cell for 60 min. Reproduced from ref. Ngo et al.[2]

In summary, the interaction of HCHO and NH_3 forms $HCONH_2$ on the surface of the commercial V_2O_5-WO_3/TiO_2 catalyst, and this reaction occurs independently from the reaction of NO and NH_3. This shows that the presence of HCHO in NH_3-SCR consumes a certain amount of NH_3, which is then no longer available for the reduction of NO_x, and the formation of $HCONH_2$ as a surface intermediate is a consequence of the reaction of HCHO and NH_3.

3.1.3 Reaction of $HCONH_2$ on the commercial V_2O_5-WO_3/TiO_2 catalyst

To prove the role of $HCONH_2$ for the formation of gas products from HCHO reactions, a flow of 300 ppm $HCONH_2$, 5 vol % O_2/He was directly flushed over the V_2O_5-WO_3/TiO_2 catalyst in the NH_3-SCR reactor. All the conditions of the reaction were kept the same as in the SCR reaction. The conversion and formation of products from this reaction are shown in Figure

31. $HCONH_2$ is converted completely above 250 °C and mainly formed HCN, CO, NH_3, N_2, and CO_2. Above 400 °C, trace amounts of NO and N_2O were also detected. The formation of products from the $HCONH_2$ reaction is based on two decomposition pathways (Equations 21-22):

$$HCONH_2 \rightarrow HCN + H_2O \quad (21)$$

$$HCONH_2 \rightarrow CO + NH_3 \quad (22)$$

The lower concentration of NH_3 than CO concentration is due to its partial oxidation on the catalyst, matching with the results plotted in Figure A2. HCN is formed in the whole temperature range, and its concentration is also higher than that of the other products. This confirms the role of $HCONH_2$ for the emission of HCN from the reaction of HCHO in NH_3-SCR and matches with the in situ FTIR results above. Like catalytic tests, CO_2 is significantly formed above 400 °C, and interestingly, a small maximum at 200 °C is also found. It could be explained by the hydration of $HCONH_2$ to form $HCOONH_4$, which further decomposes to form CO_2, NH_3, and H_2 (Equations 51-52).[83]

$$HCONH_2 + H_2O \rightarrow HCOONH_4 \quad (51)$$

$$HCOONH_4 \rightarrow CO_2 + NH_3 + H_2 \quad (52)$$

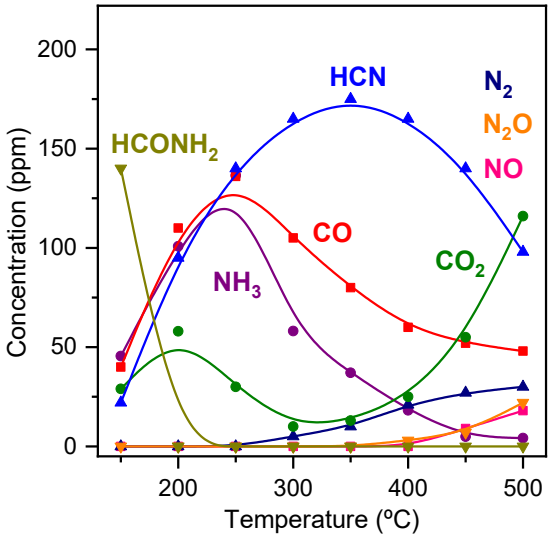

Figure 31. The reaction of 300 ppm $HCONH_2$, 5 vol % O_2 over the commercial V_2O_5-WO_3/TiO_2 catalyst. Reproduced from ref. Ngo et al.[2]

The emission of HCN from the HCHO reaction in NH_3-SCR is a matter of concern and should be restricted in any case. The results from catalytic tests and the reaction of $HCONH_2$ above have shown the decline of HCN at high temperatures and the simultaneous increase of CO_2 formation. This could be due to the oxidation of HCN on the commercial V_2O_5-WO_3/TiO_2 catalyst. This oxidation could be an interesting strategy to remove toxic HCN, which will be studied by the transient pulse experiments below.

3.1.4 The oxidation of HCN

The transient pulse experiments were performed in the TAP-2 reactor to analyze the oxidation of HCN. At first, only HCN was pulsed on the V_2O_5-WO_3/TiO_2 catalyst in the absence of O_2 between 350 – 500 °C. The result shows that HCN is oxidized by lattice oxygen above 400 °C to form CO_2 and NO (Figure 32a). The negligible emission of NO from 400 to 450 °C could be explained by its adsorption on the surface of the catalyst. At 500 °C, it could be seen clearly the decline of the HCN signal occurs simultaneously with the rise of the CO_2 and NO signals. The oxidation of HCN can be described by Equation 53 below:

$$2\ HCN + 7/2\ O_2 \rightarrow 2\ CO_2 + 2\ NO + H_2O \qquad (53)$$

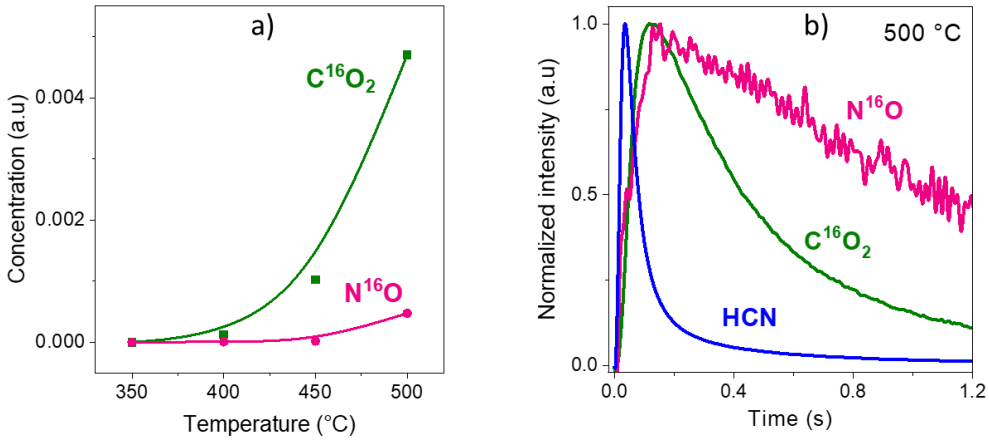

Figure 32. Oxidation of HCN in the absence of gas-phase O_2 over the VWT catalyst: a) temperature induced changes of the amount of $C^{16}O_2$ and $N^{16}O$ upon pulsing of HCN (10 vol% in N_2), b) normalized transient responses of HCN, $C^{16}O_2$, and $N^{16}O$ recorded at 500 °C. Reproduced from ref. Ngo et al.[2]

To check whether gaseous oxygen is also involved in HCN oxidation, the same pulse experiments were performed with $^{18}O_2$ and HCN. The same results are obtained as in the absence of gaseous $^{18}O_2$ and no $C^{18}O_2$ and $N^{18}O$ are detected (Figure A4). Hence, HCN can be oxidized by the lattice oxygen of the catalyst to form CO_2 and NO. The latter is involved in the standard SCR (Equation 7) reaction and it could be one more reason for the decrease of NH_3 concentration and the formation of N_2 above 300 °C in Figure 31.

$$4\,NO + 4\,NH_3 + 3\,O_2 \rightarrow 2\,N_2 + 6\,H_2O \qquad (7)$$

The pathway of HCHO reaction in NH_3-SCR on a commercial V_2O_5-WO_3/TiO_2 catalyst is summarized in Figure 33. Many negative effects of HCHO have been detected and are proved by its reaction with NH_3 to form $HCONH_2$ as the intermediate. The further decomposition of $HCONH_2$ leads to different gas products. Dehydration to HCN is the major pathway and its liberation is the matter of concern. HCN can be removed by the oxidation but this forms NO which must be efficiently reduced to N_2 in the SCR reaction.

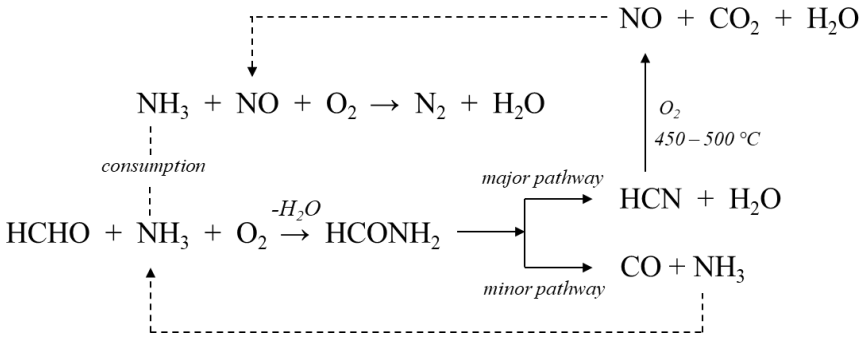

Figure 33. The pathway of the formation of gas products from the interaction of HCHO/O_2 with NH_3 on a commercial catalyst V_2O_5-WO_3/TiO_2. Reproduced from ref. Ngo et al.[2]

To explore explicitly, the role of vanadium and tungsten for the reaction of HCHO, V_2O_5-WO_3/TiO_2 catalysts with different compositions of vanadium and tungsten have been prepared and tested to identify the role of active sites for HCHO reaction. This could be the basis for developing catalysts able to restrict the negative effects of HCHO for the NH_3-SCR.

3.2 Effects of HCHO on different V_2O_5-WO_3/TiO_2 catalysts

3.2.1 Catalyst characterizations

The surface area, elemental composition, and the corresponding surface density of V and W are shown in Table 3. In principle, the impregnation of metal oxides on TiO_2 P25 does not change that much the surface area of the catalysts. The results from ICP-OES confirm that the elemental composition of prepared catalysts (W-Ti, V-Ti, and V-W-Ti) are the same as the used commercial catalyst (1 wt. % V, 6 wt. % W), which facilitates comparison with the results of the latter described above. The surface densities of V and W on the surface of TiO_2 support are calculated from the BET surface area and the elemental compositions. The total surface area of the catalyst is calculated according to Equation 54.

$$S_{total} = 10^{9.2} \cdot m_{catalyst} \cdot S_{BET} \quad (nm^2) \qquad (54)$$

S_{total} is the total surface area of catalyst (nm^2)

$m_{catalyst}$ is the weight of catalyst (g)

S_{BET} is the BET surface area of catalyst (m^2/g)

The total atoms of elements are calculated based on their composition from ICP-OES (Equation 55).

$$N_{element} = N_A \cdot \frac{\%m_{element} \cdot m_{catalyst}}{100 \cdot M_{element}} \quad (atoms) \qquad (55)$$

$N_{element}$ is the total number of atoms of the elements on a catalyst (atom)

N_A is the Avogadro number ($N_A = 6.022 \cdot 10^{23}$ mol^{-1})

$\%m_{element}$ is the mass percentage of elements from ICP-OES results (%)

$m_{catalyst}$ is the weight of catalyst (g)

$M_{element}$ is the molar mass of the elements (g/mol)

Assuming that vanadium oxides and tungsten oxides evenly disperse on the surface of a support, the surface densities ($S_{density}$) of these elements will be calculated by the division of the total number of elements with the total surface area of the catalyst (Equation 56).

$$S_{density} = \frac{N_{element}}{S_{total}} \quad (atoms/nm^2) \qquad (56)$$

The surface densities calculated can provide information about the possibility of the multilayer formation of metal oxides on the surface of a support. It shows that on W-Ti and V-Ti

catalyst, the coverage with VO_x respectively WO_x is still below that of a monolayer of VO_x (~ 7-8 V atoms/nm^2)[84-85] and WO_x on TiO_2 (~ 5 W atoms/nm^2).[86-87] The surface density of V and W on V-W-Ti catalyst are still below the monolayer coverage of both VO_x and WO_x. However, the presence of both VO_x and WO_x will increase the coverage density of metal oxides on the surface of a support. It can lead to the surrounding of the metal oxides by the others, which will be discussed more below. The results from powder XRD measurement show that only anatase and rutile TiO_2 could be detected (Figure A5). There are no crystalline V_2O_5 or WO_3 phases seen in all cases, corresponding with the results from the surface density calculated above.

Table 3. The indicators of the characterizations of vanadium-tungsten supported catalysts measured by ICP-OES, BET

Catalyst	BET *(m^2/g)*	V(ICP) *(%wt. V)*	W(ICP) *(%wt. W)*	Surface density (V atoms /nm^2)	Surface density (W atoms /nm^2)
Ti	52.9	_	_	_	_
W-Ti	55.2	_	6.26	_	3.71
V-Ti	49.5	1.13	_	2.70	_
V-W-Ti	48.7	1.14	6.24	2.76	4.20

The dispersion of vanadium and tungsten oxides on catalysts is also studied by *in situ* UV-Vis DRS characterization method. The local structures of vanadium and tungsten are often associated with the bands of the ligand-to-metal charge-transfer transitions, which are showed in the UV-Vis DRS spectra (Figure A6). However, many publications indicated that the E_g values calculated are more quantitative and informative for the local structures.[88-90] The correlation of the edge energy E_g with the average number of V-O-V bonds ($N_{V\text{-}O\text{-}V}$) and W-O-W bonds ($N_{W\text{-}O\text{-}W}$) has been proposed in previous studies (Equation 57-58).[91-93] These experimental formulas are built based on the relationship of E_g calculated and the polymerization degree of vanadium and tungsten on different samples. This relationship can be considered linear. Samples with a higher degree of polymerization of vanadium and tungsten oxide will display lower E_g values and vice versa. An average number higher than 1 indicates the formation of bonding chains of metal

oxides on the surface of a support. In contrast, the average number less than 1 point, mainly to the formation of single sites.

$$N_{V\text{-}O\text{-}V} = 14.03 - 3.95 \cdot E_g \quad (57)$$

$$N_{W\text{-}O\text{-}W} = 11.89 - 2.37 \cdot E_g \quad (58)$$

The E_g of W-Ti catalyst calculated from the Kubelka-Munk function and the Tauc's plot method is 3.47 eV (Figure 34a). According to Equation 54, the average number of W-O-W bonds is 3.7, indicating the formation of WO_x chains on the surface of a support. The edge energy calculated of the V-Ti catalyst is 3.48 eV (Figure 34b). Therefore, the average number calculated of V-O-V bonds according to Equation 57 is ~ 0.28. Hence, the dispersion of vanadium on the support of V-Ti catalyst mainly forms the single sites. It matches with the result of the surface density of VO_x calculated above; the surface density of VO_x is still quite far to reach to the VO_x monolayer on support. The E_g value calculated of V-W-Ti is 3.42 eV, not much different compare to V-Ti and W-Ti catalyst. Therefore, the formation of VO_x chains and WO_x chains on V-W-Ti is not significantly different. The coverage of both metal oxides on support will lead to the surrounding of a metal oxide by the other one. This could affect to the catalytic characterizations such as surface acidity and the symmetry of vanadium ions, which will also be discussed by the other characterization methods below.

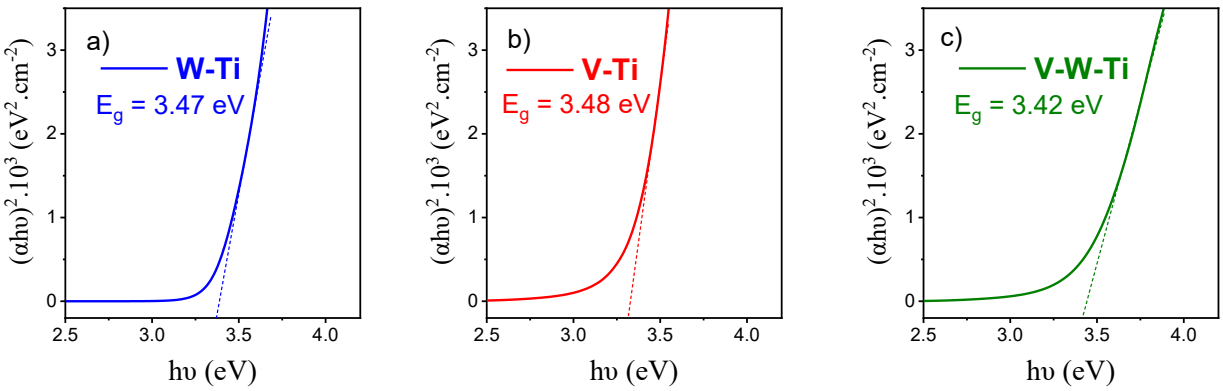

Figure 34. The edge energy of catalysts calculated from the UV-Vis DRS spectra using Kubelka-Munk function

The surface acidity of catalysts was studied by FTIR spectra using pyridine adsorption (Figure 35). The corresponding quantities of Brønsted and Lewis acid sites are shown in Table 4.

The bare support TiO_2 P25 has only Lewis acid sites. The Brønsted acid sites only present when vanadium and tungsten were introduced. The coverage of VO_x and WO_x leads to the decrease of Lewis acid sites of TiO_2, which is also indicated by a slight shift of the bands above 1600 cm^{-1} of TiO_2 to the higher wavenumbers.[76] The higher amount of Brønsted sites and stronger decrease of Lewis sites on W-Ti catalyst is due to the higher surface density of WO_x (3.71 atoms/nm^2) compare to VO_x (2.7 atom/nm^2) on support.

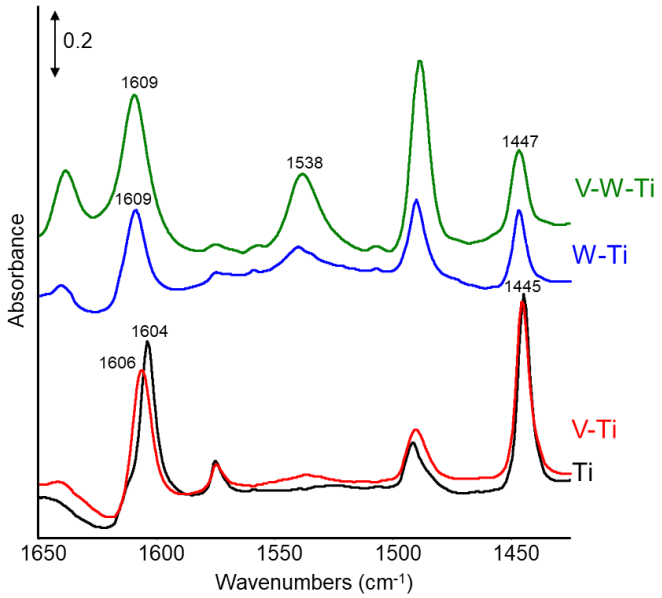

Figure 35. FT-IR spectra at 150 °C of the pyridine adsorption on vanadium-tungsten supported catalysts and the bare support TiO_2 P25

Table 4. The relative intensity of Brønsted sites (integration of the band at 1538 cm^{-1}) and Lewis sites (integration of the band at 1445 cm^{-1})

Catalyst	Ti	W-Ti	V-Ti	V-W-Ti
Brønsted site	0.00	0.74	0.25	3.33
Lewis site	3.85	1.50	3.67	1.78

Interestingly, the V-W-Ti catalyst creates the highest amount of Brønsted sites and even more than the sum of Brønsted sites from the W-Ti and V-Ti catalyst. In addition, the band of Lewis sites on the V-W-Ti catalyst shifts from 1445 cm^{-1} to 1447 cm^{-1}, and the total amount of

Lewis sites on V-W-Ti is also higher than the W-Ti catalyst. It has been studied that the amount of Lewis sites on vanadium is negligible.[18] Therefore, the changes are due to the effect of the synergistic of vanadium and tungsten on the surface of V-W-Ti. This might come from the surrounding of the metal oxide by the other one, as discussed above.

The *in situ* Raman spectra of catalysts after removing the surface water are shown in Figure 36. For the W-Ti catalyst, the broadband from 1001 - 1018 cm^{-1} could be ascribed to the vibration of W=O of both mono-tungstates and surface WO_5/WO_6 poly-tungstates, matching with the formation of W-O-W moieties as suggested by the result of in situ UV-Vis DRS investigations above.[86, 94] On V-Ti catalyst, the band of anatase TiO_2 at 795 cm^{-1} is seen clearly due to the uncompleted coverage of VO_x on the surface. Broadband at 1032 cm^{-1} has been assigned to V=O bonds of VO_x species on the support.[94-95] Therefore, also considering the edge energy result from the UV-vis spectra (Figure 34), both single sites and oligomers of vanadium oxide might exist on the surface of the TiO_2 support, which has also been confirmed by the *in situ* EPR results described in part 3.2.4 below.

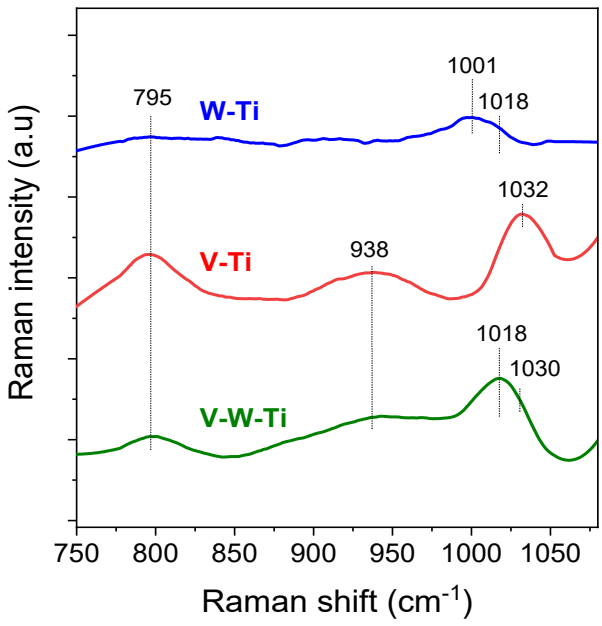

Figure 36. *In situ* Raman spectra of the catalyst after pretreatment by synthetic air at 300 °C in 1 h and cooling down to room temperature for measurement (for W-Ti is 300 °C)

The bridging V-O-V bonds are seen clearly by the broadband around 938 cm^{-1}. On the V-W-Ti catalyst, the band of V-O-V bonds at 938 cm^{-1} is broader and weaker. It may point to a partial cleavage of V-O-V bonds by WO_x species, as it was found previously by Kompio et al.[96] This goes along with a shift of the V=O vibration from 1030 to 1018 cm^{-1}, to which the W=O vibration may also contribute (compare the blue spectrum of W-Ti in Figure 36). The shift of the V=O band in catalyst V-W-Ti could be explained by the intimate mixing of WO_x and VO_x on the surface.[96] On the V-W-Ti catalyst, the surface dispersion of VO_x seems not to be much different from that of the V-Ti catalyst, but on the former, VO_x may be surrounded by WO_x species, creating V-O-W bonds. This could affect the catalytic performance, which will be discussed in more detail in the *in situ* EPR part 3.2.4 later.

The reducibility of the catalysts analyzed by TPR is shown in Figure 37. The W-Ti catalyst shows a broad peak of H_2 consumption from 400 °C to 723 °C, resulting from the reduction of sulfate present in commercial TiO_2 P25, on which a sharp peak at 723 °C from the reduction of W^{6+} to W^{4+} is superimposed.[96] The V-Ti catalyst shows the maximum of H_2 consumption at 434 °C from the reduction of V^{5+} to V^{3+}. The less pronounce of the broad peak from 400 °C to 723 °C compare to the W-Ti catalyst is due to the co-reduction of vanadium and sulfate.[96]

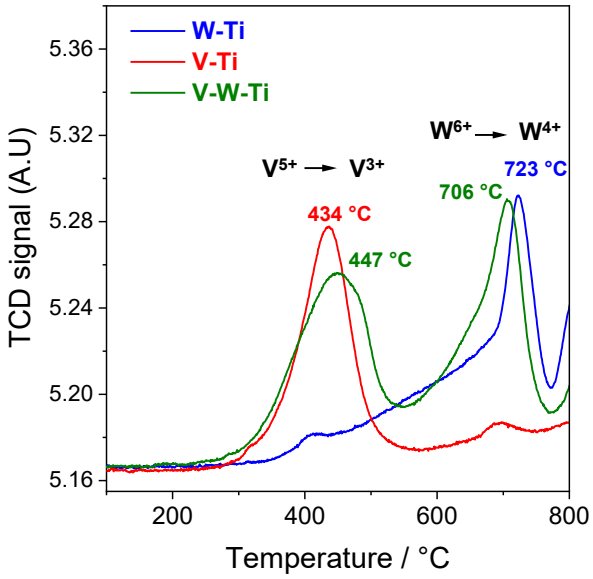

Figure 37. Temperature program reduction of W-Ti, V-Ti, and V-W-Ti catalysts

On the V-W-Ti catalyst, the reduction of V^{5+} to V^{3+} is delayed to the maximum H_2 consumption at 447 °C, the reduction of W^{6+} to W^{4+} was shifted from 723 °C to 706 °C. The reducibility of vanadium species on V-W-Ti is not better than on V-Ti in H_2 as the reducing agent. However, the shift of the H_2 consumption peaks indicates the change of the surface structure when both VO_x and WO_x present on the surface compared to the presence of only one oxide species. Combining with the results of pyridine adsorption and Raman results above, the change of the V-W-Ti catalyst's reducibility might come from the formation of V-O-W bonds, created by the surrounding of VO_x by WO_x species.[97]

In short summary, by several characterization methods, the dispersion and morphology of vanadia-tungsta supported catalysts have been studied in detail. No crystalline of V_2O_5 and WO_3 was formed, vanadia and tungsta are dispersed on the TiO_2 support as amorphous species. At the low loading content of vanadium (1 wt. % V), there is not much difference between the dispersion of vanadia on the V-Ti and V-W-Ti catalysts. Vanadia is dispersed on titania and tungsta both as single sites and clusters. The difference of the V-W-Ti catalyst is the surrounding of vanadia by tungsta, which creates a lot of Brønsted sites and V-O-W bonds, which might be the decisive factor for catalytic performance in the SCR reaction and the reaction of HCHO.

3.2.2 Catalytic test

The changes of NO_x, NH_3 conversion, and the formation of products from standard SCR reaction (N_2 and N_2O) are plotted in Figure 38. In this case, it would be more beneficial to plot N_2 directly and N_2O concentrations to observe the effect of HCHO on product formation from standard SCR reactions since the formation of N_2O on vanadium supported catalyst and vanadium-free catalyst is very different. In addition, a part of NH_3 will react with HCHO to form different amounts of HCN on different catalysts. Therefore, plotting N_2 selectivity will be challenging to explain and link the results together.

In the absence of HCHO, the NO_x conversion on W-Ti catalyst reaches its maximum from 350 – 400 °C and declines again at the higher temperature (Figure 38a, dashed pink line). The conversion of NH_3 is quite like the NO_x conversion below 350 °C but increases at a higher temperature and reaches 100 % above 400 °C (Figure 38a, dashed blue line). It could be explained by the partial oxidation of NH_3 at high temperature (Figure A7a), the same as the

results of the commercial V_2O_5-WO_3/TiO_2 catalyst (Figure A2). N_2 was the main product of the SCR reaction on W-Ti catalyst; a small amount of N_2O was only formed in the range of 300 – 400 °C (Figure 38a, dashed orange line). The decrease of N_2 concentration above 400 °C is due to the limited reduction of NO_x by NH_3. NH_3 is oxidized completely, but the formation of N_2 from its oxidation is only half of the same NH_3 amount that reacts with NO_x. In the presence of HCHO, generally, the conversion of NO_x and NH_3 on W-Ti catalyst does not change that much. However, NO_x conversion decreases above 450 °C. This might be related to the oxidation of HCN, which will be described in more detail in Figure 39a below. Corresponding with the insignificant change of NO_x and NH_3 conversion, the formation of N_2 and N_2O is almost unchanged in the presence of HCHO.

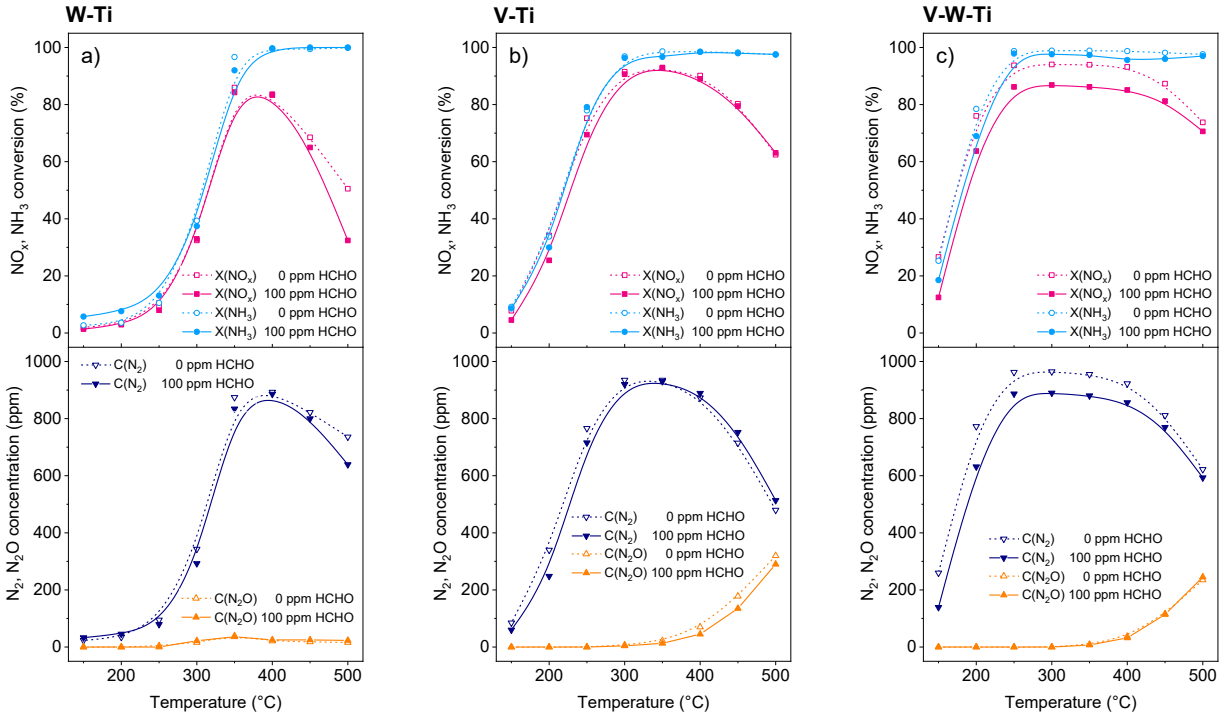

Figure 38. The conversion of NH_3 and NO_x , and the formation of N_2 and N_2O in the absence (dash line) and in the presence of 100 ppm HCHO (solid line) from reaction of 0-100 ppm HCHO, 0.1 vol % NH_3, 0.1 vol % NO, 5 vol % O_2/He on a) W-Ti, b) V-Ti, c) V-W-Ti catalysts

In the absence of HCHO, the conversion of NO_x on V-Ti catalyst reaches its maximum in the range of 300 – 400 °C and declines again at the higher temperature (Figure 38b, dashed pink line). Compare to the W-Ti catalyst, V-Ti shows much better activity in the whole temperature

range, especially at low temperatures. For example, at 250 °C, only 6 % NO_x is reduced, while on V-Ti catalyst, it is 72 %. This is clearly since vanadium is the main active site for SCR reaction, and tungsten plays the promoter's role. The conversion of NH_3 is quite similar to NO_x conversion and reaches 100 % above 300 °C. Similar to the other catalysts, the difference of NH_3 and NO_x conversion could be explained by the partial oxidation of NH_3 at high temperature (Figure A7b). N_2 is the main product, but a significant amount of N_2O was formed above 400 °C. This indicates that vanadium is the main factor for the formation of N_2O in NH_3-SCR. In the presence of 100 ppm HCHO, the NO_x and NH_3 conversion on the V-Ti catalyst does not change that much. The NO_x conversion only slightly decreases (~ 5%) below 300 °C. Corresponding with the insignificant change of the NO_x and NH_3 conversion, the formation of N_2 and N_2O on the V-Ti catalyst is also almost unchanged. Only slightly can be observed is the slightly decrease of N_2O formation (~ 20 ppm) at a temperature higher than 400 °C and the slight decrease of N_2 concentration (~ 30 ppm) below 300 °C.

The efficiency of the V-W-Ti catalyst is shown in Figure 38c. For the standard SCR reaction, V-W-Ti shows the highest activity in the whole temperature range. For instance, at 250 °C, the conversion of NO_x reaches 78 % on the V-W-Ti catalyst compared to only 32 % on the V-Ti catalyst. The conversion of NO_x on V-W-Ti catalyst reaches its maximum in the range of 250 – 450 °C (up to 92 %) and declines above 450 °C due to the partial oxidation of NH_3 (Figure 38c, dashed pink line). However, compare to W-Ti and V-Ti catalyst, the gap between NH_3 conversion and NO_x on V-W-Ti catalyst at high temperature is narrower. N_2 is still the main product, and N_2O is also formed at high temperatures. Therefore, the promotion effect of tungsten increases the SCR activity but does not change the formation of N_2O on vanadium sites at high temperatures. In the presence of HCHO, the NO_x conversion on the V-W-Ti catalyst decreases approximately 10 % in the whole temperature range, very similar to the commercial catalyst. The conversion of NH_3 is almost unchanged, suggesting that HCHO also prefers to react with NH_3, reduces the NH_3 amount for SCR reaction, and leads to the reduction of the NO_x conversion. Due to the decrease of the NO_x conversion, the concentration of N_2 also decreases in the whole temperature range. Meanwhile, the formation of N_2O is almost unchanged in the presence of HCHO.

The formation of products from the HCHO reaction is shown in Figure 39. HCHO is completely converted in all cases, so its conversion curves are not added. Generally, the reaction

of HCHO in NH_3-SCR forms HCN, CO_2, and CO. Different from the commercial catalyst, the formation of $(CH_2)_4N_6$ is too low to be detected.

The formation of products from HCHO reaction on W-Ti catalyst is shown in Figure 39a. HCN and CO_2 are the main products, and no CO was detected. The formation of HCN reaches its maximum at 300 °C and decreases at high temperatures. The concentration of CO_2 increases at high temperatures and up to 100 ppm above 450 °C. As proved in part 3.1.4, these could result from the HCN oxidation on W-Ti catalyst at high temperature to form CO_2 and NO (Equation 53). This result also explains the reduction of NO_x conversion on W-Ti catalyst above 400 °C in Figure 38a.

Interestingly, the total concentration of products below 250 °C does not add to 100 %. This is due to the formation of intermediate species on the surface of the catalyst, which does not completely decompose at low temperatures. The formation of intermediate species will be shown in part 3.2.3 below.

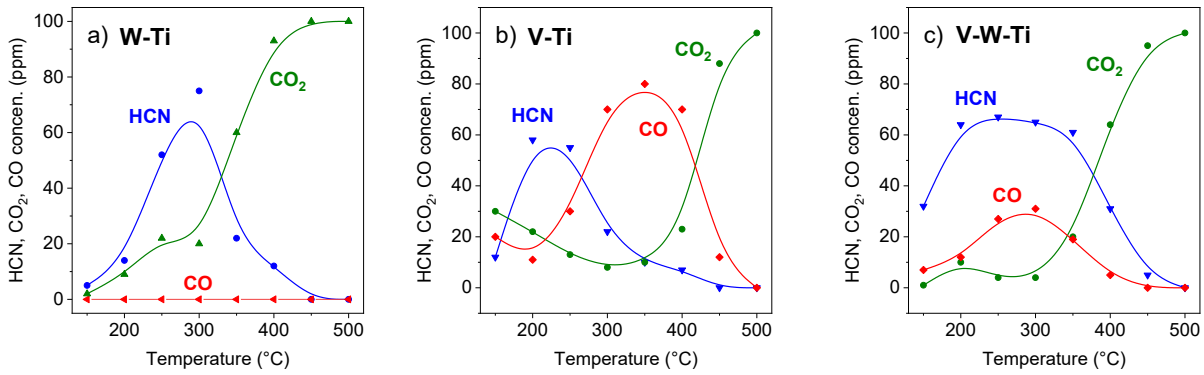

Figure 39. The formation of products of HCHO from the reaction of 100 ppm HCHO, 0.1 vol % NH_3, 5 vol % O_2/He on W-Ti, V-Ti, and V-W-Ti catalysts

The formation of products from HCHO reaction in NH_3-SCR on V-Ti catalyst is shown in Figure 39b. Different from the W-Ti catalyst, a lot of CO is formed on the V-Ti catalyst. The formation of products depends on the temperature of the reaction. In principle, HCN is mainly formed in the range of 150 – 250 °C, CO is formed primarily in the range of 250 – 400 °C and CO_2 is mainly formed above 400 °C. Below 250 °C, the total concentration of products still does not add to 100 ppm, but higher compared to W-Ti catalyst.

The formation of products from the reaction of HCHO on V-W-Ti catalyst is shown in Figure 39c. Like V-Ti catalyst, HCN, CO, and CO_2 are the main products, but the curves of its concentration based on temperature ranges are different. CO_2 is also the main product at a high temperature, which might come from the oxidation of HCN. The formation of CO on V-W-Ti catalyst is less than on V-Ti catalyst, and in return, more HCN is formed. The total concentration of CO, CO_2, and HCN below 200 °C is still less than 100 ppm but not that much. This result indicates that the decomposition of the intermediate species on V-W-Ti is better than on V-Ti and W-Ti catalyst.

In short summary, the effect of HCHO on NH_3-SCR of NO_x is different on different catalysts. The V-W-Ti catalyst shows the highest SCR activity and is affected by HCHO the most. In the presence of HCHO, the conversion of NO_x on V-W-Ti catalyst decreases in the whole temperature range, and HCN is formed the most. It has been proved above that the negative effects of HCHO on commercial V_2O_5-WO_3/TiO_2 catalyst come from its reaction with NH_3. Hence, the reaction of 100 ppm HCHO, 0.1 vol % NH_3, 5 vol % O_2/He will also be carried out on these catalysts.

Conversion of NH_3 and the formation of products from the reaction of HCHO/NH_3/O_2 on catalysts are shown in Figure 40. HCHO was converted in all cases, so its conversion is not plotted. The conversion of NH_3 substantially increases at high temperatures due to its oxidation which has been confirmed its a separate reaction with only O_2 (Figure A7). The oxidation capacity of the catalysts is also demonstrated in this reaction. V-W-Ti shows the highest conversion of NH_3, and W-Ti catalyst shows the lowest, as the sequence of their SCR activity (Figure 38).

The formation of products from the reaction of HCHO/NH_3/O_2 on W-Ti is shown in Figure 40b. The liberation of CO_2 and HCN, in this case, is the same as the reaction of HCHO in NH_3-SCR (Figure 39a). N_2 is the main product of NH_3 oxidation, and the formation of N_2O is negligible. This confirms that the formation of N_2O is not facilitated by tungsten.

On the V-Ti catalyst, the oxidation of NH_3 forms a large amount of N_2O at high temperatures, confirming the role of vanadium in its formation in NH_3-SCR. CO_2, HCN, and CO are the main products of the HCHO reaction. The increase of CO_2 and the decline of HCN at high temperatures are due to the oxidation of HCN, which has been proved above. Interestingly,

the formation of CO in this reaction (Figure 40c) is much less in comparison to the reaction of HCHO in NH_3-SCR (Figure 39b). This could be explained by the formation of nitrate species on the surface of catalyst from NO, which then oxidized HCHO to form CO as tested from the commercial catalyst (Figure A3).

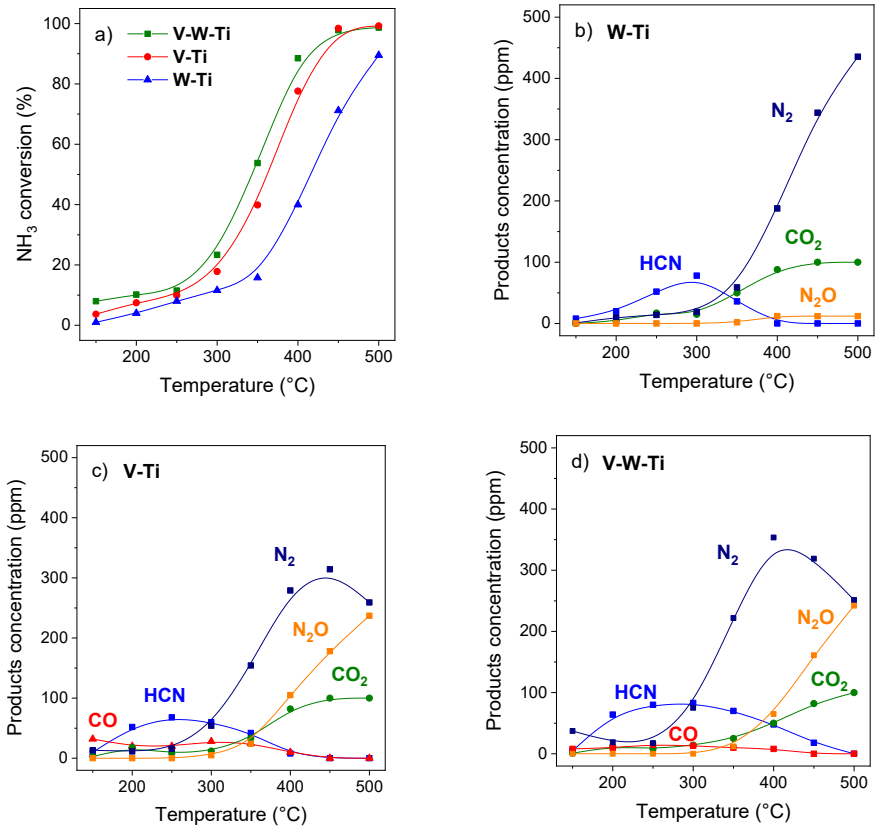

Figure 40. a) Conversion NH_3, and the formation of products from the reaction of 100 ppm HCHO, 0.1 vol % NH_3, 5 vol % O_2/He on b) W-Ti, c) V-Ti, and d) V-W-Ti catalysts

On the V-W-Ti catalyst, the oxidation of NH_3 is like that of the V-Ti catalyst, N_2 is the main product, but it is suppressed by the formation of N_2O at high temperature. The formation of CO_2 and HCN from HCHO in this case (Figure 40d) is similar to the reaction of HCHO in the full feed of NH_3-SCR (Figure 39c). However, the formation of CO, in this case, is also less than in the reaction of HCHO in NH_3-SCR. Same as on V-Ti catalyst, it could be explained by the effect of NO, it can create nitrates on the surface, which then oxidizes HCHO to from CO.

Therefore, same as the commercial catalyst, the effects of HCHO on V_2O_5-WO_3/TiO_2 prepared catalysts above are also determined by its reaction with NH_3. However, the performance is not the same on these catalysts. The best V-W-Ti catalyst is more affected than the others. The formation of the intermediate species on the surface of catalysts could explain these differences, and it will be studied by *in situ* FT-IR experiments below.

3.2.3 In situ FT-IR experiments

On commercial V_2O_5-WO_3/TiO_2, it has been demonstrated that the formation of $HCONH_2$ does not depend on the sequence of the adsorption – the reaction of HCHO and NH_3. Either HCHO reacts with the adsorbates of NH_3 ($NH_{3\ ads}$, $NH_4^+{}_{ads}$) or NH_3 reacts with the adsorbates of HCHO (formates) to form $HCONH_2$. However, the oxidation of HCHO on the prepared catalysts is not the same as the catalytic test (Figure 41a). At 150 °C, HCHO has completely oxidized on V-Ti and V-W-Ti catalyst, but only 30 % of total HCHO is reacted on W-Ti catalyst. The gap between the total concentration of CO and CO_2 and the reacted concentration of HCHO is due to the formation of the intermediate species on the surface of catalysts (Figure 41b).

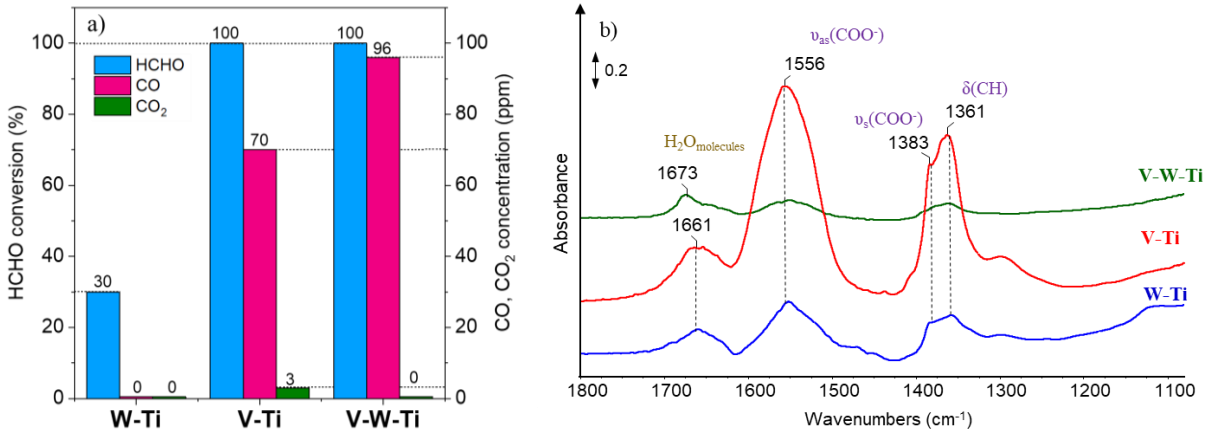

Figure 41. a) The conversion and formation of gas products from reaction of 100 ppm HCHO, 5 vol % O_2/He on W-Ti, V-Ti and V-W-Ti catalyst at 150 °C, b) FT-IR spectra of the adsorption of 200 ppm HCHO, 5 vol % O_2/He on W-Ti, V-Ti and V-W-Ti catalysts at 150 °C

On the V-W-Ti catalyst, HCHO is almost completely converted to CO, and the remaining adsorbates on the surface of the catalyst are not much. The band at 1673 cm^{-1} could be ascribed for the vibration of an adsorbed water molecule.[98] On W-Ti and V-Ti catalyst, the typical bands

of formate at 1361 cm^{-1} of δ(CH), 1383 cm^{-1} of $\upsilon_s(COO^-)$, and 1556 cm^{-1} of $\upsilon_{as}(COO^-)$ are seen clearly.[75, 99] The shoulder at 1661 cm^{-1} is ascribed for the adsorbed water molecules on the surface of catalysts generated from the oxidation of HCHO.[98]

Therefore, the number of intermediate species remaining on the surface of W-Ti, V-Ti, and V-W-Ti catalysts are completely dissimilar. This would make it very difficult to compare the differences in the formation of intermediate species on the surface of catalysts when NH_3 is subsequently exposed. On the other hand, the interaction of NH_3 with the adsorbates of $HCHO/O_2$ and the interaction of $HCHO/O_2$ with the adsorbent of NH_3 both yield the same result. Therefore, only the *in situ* FTIR spectra recorded upon the interaction of $HCHO/O_2$ with preabsorbed NH_3 are discussed below. The oxidation of NH_3 on the above catalysts at 150 °C has been shown to be negligible (Figure A7).

Interaction of $HCHO/O_2$ with the pre-adsorbates of NH_3 on bare support TiO_2 P25 is shown in Figure 42. On the bare support TiO_2, NH_3 adsorbs only on Lewis sites (the bands at 1170 and 1594 cm^{-1} of the coordinated NH_3 on Lewis sites).[100-101] No band of NH_3 adsorption on Brønsted acid sites (NH_4^+) is formed, corresponding with the result of the pyridine adsorption (Figure 35, Table 4).

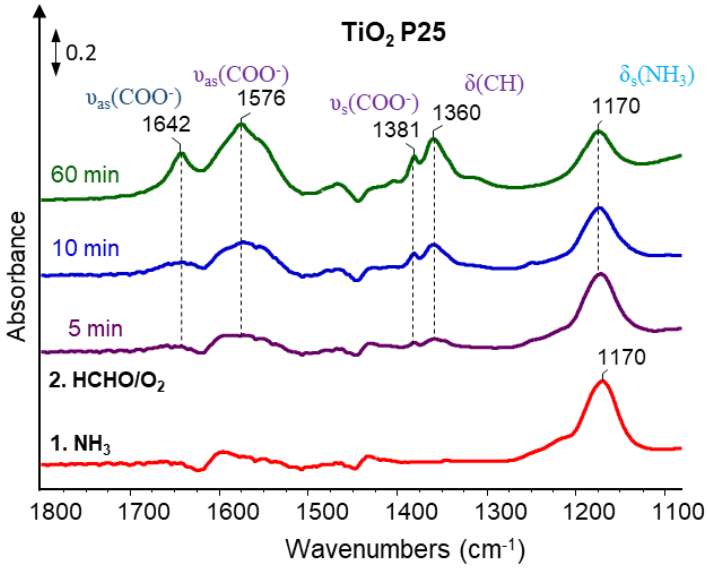

Figure 42. FT-IR spectra of the interaction of $HCHO/O_2$ with the adsorbate species of NH_3 on bare support TiO_2 P25

The exposure of $HCHO/O_2$ leads to the rise up of the bands at 1576 cm^{-1}, 1381 cm^{-1}, and 1360 cm^{-1}, which could be ascribed for $\upsilon_{as}(COO^-)$, $\upsilon_s(COO^-)$ and $\delta(CH)$ of bidentate formate, respectively.[75, 99] Band at 1642 cm^{-1} is ascribed for the $\upsilon_{as}(COO^-)$ of the surface monodentate formate with asymmetric coordination of the COO^- group.[102] No formamide is formed. The slight decrease in the band intensity of pre-adsorbed NH_3 (1170 cm^{-1}) can be explained by replacing the NH_3 adsorbate on the TiO_2 surface with formate.

On the W-Ti catalyst, NH_3 adsorbs on both Brønsted (1445 cm^{-1}) and Lewis acid sites (1223 cm^{-1}) (Figure 43, red line). A band at 1170 cm^{-1} of the Lewis site on TiO_2 is not found, indicating that the surface of bare support is almost completely covered by tungsten. The exposure of $HCHO/O_2$ leads to the decrease of both bands of NH_4^+ and adsorbed NH_3 at 1445 cm^{-1} and 1225 cm^{-1}, respectively. Simultaneously, the typical bands of formate at 1574 cm^{-1}, 1381 cm^{-1}, and 1362 cm^{-1} are also found. However, compare to the formation of formate on bare support TiO_2, it is much less. Differently, formamide is formed as indicated by its typical bands of $\upsilon(CO)$ at 1672 cm^{-1} and $\delta(NH_2)$ at 1634 cm^{-1} (Figure 43).[80-81]

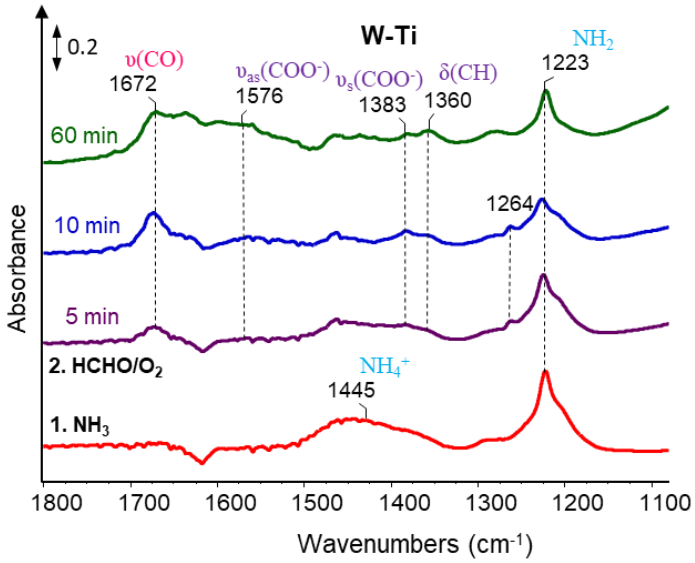

Figure 43. FT-IR spectra of the interaction of $HCHO/O_2$ with the adsorbate species of NH_3 on bare support W-Ti catalyst

The formation of $HCONH_2$ on W-Ti catalyst occurs on both Brønsted and Lewis acid sites, but it seems that the reaction on Brønsted acid sites was more substantial than on Lewis sites.

After 60 min exposure with $HCHO/O_2$, the band of NH_4^+ at 1445 cm^{-1} completely disappears, but the amount of $NH_{3\ ads}$ on Lewis sites remains. Possibly, the Lewis sites do not involve the formation of $HCONH_2$ in this case. The slight decrease of the band at 1170 cm^{-1} is due to the replacement of formates, same as on bare support TiO_2 P25. The formation of formates and $HCONH_2$ simultaneously occurs. Therefore, the more acid sites created on the catalyst surface, the more formation of $HCONH_2$. And vice versa, when the amount of NH_3 adsorbates on metal oxides is not large enough, HCHO will interact with the lattice oxygen of TiO_2 to create formates.

A similar result is also found on the V-Ti catalyst, NH_3 adsorb on V-Ti catalyst on both Brønsted sites (1425 cm^{-1}) and Lewis sites (1189 cm^{-1}) (Figure 44, red line). Since the vanadium content on TiO_2 is not large enough to cover the entire surface of the support, the shift acid band from 1170 cm^{-1} to 1189 cm^{-1} could be ascribed for the mixing effect of vanadium support TiO_2 on Lewis sites.

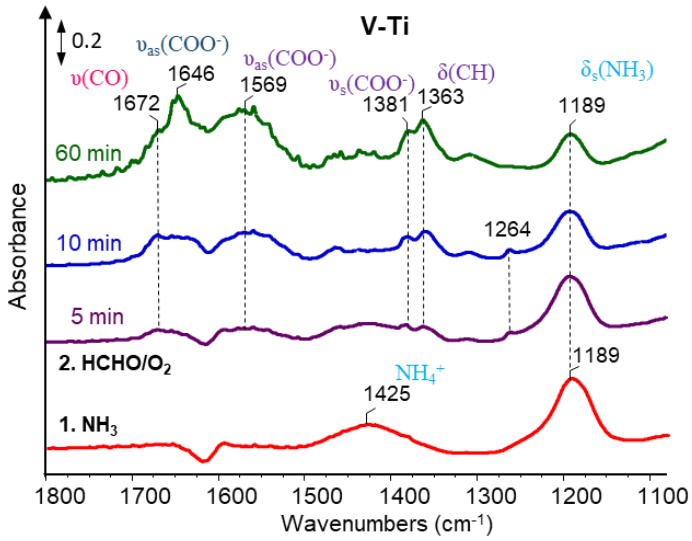

Figure 44. FT-IR spectra of the interaction of $HCHO/O_2$ with the adsorbate species of NH_3 on bare support V-Ti catalyst

The exposure of $HCHO/O_2$ leads to the decrease of both bands at Brønsted and Lewis sites. Same as on W-Ti catalyst, the adsorbates of NH_3 on Brønsted acid sites completely react after 60 min interaction. Meanwhile, a significant amount of NH_3 on Lewis sites remains. The formation

of both formate (1568 cm^{-1}, 1380 cm^{-1} and 1362 cm^{-1}) and formamide (1672 cm^{-1}) simultaneously occurs. The band at 1646 cm^{-1} could be ascribed for $\upsilon_{as}(COO^-)$ of monodentate formate, overlaps with the band of $\delta(NH_2)$ (1636 cm^{-1}) of formamide. However, the intensity of formate bands on V-Ti is significantly higher than on W-Ti catalyst. This could be explained by the interaction of HCHO with the lattice oxygen of bare support TiO_2 since the dispersion of vanadium on V-Ti catalyst cannot cover the entire surface of TiO_2, as discussed above.

Therefore, $HCONH_2$ is only formed when the metal oxides (VO_x, WO_x) are loaded on TiO_2. The role of the surface acidic sites for the formation of $HCONH_2$ could be seen more clearly on the V-W-Ti catalyst. The adsorption of NH_3 on V-W-Ti catalyst forms a strong and broadband at 1425 cm^{-1} on Brønsted sites (Figure 45).

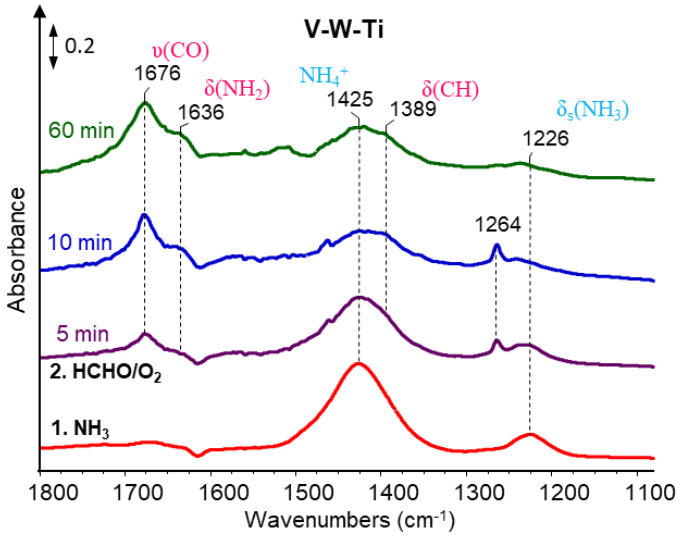

Figure 45. FT-IR spectra of the interaction of $HCHO/O_2$ with the adsorbate species of NH_3 on bare support V-W-Ti catalyst

Dosing $HCHO/O_2$ to the adsorbates of NH_3 leads to the decrease in the band intensity of NH_4^+ and NH_3 (at 1425 cm^{-1} and 1223 cm^{-1}, respectively). Formamide is the only product that is indicated by typical bands at 1675 cm^{-1}, 1636 cm^{-1}, and 1395 cm^{-1} of υ(CO), δ (NH_2), and δ(CH), respectively. A small amount of $NH_{3\ ads}$ (1226 cm^{-1}) on Lewis sites remains on the surface of the catalyst. Different from W-Ti and V-Ti catalyst, the amount of NH_4^+ remains after 60 min exposure with $HCHO/O_2$ and could be the reason that there was no formate is formed. This also

indicates the role of NH_4^+ for the formation of $HCONH_2$: a certain amount of the adsorbate of NH_3 on Lewis sites can react with HCHO to form $HCONH_2$ but the adsorbate of NH_3 on Brønsted sites predominates. The reaction of NH_4^+ occurs more intensely, and while NH_4^+ is still on the surface, HCHO will only interact with it to form $HCONH_2$. Interestingly, a sharp peak at 1264 cm^{-1} is always present in the first 10 minutes of the exposure of $HCHO/O_2$ and disappears after 60 minutes when the formation of $HCONH_2$ reaches to its maximum on all catalysts. It could be ascribed to an intermediate formed during the formation of $HCONH_2$.

In summary, these *in situ* FTIR results above have indicated the role of surface acidity for the reaction of HCHO in NH_3-SCR. $HCONH_2$ is only formed by the reaction of HCHO with the adsorbates of NH_3 on the surface of catalysts. Both Brønsted and Lewis acid sites on metal oxides can involve the interaction of HCHO, but Brønsted acid sites play the primary role for HCHO interaction. These results are a critical point to explain the various effects of HCHO on V_2O_5-WO_3/TiO_2 prepared catalysts in Figure 38. On the V-W-Ti catalyst, pre-adsorbed NH_4^+/NH_3 species will react with NO as the standard SCR or with HCHO to form $HCONH_2$. It leads to the decrease of NH_3 amount for SCR reaction, thus reduces the NO_x conversion in the whole temperature range.

In contrast, on the V-Ti and W-Ti catalyst, the amount of pre-adsorbed NH_4^+/NH_3 is not large enough for both reactions of NO and HCHO. A part of HCHO will interact with the bare support to form formate, which further decomposes or be oxidized to liberate CO and CO_2. Therefore, the presence of HCHO does not affect that much the NO_x conversion on the W-Ti, and V-Ti catalyst (Figure 38a, b), and the formation of HCN on these catalysts is also less than on the V-W-Ti catalyst and (Figure 39).

3.2.4 In situ EPR experiments

As mentioned above, the redox pair V^{5+}/V^{4+} plays a critical role in the catalytic activity of SCR reaction. *In situ* EPR experiment can very well detect V^{4+}, which can provide information on the participation of different vanadium species for each period of the SCR reaction. In addition, the behavior of the redox property for the formation of $HCONH_2$ can indicate the relationship between the SCR activity and the effect of HCHO on each catalyst.

All catalysts are pretreated with 5 vol % O_2/He at 300 °C for 1 h before the reaction to remove the surface contaminants, then are cooled down to 150 °C for the measurement. Because the EPR spectra of tungsten (W^{5+}) and titania (Ti^{3+}) only can be detected at very low temperatures, the spectra observed at 150 °C below can only be ascribed for the EPR spectra of V^{4+}.[103-104] Furthermore, the values observed from the simulation could provide information on the local structures of vanadia species. The axial distortion of the V^{4+} center has been investigated by the parameter $\Delta g_{\parallel}/\Delta g_{\perp}$ ($\Delta g_{\parallel} = g_{\parallel} - g_e$, $\Delta g_{\perp} = g_{\perp} - g_e$, g_e= 2.0023 for the free electron) and the delocalization coefficient β_2^{*2} obtained from Equation 59 can provide the information of the single electron delocalized toward the O ligands in the plane of O_4V=O site.[105] $\beta_2^{*2} = 1$ corresponds to the localization of the single electron totally at the vanadium nucleus. P value was set to 184.5 G and is known as the elecment – specific parameter which cover the relation of the Bohr magneton μ_b and the nuclear magneton μ_N.[106] The signal area of V^{4+} EPR spectra during the reaction is calculated by the double integration of the V^{4+} EPR peak. This area includes both the cluster and isolated VO^{2+} species.

$$\beta_2^{*2} = (7/6)\cdot\Delta g_{\parallel} - (5/12)\cdot\Delta g_{\perp} - (7/6)\cdot[(A_{\parallel} - A_{\perp})/P] \quad (59)$$

The representative EPR spectra of the interaction of NO/O_2 with the pre-adsorbates of NH_3 on vanadium supported catalysts and the corresponding signal area of V^{4+} with time (collected every 3 min) are shown in Figure 46. The axial distortion $\Delta g_{\parallel}/\Delta g_{\perp}$ and the delocalization coefficient β_2^{*2} of the simulated spectra are summarised in Table 5. The detailed simulated values ($g_{\parallel}$, $g_{\perp}$, $A_{\parallel}$, $A_{\perp}$) of the representative spectra are shown in Table A1-4. The corresponding simulated spectra, together with the experimental ones, are shown in Figure S8-9.

After the pretreatment, both V-Ti and V-W-Ti catalysts still contained a small amount of V^{4+} (Figure 46a, b, black lines), which survived oxidative pretreatment. The exposure of NH_3 on both catalysts increases the amount of V^{4+}, which could be ascribed to the reduction of V^{5+}. As shown by the results of the *in situ* FTIR experiments above (Figure 44-45), NH_3 adsorbs on V-Ti and V-W-Ti on both Brønsted acid sites (NH_4^+) and Lewis acid sites (NH_3). The formation of the adsorbates of NH_3 might be the reason for the reduction of V^{5+}, but both NH_4^+ and $NH_{3\ ads}$ contain the valence state of N at -3. On the other hand, there were no products detected of the NH_3 oxidation on both catalysts at 150 °C (Figure A7). Therefore, the reduction of V^{5+} to V^{4+} should be ascribed for the oxidation of a small amount of NH_3 at 150 °C, which cannot be

detected by the current conditions of the equipment. The other possibility is due to the formation of a type of chemical bond between a nitrogen atom (N^{-3}) and a vanadium atom (V^{5+}) where the nitrogen atom will produce donor electron to vanadium atom. The mechanism of SCR reaction is a controversial topic for a long time, and this could be an interesting topic of further research. The exposure of NO/O_2 leads to the decrease of the V^{4+} EPR signal. As mentioned in part 1.2.2, NO will react with the adsorbates of NH_3 on the surface of the catalyst to form N_2, and O_2 will oxidize V^{4+} to V^{5+}, which is the reason for the reducing of V^{4+} EPR signal.

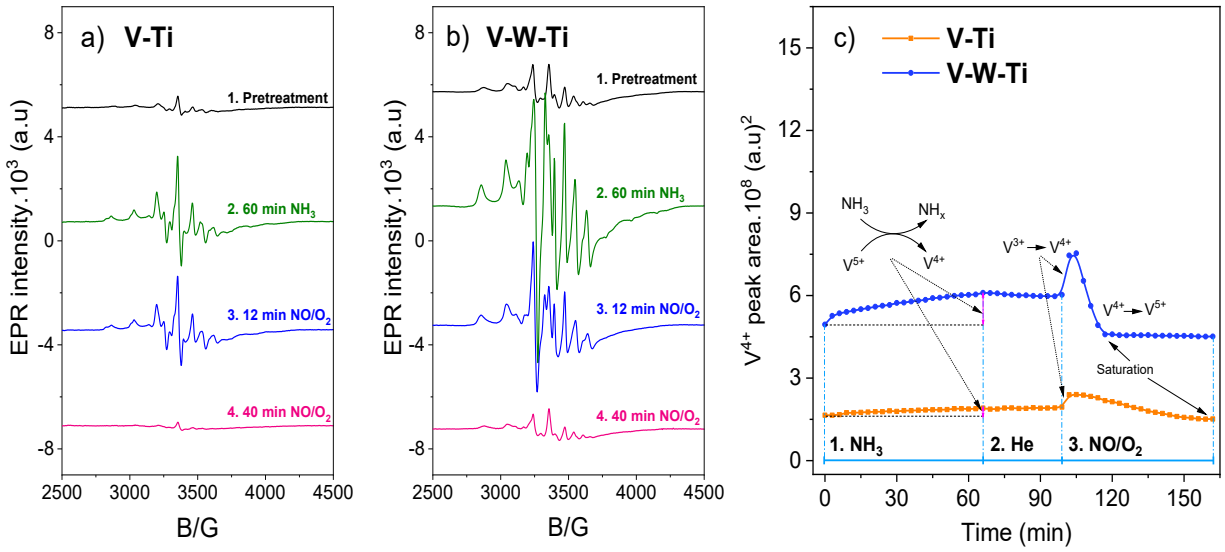

Figure 46. The *in situ* EPR spectra of a) V-Ti and b) V-W-Ti catalysts after the pretreatment at 300 °C in 5 vol % O_2/He, 60 min treatment with 0.2 vol % NH_3/He, 30 min flushing He and 60 min exposure to 400 ppm HCHO, 5 vol % O_2/He at 150 °C, c) the EPR spectra area of vanadium supported catalysts with time resulted from the integration

The signal area of V^{4+} EPR spectra during the interaction of NO/O_2 with NH_3 is obtained from the double integration (Figure 46c). The exposure of NH_3 leads to the formation of V^{4+} on both catalysts but more on the V-W-Ti catalyst. It could be due to the promotion effect of W which facilitates the reducibility of V. The flushing with He does not change the amount of V^{4+}. Interestingly, the amount of V^{4+} increases on both catalysts in the first 6 min exposure of NO/O_2. It could be explained by the formation of V^{3+} during the adsorption of NH_3, which is then oxidized by O_2 to form V^{4+}. After 6 min exposure with NO/O_2, the amount of V^{4+} decreased due

to the oxidation by O_2 to form V^{5+} as the redox cycle of the standard SCR. The rate of the V^{4+} oxidation is much faster on the V-W-Ti catalyst. After approximately 12 min exposure to NO/O_2, the EPR signal of V^{4+} on V-W-Ti becomes stable. Meanwhile, on the V-Ti catalyst, it takes approximately 60 min (Figure 46c). This could be why the higher SCR activity on V-W-Ti compared to V-Ti catalysts; the redox cycle faster will accelerate the reaction rate and produce more products.

The axial distortion ($\Delta g_{\parallel}/\Delta g_{\perp}$), delocalization coefficient ($\beta^*_2{}^2$) and the relative intensities (I_{rel} %) of vanadium species from the simulated values are shown in Table 5. The simulation indicates that V^{4+} on both catalysts comprises two single VO^{2+} species and the cluster to fit the original spectra. This matches with the results from UV-Vis DRS and Raman above that both single sites and vanadium clusters exist on the catalysts.

Table 5. Simulate parameters of the EPR spectra and parameters calculated thereof. g and A values, relative intensity (I_{rel}) (axial distortion of VO^{2+} site), and delocalization coefficient $\beta_2{}^*{}^2$ (see text) from the interaction of NO/O_2 with the adsorbents of NH_3 on vanadium supported catalysts

Time	V species	V-Ti			V-W-Ti		
		$\Delta g_{\parallel}/\Delta g_{\perp}$	$\beta^*_2{}^2$	I_{rel} %	$\Delta g_{\parallel}/\Delta g_{\perp}$	$\beta^*_2{}^2$	I_{rel} %
After pretreatment	VO^{2+} (I)	2.02	0.676	30.4	2.43	0.680	16.9
	VO^{2+} (II)	3.70	0.570	8.8	5.24	0.541	17.8
	Singlet			60.8			65.3
60 min NH_3	VO^{2+} (I)	1.72	0.696	32.2	2.61	0.678	28.0
	VO^{2+} (II)	3.44	0.603	21.7	3.97	0.622	25.3
	Singlet			46.2			46.6
12 min NO/O_2	VO^{2+} (I)	1.75	0.692	28.0	2.39	0.690	16.3
	VO^{2+} (II)	3.43	0.625	22.2	3.90	0.630	33.1
	Singlet			49.9			50.7
60 min NO/O_2	VO^{2+} (I)	2.02	0.685	20.5	2.38	0.674	17.9
	VO^{2+} (II)	3.24	0.545	4.5	4.04	0.566	16.1
	Singlet			74.6			67.0

On catalyst V-Ti, two species of isolated VO^{2+} have different axial distortion and delocalization coefficient values. The adsorption of NH_3 increases the contribution of single sites for the V^{4+} EPR spectra. It indicates that the exposure of NH_3 is dispersed relatively evenly on the catalyst surface. The contribution of specie VO^{2+}(II) is not that much after the pretreatment (8.8 %) but increases a lot after the adsorption of NH_3 (21.7%). However, after 60 min exposure with NO/O_2, its contribution to the EPR spectra is significantly reduced (4.5 %). Hence, the involvement of specie VO^{2+}(II) for the SCR reaction is stronger than specie VO^{2+}(I). This might be due to the outermost surface-exposed of VO^{2+}(II) more than specie VO^{2+}(I), which also agrees with the higher $\Delta g_{\parallel}/\Delta g_{\perp}$ value on VO^{2+}(II). The local environment is more distorted on the surface where the coordination vacancies exist. In addition, the $\beta^*_2{}^2$ also changes more during the interactions on VO^{2+}(II) species. This should be the consequence of the surrounding environment of VO^{2+}(II) species being changed more.

On the V-W-Ti catalyst, two isolated VO^{2+} and the cluster are found to fit the original spectra. Despite the delocalization, the coefficient does not change that much compare to V-Ti catalyst, the axial distortion $\Delta g_{\parallel}/\Delta g_{\perp}$ of vanadium species on V-W-Ti catalyst is higher (Table 5). This result can be pointed to the close intimate of V and W on the surface, resulting from the surrounding of tungsten oxides for vanadium oxides. In the vicinity of W, V will tend to exist in its reduced state since the reduction potential of VO^{3+}/VO^{2+} (0.957V) is much higher compared to the potential of W^{6+}/W^{5+} (-0.029V) or W^{6+}/W^{4+} (0.036V).[107] The involvement of both vanadium species is quite similar on the V-W-Ti catalyst. Therefore, the intimate coordination of V and W in the vicinity will accelerate the redox property of both species, which should be the reason for the higher activity of the V-W-Ti catalyst.

The EPR spectra of vanadium supported catalysts from the interaction of $HCHO/O_2$ with the adsorbates of NH_3 are shown in Figure 47. Unlike the interaction of NO/O_2, the interaction of $HCHO/O_2$ strongly increases the EPR signal of V^{4+}. It could be explained by the oxidation from HCHO (C^0) to either $HCONH_2$ (C^{2+}) on V-W-Ti catalyst or both $HCONH_2$ and formate $HCOO^-$ (C^{2+}) on V-Ti catalyst (Figure 44-45). Resulting from the reduction of V^{5+}, the rate of V^{4+} formation on V-W-Ti is faster. The intensity of V^{4+} reaches saturation earlier than on the V-Ti catalyst (Figure 46c).

The axial distortion ($\Delta g_{\parallel}/\Delta g_{\perp}$), delocalization coefficient ($\beta^*{}_2{}^2$) and the relative intensities (I_{rel} %) of vanadium species from the simulated values are shown in Table 6. There are some minor changes of the simulated parameters of EPR spectra of V-Ti and V-W-Ti catalyst after pretreatment and 60 min NH_3 adsorption compare to Table 5. This is due to the experimental error from two various experiments despite the same procedure on the same catalysts (pretreatment – NH_3 adsorption). However, in general, the error is negligible; the components of the EPR spectra are still like the previous experiments. Therefore, these experimental errors can be ignored.

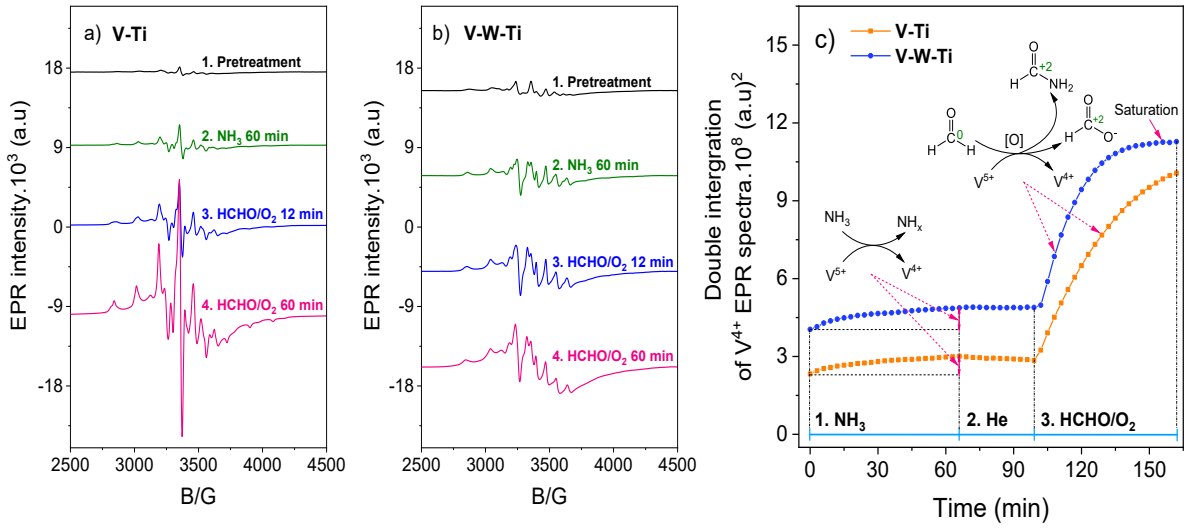

Figure 47. The *in situ* EPR spectra of a) V-Ti catalyst and b) V-W-Ti catalyst following by the pretreatment at 300 °C by 5 vol % O_2/He, 60 min pre-adsorption with 0.2 vol % NH_3/He, 30 min flushing He and 60 min exposure with 400 ppm HCHO, 5 vol % O_2/He at 150 °C, c) the EPR spectra area of vanadium supported catalysts with time resulted from the integration

The simulated results show the decrease of the contribution of isolated VO^{2+} and the increase of cluster for V^{4+} spectra during the exposure of HCHO/O_2. It could be explained by the formation of V^{4+} in the vicinity of V^{4+} sites created by NH_3 adsorption before, forming the V^{4+} cluster and reducing the contribution of the isolated VO^{2+} species. Since the content of vanadium loading on the surface of V-Ti and V-W-Ti is equal (1 wt.%), the dispersion of VO_x on both catalysts is not unlike that much; the higher oxidation property of V-W-Ti only can be explained by the promotion effect of W for the reducibility of V as discussed above.

This result indicates the role of redox cites for the effects of HCHO on different catalysts. V-W-Ti catalyst was affected more than W-Ti and V-Ti catalyst because V-W-Ti contains more acidic sites for the interaction of $HCHO/O_2$ and NH_3 and its high redox property accelerates the oxidation of HCHO to form $HCONH_2$, which will further decompose to form HCN. This is the explanation that why HCN was created the most on V-W-Ti catalyst.

Table 6. Simulate parameters of the EPR spectra and parameters calculated thereof. g and A values, relative intensity (I_{rel}) (axial distortion of VO^{2+} site), and delocalization coefficient $\beta_2{}^{*2}$ (see text) from the interaction of $HCHO/O_2$ with the adsorbents of NH_3 on vanadium supported catalysts

Time	V species	V-Ti			V-W-Ti		
		$\Delta g_{\parallel}/\Delta g_{\perp}$	$\beta^*{}_2{}^2$	I_{rel} %	$\Delta g_{\parallel}/\Delta g_{\perp}$	$\beta^*{}_2{}^2$	I_{rel} %
After pretreatment	VO^{2+} (I)	1.93	0.697	27.5	2.43	0.693	16.9
	VO^{2+} (II)	4.05	0.587	11.0	5.25	0.602	17.8
	Singlet			61.5			65.3
60 min NH_3	VO^{2+} (I)	1.77	0.690	35.1	2.49	0.765	24.2
	VO^{2+} (II)	3.62	0.617	20.8	4.00	0.651	20.2
	Singlet			44.1			55.6
12 min $HCHO/O_2$	VO^{2+} (I)	1.77	0.712	25.6	2.64	0.715	10.7
	VO^{2+} (II)	3.65	0.618	21.4	3.76	0.647	17.9
	Singlet			53.0			71.4
60 min $HCHO/O_2$	VO^{2+} (I)	1.86	0.701	27.8	2.19	0.676	4.9
	VO^{2+} (II)	3.77	0.584	12.2	3.75	0.631	11.4
	Singlet			60.0			83.8

3.2.5 Effect of H_2O

In the flue gas, water vapor from the combustion of fuel always presents and could affect the NH_3-SCR. Therefore, the effect of HCHO is also studied in the presence of H_2O to approach the practical condition. The conversion of NO_x, NH_3, and formation of products from the reaction of HCHO in NH_3-SCR in the presence of H_2O on V-W-Ti catalyst are shown in Figure 48. In the presence of 8 vol % H_2O, NO_x conversion increases above 300 °C but decreases below 300 °C in comparison to the absence of H_2O. Meanwhile, NH_3 conversion was unchanged above 300 °C

and decreased at a temperature lower than 300 °C (15 – 20 %). N_2 is still the main product from the SCR reaction, but the formation of N_2O reduces a lot. The effect of H_2O at a temperature higher than 300 °C could be explained by its hindering the partial oxidation of NH_3.[108]

In the presence of both HCHO and H_2O, the conversion of NO_x and NH_3 decreased significantly in the whole temperature range (Figure 48a-b, pink lines), especially below 300 °C in comparison to the presence of only HCHO (Figure 48a-b, blue lines). The NO_x conversion reaches to its maximum above 300 °C but does not decline that much at a temperature higher than 450 °C. Same as the presence of the only H_2O, it could be explained by the limited partial oxidation of NH_3. It was also confirmed by the negligible formation of N_2O (Figure 48c, dashed pink line, overlapped with the green line).

Formaldehyde was converted completely in the presence of H_2O. CO_2 is formed above 400 °C and the curve of HCN formation is the same as its formation in the absence of H_2O (Figure 49a). Interestingly, the total concentration of HCN and CO_2 only reaches to maximum ~ 20 ppm in the whole temperature range. This result suggests that in the presence of H_2O, the decomposition of $HCONH_2$ is limited, remains on the surface of the catalyst, and blocks the active sites, then strongly reduced the SCR activity. To confirm this, the catalyst after the reaction is heated up to 350 °C and flushing by He. The result shows that HCN is released a lot from the catalyst, and it needs approximately 6 h to remove all $HCONH_2$ on the surface of the catalyst (Figure 49b). Although the coverage of $HCONH_2$ on the surface of the catalyst can be removed at 350 °C, it will take a long time. This explains why the conversion of NO_x and NH_3 above 350 °C is still much lower than the absence of H_2O. The delay of $HCONH_2$ decomposition inhibits the reaction of NO and NH_3 on the surface of the catalyst.

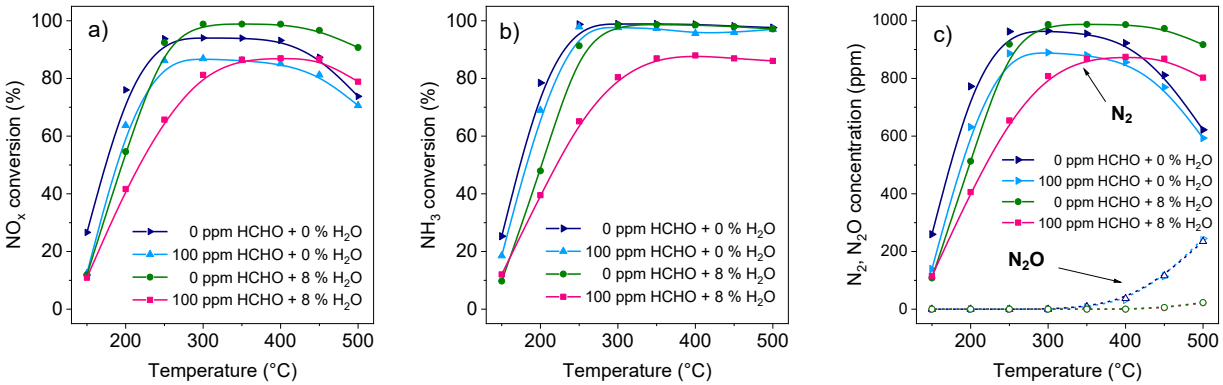

Figure 48. Conversion of NO_x, NH_3 and the formation of N_2, N_2O from the reaction of 0.1 vol % NO, 0.1 vol % NH_3, 0 - 8 vol % H_2O, 0 – 100 ppm HCHO, 5 vol % O_2/He on V-W-Ti catalyst

Therefore, the effect of HCHO on the presence of H_2O is worse compared to the dry condition. HCHO is converted completely, but the NO_x conversion and N_2 formation decrease more than in the absence of H_2O, especially at low temperatures. The reaction of HCHO in this case also forms HCN and CO_2 but less than in dry conditions. In contrast, the formation of $HCONH_2$ from the interaction of HCHO and NH_3 remains on the surface in the wet condition. This uncompleted decomposition will block the active sites, and the catalyst need to be heated up at high temperature to unblock the surface-active sites.

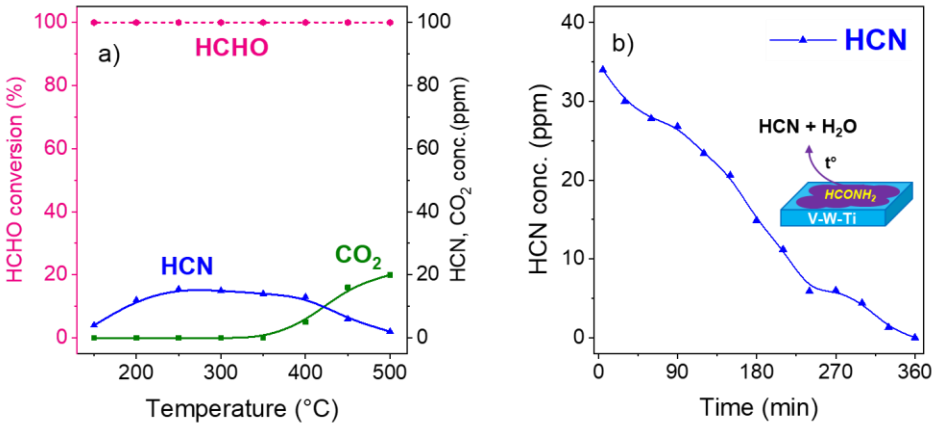

Figure 49. a) Conversion and formation of products of HCHO from the reaction of 100 ppm HCHO, 8 vol % H_2O, 0.1 vol % NO, 0.1 vol % NH_3, 5 vol % O_2/He on catalyst V-W-Ti, b) The liberation of HCN with time by heat up catalyst V-W-Ti after reaction of 100 ppm HCHO, 8 vol % H_2O, 0.1 vol % NO, 0.1 vol % NH_3, 5 vol % O_2/He

4. Conclusions and outlook

In this study, the effect of HCHO in NH_3-SCR of NO_x has been studied on V_2O_5-WO_3/TiO_2 catalysts with different compositions. The formation of intermediate species on the surface of catalysts and the redox behavior of the active sites of the reaction of HCHO in NH_3-SCR have also been studied by *in situ* FTIR and *in situ* EPR experiments, respectively.

The first results on a commercial V_2O_5-WO_3/TiO_2 (1 wt. % V, 6 wt. % W) catalyst shows many negative effects of HCHO. In the standard SCR feed gas (NH_3, NO, O_2), HCHO prefers to react with NH_3 to form HCN as the main product. This undesired reaction leads to the decrease of both NO_x conversion and N_2 selectivity. Results from *in situ* FTIR experiments indicate that the interaction of HCHO and NH_3 will form $HCONH_2$ as the intermediate species on the surface of the catalyst. The latter can be formed by either gaseous HCHO reacts with the adsorbates of NH_3 ($NH_4^+{}_{ads}$, $NH_{3\ ads}$) or gaseous NH_3 reacts with the adsorbates of HCHO (formates). The decomposition of $HCONH_2$ is the source of the HCN liberation from the reaction of HCHO in NH_3-SCR. HCN is a very harmful compound, and it can be oxidized by the lattice oxygen of catalyst at high temperatures. However, this oxidation will form NO, which will return to the SCR reaction and reduce the NO_x conversion again.

The role of active sites has been studied by carried out the effect of HCHO on catalysts with different compositions: WO_3/TiO_2 (W-Ti), V_2O_5/TiO_2 (V-Ti), and V_2O_5-WO_3/TiO_2 (V-W-Ti) catalyst. Catalysts are prepared by the wetness impregnation method, and the content of vanadium and tungsten are based on the used commercial one. Several characterization methods have been applied to investigate the dispersion of metal oxides on the surface of the support. It shows that at low loading content of vanadium (1 wt. % V), there is not much different between the dispersion of vanadium on bare support TiO_2 (V-Ti catalyst) and WO_3/TiO_2 (V-W-Ti catalyst). However, on the V-W-Ti catalyst, vanadium oxides are surrounded by tungsten oxides, and the synergistic of these oxides will create more surface acid sites and the V-O-W bonds. The latter accelerates the redox cycle of vanadium sites, which will increase the activity of SCR reaction.

The effect of HCHO on different catalysts is strongly related to their catalytic activity of SCR reaction. In the same condition, the V-W-Ti catalyst shows the highest SCR activity and is

affected the most by the reaction of HCHO. HCHO causes the decline of NO_x conversion on V-W-Ti catalyst in the whole temperature range and releases the highest amount of HCN. *In situ* FTIR experiments reveal that the high acidic property on V-W-Ti catalyst provides enough NH_3 surface adsorbates for the reaction of HCHO to form $HCONH_2$ as the intermediate species. In contrast, on W-Ti and V-Ti catalyst, where the amount of NH_3 adsorbates is not large enough, HCHO will interact with lattice oxygen of bare support to form formates further decomposed or oxidized to form CO and CO_2. Besides, results from *in situ* EPR indicates that the high redox property of catalyst also accelerates the oxidation rate of HCHO (C^0) to $HCONH_2$ (C^{2+}) (Figure 50). These are the reasons for the highest liberation of HCN on the best SCR catalyst V-W-Ti.

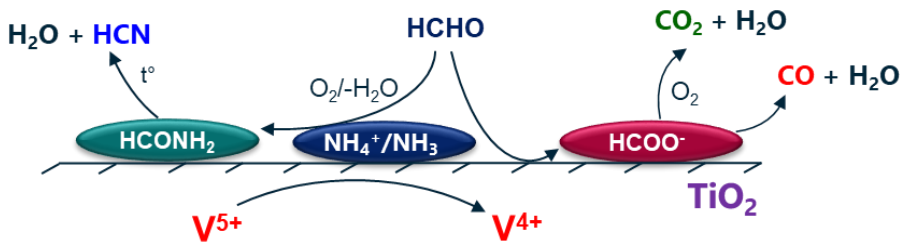

Figure 50. The pathways of HCHO reaction on NH_3-SCR of NO_x on V_2O_5-WO_3/TiO_2 catalysts

In the presence of H_2O, the effect of HCHO becomes even worse than in the dry condition. The NO_x conversion on V-W-Ti declines more than the absence of H_2O, especially at a temperature lower than 250 °C. The emission of HCN is much less than the reaction of only HCHO, but the reason is due to the deposition of $HCONH_2$ on the catalyst surface. The presence of H_2O inhibits the decomposition of $HCONH_2$, leads to the coverage of $HCONH_2$ on the surface of the catalyst, blocks the active sites, and enormously decreases the catalytic activity. This contamination can be removed by heating the catalyst after reaction at a high temperature (above 350 °C) and liberate a lot of HCN.

Further works. Since HCHO causes several negative effects on the NH_3-SCR, solutions need to be found to limit them. However, there is a disadvantage that the catalyst which has high SCR activity will also strongly accelerate the formation of HCN from the HCHO reaction. The formation of $HCONH_2$ is inevitable whenever HCHO is present on the catalyst surface containing NH_3 adsorbates, and even it is accelerated by the high catalytic redox property. Therefore, the removal of HCHO before it can affect the SCR could be necessary and applied by

the DOCs. Though, in some conditions, the DOCs can even generate HCHO from the partial oxidation of unburned hydrocarbon. Thus, minimizing the formation of HCHO should be an important factor to consider for applying the DOCs.

Another possibility is that since the HCHO reaction will induce HCN, developing a new catalyst that can perform high SCR activity and good HCN treatment may be of interest. The oxidation of HCN on V_2O_5-WO_3/TiO_2 only occurs at high temperature and liberates NO, which will further return to the feed gas and decrease the NO_x conversion again. Therefore, the acceleration of HCN oxidation should increase NH_3 concentration in the feed gas to ensure enough amount of NH_3 for SCR reaction. Since H_2O is always present in the exhaust gas, the hydrolysis HCN on the SCR catalyst could also be an exciting pathway. The hydrolysis of HCN is the reverse reaction of the decomposition of $HCONH_2$. The latter can also be hydrolyzed to form $HCOONH_4$, which will further decompose to form NH_3 and CO_2, limiting the emission of HCN to the environment.

References

1. Han, L.; Cai, S.; Gao, M.; Hasegawa, J.-y.; Wang, P.; Zhang, J.; Shi, L.; Zhang, D., Selective Catalytic Reduction of NO_x with NH_3 by Using Novel Catalysts: State of the Art and Future Prospects. *Chem. Rev.* **2019,** *119* (19), 10916-10976.

2. Ngo, A. B.; Vuong, T. H.; Atia, H.; Bentrup, U.; Kondratenko, V. A.; Kondratenko, E. V.; Rabeah, J.; Ambruster, U.; Brückner, A., Effect of Formaldehyde in Selective Catalytic Reduction of NO_x by Ammonia (NH_3-SCR) on a Commercial V_2O_5-WO_3/TiO_2 Catalyst under Model Conditions. *Environ. Sci. Technol.* **2020,** *54* (19), 11753-11761.

3. Agency, U. S. E. P. *Nitrogen oxides (NO_x), why and how they are controlled*; **1999**.

4. Mollenhauer, K. T., Helmut, *Handbook of Diesel Engines*. **2010**.

5. Moosmann, L. T., Melanie ; Haider, Simone ; Gager, Michael ; Schindlbacher, Sabine ; Kampel, Elisabeth *European Union emission inventory report 1990–2011 under the UNECE Convention on Long-range Transboundary Air Pollution (LRTAP)*; European Environment Agency: **2013**.

6. Bartok, W.; Sarofim, A. F., *Fossil fuel combustion: A source book*. John Wiley & Sons, New York, NY (United States): United States, **1991**.

7. Agency, E. S., Nitrogen dioxide pollution mapped. *Copernicus Sentinel-5P mission* **2019**.

8. Eurostat, Air pollution statistics - air emissions accounts. **2018,** *online data code: env_ac_ainah_r2*.

9. EPA., U. S., Integrated Science Assessment (ISA) For Oxides of Nitrogen. *Health Criteria (Final Report, 2016)* **2016,** *EPA/600/R-15/068, 2016.*

10. Potera, C., Air Pollution: Salt Mist Is the Right Seasoning for Ozone. *Environ. Health Perspect.* **2008,** *116* (7), A288-A288.

11. Nowlan, C. R.; Martin, R. V.; Philip, S.; Lamsal, L. N.; Krotkov, N. A.; Marais, E. A.; Wang, S.; Zhang, Q., Global dry deposition of nitrogen dioxide and sulfur dioxide inferred from space-based measurements. *Global Biogeochem. Cycles* **2014,** *28* (10), 1025-1043.

12. Agency, U. E. P., Overview of Greenhouse Gases. *Greenhouse Gas Emissions* **2018**.

13. Kyriaki, P.; Angelos, M. E., NO_x Control via H_2-Selective Catalytic Reduction (H_2-SCR) Technology for Stationary and Mobile Applications. *Recent. Pat. Mater. Sci.* **2012,** *5* (2), 87-104.

14. Latha, H. S.; Prakash, K. V.; Veerangouda, M.; Maski, D.; Ramappa, K. T., A Review on SCR System for NOx Reduction in Diesel Engine. *Int. J. Curr. Microbiol. Appl. Sci.* **2019,** *8*, 1553-1559.

15. Mladenović, M.; Paprika, M.; Marinković, A., Denitrification techniques for biomass combustion. *Renew. Sustain. Energy. Rev.* **2018,** *82*, 3350-3364.

16. Choung, J. W.; Nam, I.-S.; Ham, S.-W., Effect of promoters including tungsten and barium on the thermal stability of V_2O_5/sulfated TiO_2 catalyst for NO reduction by NH_3. *Catal. Today* **2006,** *111* (3), 242-247.

17. Madia, G.; Elsener, M.; Koebel, M.; Raimondi, F.; Wokaun, A., Thermal stability of vanadia-tungsta-titania catalysts in the SCR process. *Appl. Catal., B* **2002,** *39* (2), 181-190.

18. Lai, J.-K.; Wach, I. E., A Perspective on the Selective Catalytic Reduction (SCR) of NO with NH_3 by Supported V_2O_5–WO_3/TiO_2 Catalysts. *ACS Catal.* **2018,** *8* (7), 6537-6551.

19. Topsoe, N. Y.; Topsoe, H.; Dumesic, J. A., Vanadia/Titania Catalysts for Selective Catalytic Reduction (SCR) of Nitric-Oxide by Ammonia: I. Combined Temperature-Programmed in-Situ FTIR and On-line Mass-Spectroscopy Studies. *J. Catal.* **1995,** *151* (1), 226-240.

20. Topsoe, N. Y.; Dumesic, J. A.; Topsoe, H., Vanadia-Titania Catalysts for Selective Catalytic Reduction of Nitric-Oxide by Ammonia: I.I. Studies of Active Sites and Formulation of Catalytic Cycles. *J. Catal.* **1995,** *151* (1), 241-252.

21. Ramis, G.; Busca, G.; Bregani, F.; Forzatti*, P., Fourier transform-infrared study of the adsorption and coadsorption of nitric oxide, nitrogen dioxide and ammonia on vanadia-titania and mechanism of selective catalytic reduction. *App. Catal.* **1990,** *64*, 259-278.

22. Li, X.; Li, Y., Molybdenum modified $CeAlO_x$ catalyst for the selective catalytic reduction of NO with NH3. *J. Mol. Catal. A: Chem.* **2014,** *386*, 69–77.

23. Busca, G.; Lietti, L.; Ramis, G.; Berti, F., Chemical and mechanistic aspects of the selective catalytic reduction of NOx by ammonia over oxide catalysts: A review. *Appl. Catal., B* **1998,** *18* (1), 1-36.

24. Vuong, T. H.; Radnik, J.; Rabeah, J.; Bentrup, U.; Schneider, M.; Atia, H.; Armbruster, U.; Grünert, W.; Brückner, A., Efficient $VO_x/Ce_{1-x}Ti_xO_2$ Catalysts for Low-Temperature NH_3-SCR: Reaction Mechanism and Active Sites Assessed by in Situ/Operando Spectroscopy. *ACS Catal.* **2017,** *7* (3), 1693-1705.

25. Smirniotis, P. G.; Peña, D. A.; Uphade, B. S., Low-Temperature Selective Catalytic Reduction (SCR) of NO with NH3 by Using Mn, Cr, and Cu Oxides Supported on Hombikat TiO_2. *Angew. Chem. Int. Ed.* **2001,** *40* (13), 2479-2482.

26. Boningari, T.; Ettireddy, P. R.; Somogyvari, A.; Liu, Y.; Vorontsov, A.; McDonald, C. A.; Smirniotis, P. G., Influence of elevated surface texture hydrated titania on Ce-doped Mn/TiO_2 catalysts for the low-temperature SCR of NO_x under oxygen-rich conditions. *J. Catal.* **2015,** *325*, 145-155.

27. Pérez Vélez, R.; Bentrup, U.; Grünert, W.; Brückner, A., The Role of NO2 in the Fast NH3-SCR of NOx: A Combined In Situ FTIR and EPR Spectroscopic Study. *Top. Catal.* **2017,** *60*, 1-12.

28. Chen, Z.; Yang, Q.; Li, H.; Li, X.; Wang, L.; Chi Tsang, S., Cr–MnOx mixed-oxide catalysts for selective catalytic reduction of NO_x with NH_3 at low temperature. *J. Catal.* **2010,** *276* (1), 56-65.

29. Mu, J.; Li, X.; Sun, W.; Fan, S.; Wang, X.; Wang, L.; Qin, M.; Gan, G.; Yin, Z.; Zhang, D., Inductive Effect Boosting Catalytic Performance of Advanced $Fe_{1-x}V_xO_\delta$ Catalysts in Low-Temperature NH_3 Selective Catalytic Reduction: Insight into the Structure, Interaction, and Mechanisms. *ACS Catal.* **2018,** *8* (8), 6760-6774.

30. Gillot, S.; Tricot, G.; Vezin, H.; Dacquin, J.-P.; Dujardin, C.; Granger, P., Development of stable and efficient $CeVO_4$ systems for the selective reduction of NO_x by ammonia: Structure-activity relationship. *Appl. Catal., B* **2017,** *218*, 338-348.

31. Kijlstra, W.; Brands, D.; Smit, H.; Poels, E.; Bliek, A., Mechanism of Selective Catalytic Reduction of NO with NH_3 over MnO_x/Al_2O_3, I. Adsorption and Desorption of the Single Reaction Components. *J. Catal.* **1997,** *171*.

32. Jin, R.; Liu, Y.; Wang, Y.; Cen, W.; Wu, Z.; Wang, H.; Weng, X., The role of cerium in the improved SO_2 tolerance for NO reduction with NH_3 over Mn-Ce/TiO_2 catalyst at low temperature. *Appl. Catal., B* **2014,** *148-149*, 582-588.

33. Wei, L.; Cui, S.; Guo, H.; Ma, X.; Zhang, L., DRIFT and DFT study of cerium addition on SO_2 of Manganese-based Catalysts for low temperature SCR. *J. Mol. Catal. A: Chem.* **2016,** *421*, 102-108.

34. Sheng, Z.; Hu, Y.; Xue, J.; Wang, X.; Liao, W., SO_2 poisoning and regeneration of Mn-Ce/TiO_2 catalyst for low temperature NO_x reduction with NH3. *J Rare Earth* **2012,** *30* (7), 676-682.

35. Xu, L.; Wang, C.; Chang, H.; Wu, Q.; Zhang, T.; Li, J., New Insight into SO_2 Poisoning and Regeneration of CeO_2–WO_3/TiO_2 and V_2O_5–WO_3/TiO_2 Catalysts for Low-Temperature NH_3–SCR. *Environ. Sci. Technol.* **2018,** *52* (12), 7064-7071.

36. Li, J.; Peng, Y.; Chang, H.; Li, X.; Crittenden, J. C.; Hao, J., Chemical poison and regeneration of SCR catalysts for NOxremoval from stationary sources. *Front. Envi. Sci. Eng.* **2016,** *10* (3), 413-427.

37. Yu, Y.; Miao, J.; Wang, J.; He, C.; Chen, J., Facile synthesis of $CuSO_4/TiO_2$ catalysts with superior activity and SO_2 tolerance for NH_3-SCR: physicochemical properties and reaction mechanism. *Catal. Sci.Technol.* **2017,** *7* (7), 1590-1601.

38. Du, X.; Wang, X.; Chen, Y.; Gao, X.; Zhang, L., Supported metal sulfates on Ce-TiO_x as catalysts for NH3-SCR of NO: High resistances to SO_2 and potassium. *J. Ind. Eng. Chem.* **2016,** *36*.

39. Jiang, Y.; Gao, X.; Zhang, Y.; Wu, W.; Luo, Z.; Cen, K., Effect of KCl on the selective catalytic reduction of NO with NH3 over vanadia-based catalysts for biomass combustion. *Environ. Prog. Sustain. Energy.* **2014,** *33* (2), 390-395.

40. Putluru, S. S. R.; Riisager, A.; Fehrmann, R., Alkali resistant Cu/zeolite deNO_x catalysts for flue gas cleaning in biomass fired applications. *Appl. Catal., B* **2011,** *101* (3), 183-188.

41. Putluru, S. S. R.; Kristensen, S. B.; Due-Hansen, J.; Riisager, A.; Fehrmann, R., Alternative alkali resistant deNO_x catalysts. *Catal. Today* **2012,** *184* (1), 192-196.

42. Gao, S.; Wang, P.; Chen, X.; Wang, H.; Wu, Z.; Liu, Y.; Weng, X., Enhanced alkali resistance of CeO_2/SO_4^{2-}–ZrO_2 catalyst in selective catalytic reduction of NO_x by ammonia. *Catal. Commun.* **2014,** *43*, 223-226.

43. Due-Hansen, J.; Boghosian, S.; Kustov, A.; Fristrup, P.; Tsilomelekis, G.; Ståhl, K.; Christensen, C. H.; Fehrmann, R., Vanadia-based SCR catalysts supported on tungstated and sulfated zirconia: Influence of doping with potassium. *J. Catal.* **2007,** *251* (2), 459-473.

44. Yan, L.; Ji, Y.; Wang, P.; Feng, C.; Han, L.; Li, H.; Yan, T.; Shi, L.; Zhang, D., Alkali and Phosphorus Resistant Zeolite-like Catalysts for NO_x Reduction by NH3. *Environ. Sci. Technol.* **2020,** *54* (14), 9132-9141.

45. Wang, S.-x.; Guo, R.-t.; Pan, W.-g.; Li, M.-y.; Sun, P.; Liu, S.-m.; Liu, S.-w.; Sun, X.; Liu, J., The deactivation mechanism of Pb on the Ce/TiO_2 catalyst for the selective catalytic reduction of NOx with NH3: TPD and DRIFT studies. *PCCP* **2017,** *19* (7), 5333-5342.

46. Lu, Q.; Pei, X.-q.; Wu, Y.-w.; Xu, M.-x.; Liu, D.-j.; Zhao, L., Deactivation Mechanism of the Commercial V_2O_5–MoO_3/TiO_2 Selective Catalytic Reduction Catalyst by Arsenic Poisoning in Coal-Fired Power Plants. *Energ Fuel* **2020,** *34* (4), 4865-4873.

47. Li, X.; Li, X.; Zhu, T.; Peng, Y.; Li, J.; Hao, J., Extraordinary Deactivation Offset Effect of Arsenic and Calcium on CeO2–WO3 SCR Catalysts. *Environ. Sci. Technol.* **2018,** *52* (15), 8578-8587.

48. Chang, H.; Jong, M. T.; Wang, C.; Qu, R.; Du, Y.; Li, J.; Hao, J., Design Strategies for P-Containing Fuels Adaptable CeO_2–MoO_3 Catalysts for $DeNO_x$: Significance of Phosphorus Resistance and N2 Selectivity. *Environ. Sci. Technol.* **2013,** *47* (20), 11692-11699.

49. Lisi, L.; Lasorella, G.; Malloggi, S.; Russo, G., Single and combined deactivating effect of alkali metals and HCl on commercial SCR catalysts. *Appl. Catal., B* **2004,** *50* (4), 251-258.

50. Chang, H.; Li, J.; Su, W.; Shao, Y.; Hao, J., A novel mechanism for poisoning of metal oxide SCR catalysts: Base-acid explanation correlated with redox properties. *Chem. Commun. (Cambridge, U. K.)* **2014,** *50*.

51. Mitchell, C. E.; Olsen, D. B., Formaldehyde Formation in Large Bore Natural Gas Engines Part 1: Formation Mechanisms. *J. Eng. Gas. Turbine. Power.* **1999,** *122* (4), 603-610.

52. Engines, I. C. o. C., Methane and Formaldehyde Emissions of Gas Engines. *CIMAC Position Paper* **2014,** *WG 17*.

53. Rodrigues, M. C.; Guarieiro, L. L. N.; Cardoso, M. P.; Carvalho, L. S.; da Rocha, G. O.; de Andrade, J. B., Acetaldehyde and formaldehyde concentrations from sites impacted by heavy-duty diesel vehicles and their correlation with the fuel composition: Diesel and diesel/biodiesel blends. *Fuel* **2012,** *92* (1), 258-263.

54. Suarez-Bertoa, R.; Clairotte, M.; Arlitt, B.; Nakatani, S.; Hill, L.; Winkler, K.; Kaarsberg, C.; Knauf, T.; Zijlmans, R.; Boertien, H.; Astorga, C., Intercomparison of ethanol, formaldehyde and acetaldehyde measurements from a flex-fuel vehicle exhaust during the WLTC. *Fuel* **2017,** *203*, 330-340.
55. Agency, U. S. E. P. Light-Duty Vehicles and Light-Duty Trucks: Clean Fuel Fleet Exhaust Emission Standards.
56. Clairotte, M.; Adam, T. W.; Zardini, A. A.; Manfredi, U.; Martini, G.; Krasenbrink, A.; Vicet, A.; Tournié, E.; Astorga, C., Effects of low temperature on the cold start gaseous emissions from light duty vehicles fuelled by ethanol-blended gasoline. *Appl. Energy* **2013,** *102*, 44-54.
57. Shukla, P. C.; Gupta, T.; Agarwal, A. K., Performance evaluation of a biodiesel fuelled transportation engine retrofitted with a non-noble metal catalysed diesel oxidation catalyst for controlling unregulated emissions. *J. Hazard. Mater.* **2018,** *344*, 615-625.
58. Wei, H.; Yao, C.; Dou, Z.; Wang, B.; Chen, C.; Liu, M., Comparison of the conversion efficiency of DOC and DPOC to unregulated emissions from a DMDF engine. *Fuel* **2017,** *204*, 71-84.
59. Danilevich, E. V.; Popova, G. Y.; Zolotarskii, I. A.; Ermakova, A.; Andrushkevich, T. V., Kinetics of formaldehyde oxidation on a vanadia-titania catalyst. *Catal. Ind.* **2011,** *2* (4), 320-328.
60. Li, Y.; Chen, X.; Wang, C.; Zhang, C.; He, H., Sodium Enhances Ir/TiO2 Activity for Catalytic Oxidation of Formaldehyde at Ambient Temperature. *ACS Catal.* **2018,** *8* (12), 11377-11385.
61. Wang, L.; Yue, H.; Hua, Z.; Wang, H.; Li, X.; Li, L., Highly active Pt/NaxTiO2 catalyst for low temperature formaldehyde decomposition. *Appl. Catal., B* **2017,** *219*, 301-313.
62. Bai, B.; Li, J., Positive Effects of K+ Ions on Three-Dimensional Mesoporous Ag/Co3O4 Catalyst for HCHO Oxidation. *ACS Catal.* **2014,** *4* (8), 2753-2762.
63. Healy, T. V., The Reaction of nitric acid with formaldehyde and with formic acid and its application to the removal of nitric acid from mixtures. *J. Appl. Chem.* **1958,** *8* (9), 553-561.
64. Richmond, H. H.; Myers, G. S.; Wright, G. F., The Reaction between Formaldehyde and Ammonia. *J. Am. Chem. Soc.* **1948,** *70* (11), 3659-3664.
65. Kröcher, O.; Elsener, M.; Jacob, E., A model gas study of ammonium formate, methanamide and guanidinium formate as alternative ammonia precursor compounds for the selective catalytic reduction of nitrogen oxides in diesel exhaust gas. *Appl. Catal., B* **2009,** *88* (1), 66-82.
66. Nguyen, V. S.; Abbott, H. L.; Dawley, M. M.; Orlando, T. M.; Leszczynski, J.; Nguyen, M. T., Theoretical Study of Formamide Decomposition Pathways. *J. Phys. Chem. A* **2011,** *115* (5), 841-851.
67. Love, A. M.; Carrero, C. A.; Chieregato, A.; Grant, J. T.; Conrad, S.; Verel, R.; Hermans, I., Elucidation of Anchoring and Restructuring Steps during Synthesis of Silica-Supported Vanadium Oxide Catalysts. *Chem. Mater.* **2016,** *28* (15), 5495-5504.

68. Delgass, W. N.; Haller, G. L.; Kellerman, R.; Lunsford, J. H., Chapter 4 - DIFFUSE REFLECTANCE AND PHOTOACOUSTIC SPECTROSCOPIES. In *Spectroscopy in Heterogeneous Catalysis*, Delgass, W. N.; Haller, G. L.; Kellerman, R.; Lunsford, J. H., Eds. Academic Press: **1979**; pp 86-131.

69. Gliemann, G., A. B. P. Lever: Inorganic Electronic Spectroscopy, Vol. 33 aus: Studies in Physical and Theoretical Chemistry, Elsevier, Amsterdam, Oxford, New York, Tokio 1984. 863 Seiten, *Ber. Bunsenges. Physik. Chem.* **1985,** *89* (1), 99-100.

70. Kumar, V. V.; Naresh, G.; Sudhakar, M.; Anjaneyulu, C.; Bhargava, S. K.; Tardio, J.; Reddy, V. K.; Padmasri, A. H.; Venugopal, A., An investigation on the influence of support type for Ni catalysed vapour phase hydrogenation of aqueous levulinic acid to γ-valerolactone. *RSC Advances* **2016,** *6* (12), 9872-9879.

71. Brückner, A., Electron Paramagnetic Resonance. *In In-situ Spectroscopy of Catalysts*, Weckhuysen, B. M., Ed. American Scientific Publishers: **2004**; pp 219-252.

72. Duin, E. In *Electron Paramagnetic Resonance Theory*, 2013.

73. Brückner, A., In situ electron paramagnetic resonance: a unique tool for analyzing structure–reactivity relationships in heterogeneous catalysis. *Chem. Soc. Rev.* **2010,** *39* (12), 4673-4684.

74. Stoll, S.; Schweiger, A., EasySpin, a comprehensive software package for spectral simulation and analysis in EPR. *J. Magn. Reson.* **2006,** *178* (1), 42-55.

75. Busca, G.; Lamotte, J.; Lavalley, J. C.; Lorenzelli, V., FT-IR study of the adsorption and transformation of formaldehyde on oxide surfaces. *J. Am. Chem. Soc.* **1987,** *109* (17), 5197-5202.

76. Busca, G., The surface acidity of solid oxides and its characterization by IR spectroscopic methods. An attempt at systematization. *PCCP* **1999,** *1* (5), 723-736.

77. Lercher, J. A.; Gründling, C.; Eder-Mirth, G., Infrared studies of the surface acidity of oxides and zeolites using adsorbed probe molecules. *Catal. Today* **1996,** *27* (3), 353-376.

78. Elisabetta Palumbo, M.; Baratta, G. A.; Collings, M. P.; McCoustra, M. R. S., The profile of the 2140 cm−1 solid CO band on different substrates. *PCCP* **2006,** *8* (2), 279-284.

79. Urso, R. G.; Scirè, C.; Baratta, G. A.; Brucato, J. R.; Compagnini, G.; Kaňuchová, Z.; Palumbo, M. E.; Strazzulla, G., Infrared study on the thermal evolution of solid state formamide. *PCCP* **2017,** *19* (32), 21759-21768.

80. Mortensen, A.; Faurskov Nielsen, O., Vibrational spectra in the carbonyl stretching region of isotopomers of formamide in the gaseous and liquid states. *Spectrochim. Acta A* **1995,** *51* (8), 1345-1354.

81. Parmeter, J. E.; Schwalke, U.; Weinberg, W. H., Interaction of formamide with the Ru(001) surface. *J. Am. Chem. Soc.* **1988,** *110* (1), 53-62.

82. Hadjiivanov, K. I., Identification of Neutral and Charged N x O y Surface Species by IR Spectroscopy. *Catal. Rev.* **2000,** *42* (1-2), 71-144.

83. Hudson, J. S.; Eberle, J. F.; Vachhani, R. H.; Rogers, L. C.; Wade, J. H.; Krishnamurthy, R.; Springsteen, G., A Unified Mechanism for Abiotic Adenine and Purine Synthesis in Formamide. *Angew. Chem. Int. Ed.* **2012,** *51* (21), 5134-5137.

84. Deo, G.; Wach, I. E., Reactivity of Supported Vanadium Oxide Catalysts: The Partial Oxidation of Methanol. *J. Catal.* **1994,** *146* (2), 323-334.

85. Wach, I. E.; Weckhuysen, B. M., Structure and reactivity of surface vanadium oxide species on oxide supports. *App. Catal., A, Gen* **1997,** *157* (1), 67-90.

86. Kim, T.; Burrows, A.; Kiely, C. J.; Wach, I. E., Molecular/electronic structure–surface acidity relationships of model-supported tungsten oxide catalysts. *J. Catal.* **2007,** *246* (2), 370-381.

87. Wach, I. E., Raman and IR studies of surface metal oxide species on oxide supports: Supported metal oxide catalysts. *Catal. Today* **1996,** *27* (3), 437-455.

88. Wei, D.; Wang, H.; Feng, X.; Chueh, W.-T.; Ravikovitch, P.; Lyubovsky, M.; Li, C.; Takeguchi, T.; Haller, G. L., Synthesis and Characterization of Vanadium-Substituted Mesoporous Molecular Sieves. *J. Phys. Chem. B* **1999,** *103* (12), 2113-2121.

89. Gao, X.; Bare, S. R.; Fierro, J. L. G.; Wach, I. E., Structural Characteristics and Reactivity/Reducibility Properties of Dispersed and Bilayered $V_2O_5/TiO_2/SiO_2$ Catalysts. *J. Phys. Chem. B* **1999,** *103* (4), 618-629.

90. Khodakov, A.; Olthof, B.; Bell, A. T.; Iglesia, E., Structure and Catalytic Properties of Supported Vanadium Oxides: Support Effects on Oxidative Dehydrogenation Reactions. *J. Catal.* **1999,** *181* (2), 205-216.

91. Gao, X.; Wach, I. E., Investigation of Surface Structures of Supported Vanadium Oxide Catalysts by UV−vis−NIR Diffuse Reflectance Spectroscopy. *J. Phys. Chem. B* **2000,** *104* (6), 1261-1268.

92. Kim, D. S.; Ostromecki, M.; Wach, I. E., Surface structures of supported tungsten oxide catalysts under dehydrated conditions. *J. Mol. Catal. A: Chem.* **1996,** *106* (1), 93-102.

93. Ross-Medgaarden, E. I.; Wach, I. E., Structural Determination of Bulk and Surface Tungsten Oxides with UV−vis Diffuse Reflectance Spectroscopy and Raman Spectroscopy. *J. Phys. Chem. C* **2007,** *111* (41), 15089-15099.

94. Vuurman, M. A.; Wach, I. E.; Hirt, A. M., Structural determination of supported vanadium pentoxide-tungsten trioxide-titania catalysts by in situ Raman spectroscopy and x-ray photoelectron spectroscopy. *J. Phys. Chem.* **1991,** *95* (24), 9928-9937.

95. Brückner, A.; Kondratenko, E., Simultaneous operando EPR/UV–vis/laser–Raman spectroscopy — A powerful tool for monitoring transition metal oxide catalysts during reaction. *Catal. Today* **2006,** *113* (1), 16-24.

96. Kompio, P. G. W. A.; Brückner, A.; Hipler, F.; Auer, G.; Löffler, E.; Grünert, W., A new view on the relations between tungsten and vanadium in $V_2O_5WO_3/TiO_2$ catalysts for the selective reduction of NO with NH3. *J. Catal.* **2012,** *286*, 237-247.

97. Wang, C.; Yang, S.; Chang, H.; Peng, Y.; Li, J., Dispersion of tungsten oxide on SCR performance of V2O5WO3/TiO2: Acidity, surface species and catalytic activity. *Chem. Eng. J.* **2013,** *225*, 520-527.

98. Góra-Marek, K., IR studies of the transformation of formaldehyde and methanol on Co-ferrierites. *Micropor. Mesopor. Mater.* **2011,** *145* (1), 93-97.

99. Nakamoto, K., Infrared and Raman Spectra of Inorganic and Coordination Compounds. In *Handbook of Vibrational Spectroscopy*, 2001.

100. Topsøe, N.-Y., Mechanism of the Selective Catalytic Reduction of Nitric Oxide by Ammonia Elucidated by in Situ On-Line Fourier Transform Infrared Spectroscopy. *Science* **1994,** *265* (5176), 1217.

101. Centeno, M. A.; Carrizosa, I.; Odriozola, J. A., NO–NH_3 coadsorption on vanadia/titania catalysts: determination of the reduction degree of vanadium. *Appl. Catal., B* **2001,** *29* (4), 307-314.

102. Funck, E., K. Nakamoto: Infrared Spectra of Inorganic and Coordination Compounds. John Wiley & Sons, New York – London, 1963. 328 Seiten, zahlreiche Abbildungen und Tabellen. Preis: 72 s. *Ber. Bunsenges. Physik. Chem.* **1963,** *67* (9-10), 996-996.

103. Studer, F.; Rih, N.; Raveau, B., Mixed valence tungsten phosphate glasses: ESR and diffuse reflectance investigation. *J. Non-Cryst. Solids* **1988,** *107* (1), 101-117.

104. Whichard, G.; Hosono, H.; Weeks, R. A.; Zuhr, R. A.; Magruder Iii, R. H., Electron paramagnetic resonance spectroscopy of titanium-ion-implanted silica. *J. Appl. Phys.* **1990,** *67* (12), 7526-7530.

105. Brückner, A.; Bentrup, U.; Stelzer, J.-B., The Influence of Sulfate-Doping on the Nature of V Sites in VO_x/TiO_2 Catalysts. *Z. Anorg. Allg. Chem.* **2005,** *631* (1), 60-66.

106. Boucher, L. J.; Tynan, E. C.; Yen, T. F. In *Spectral Properties of Oxovanadium(IV) Complexes. IV. Correlation of ESR Spectra with Ligand Type*, Electron Spin Resonance of Metal Complexes, New York, NY, 1969//; Yen, T. F., Ed. Springer US: New York, NY, **1969**; pp 111-130.

107. *Handbook of Chemistry and Physics, CRC Press*. Boca Raton: 1997-1998.

108. Liu, K.; Yan, Z.; He, H.; Feng, Q.; Shan, W., The effects of H2O on a vanadium-based catalyst for NH_3-SCR at low temperatures: a quantitative study of the reaction pathway and active sites. *Catal. Sci.Technol.* **2019,** *9* (20), 5593-5604.

Appendix

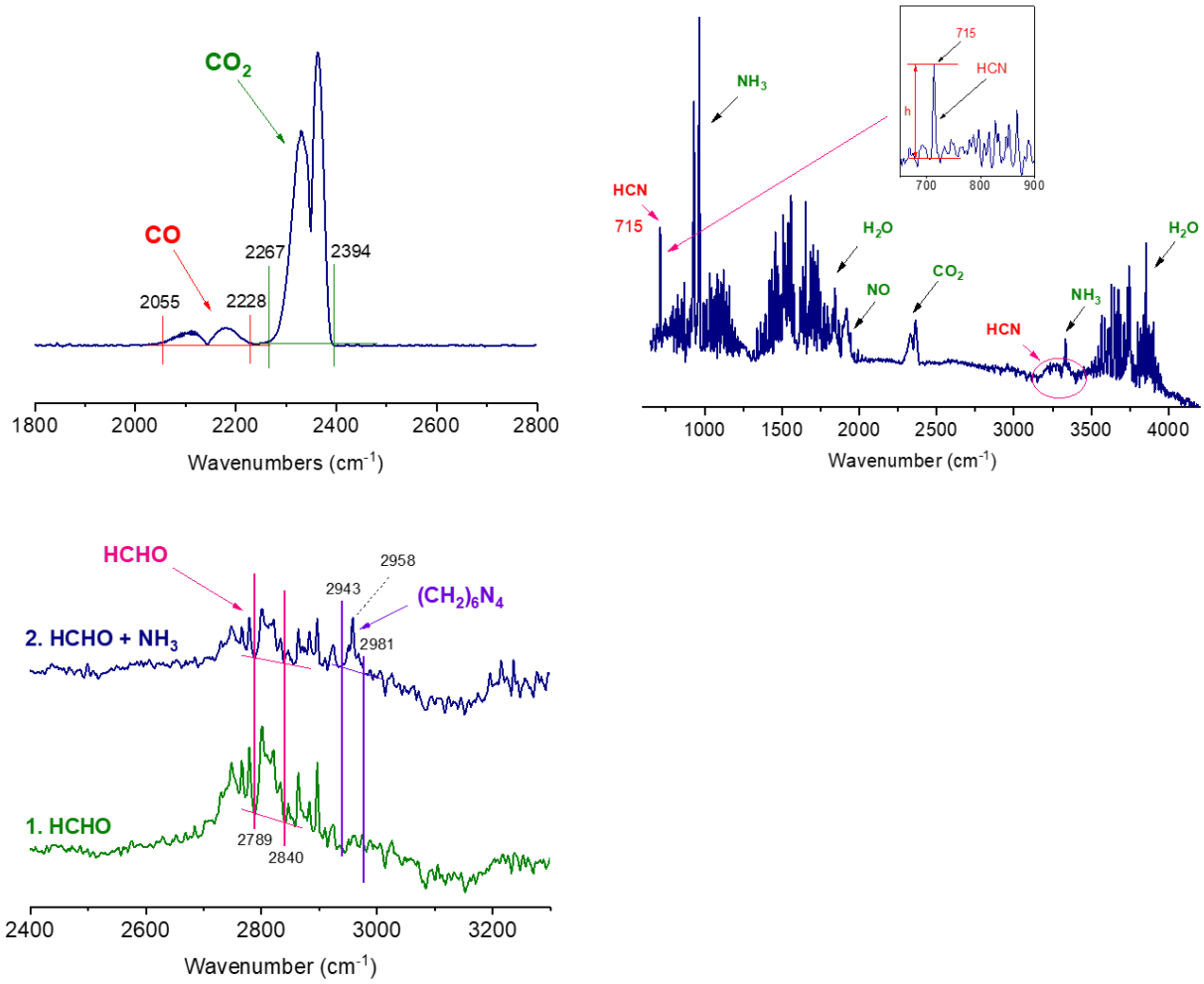

Figure A1a. The FTIR bands used to quantify HCN, CO_2, CO, $(CH_2)_6N_4$, and HCHO concentration. Reproduced from ref. Ngo et al.[2]

The concentration of HCN was calibrated by the height of the peak at 715 cm^{-1}. The concentration of HCN, CO_2, CO, $(CH_2)_6N_4$, and HCHO was calibrated by the boundaries of their typical bands shown above.

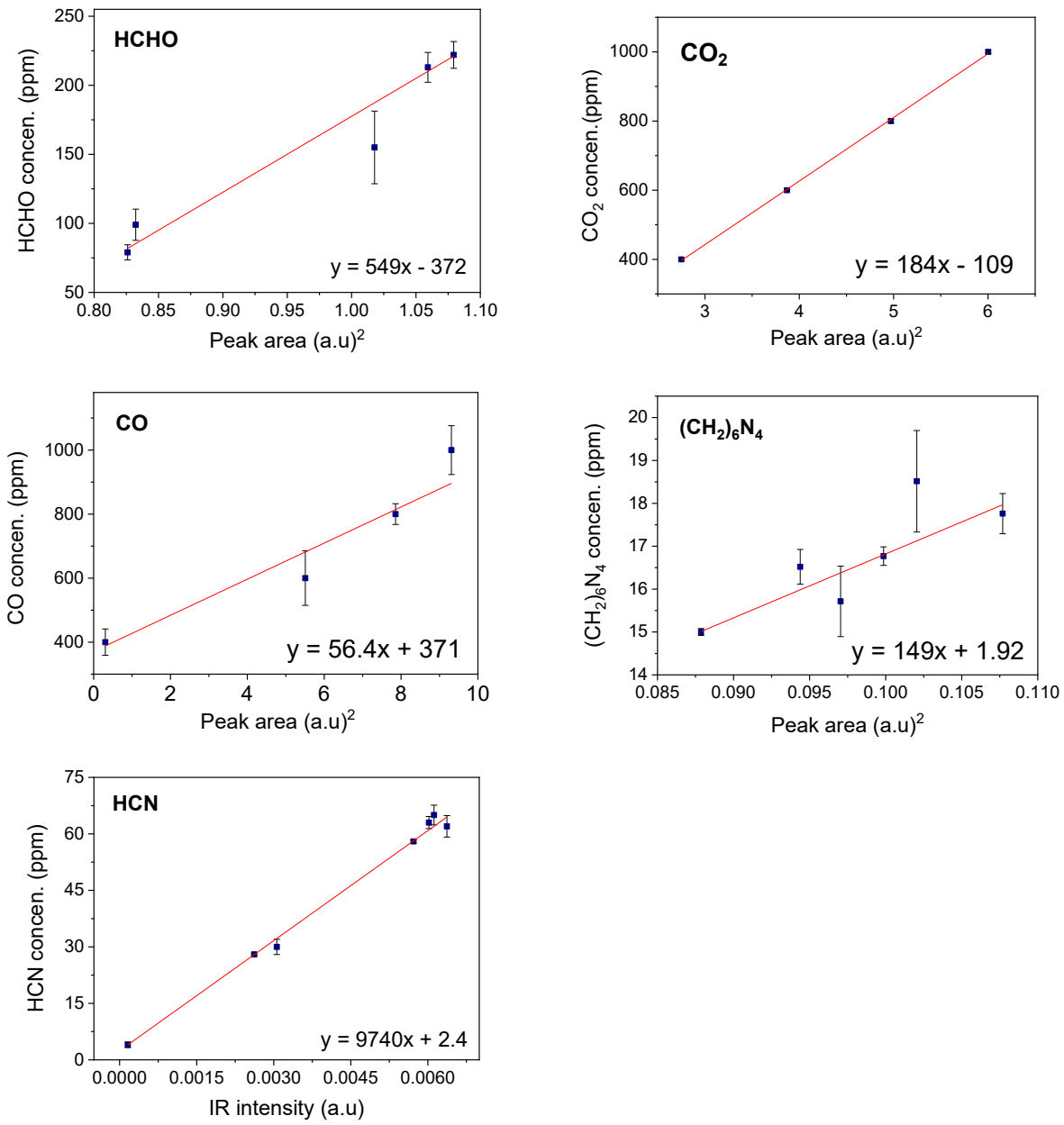

Figure A1b. The corresponding calibration curves. Reproduced from ref. Ngo et al.[2]

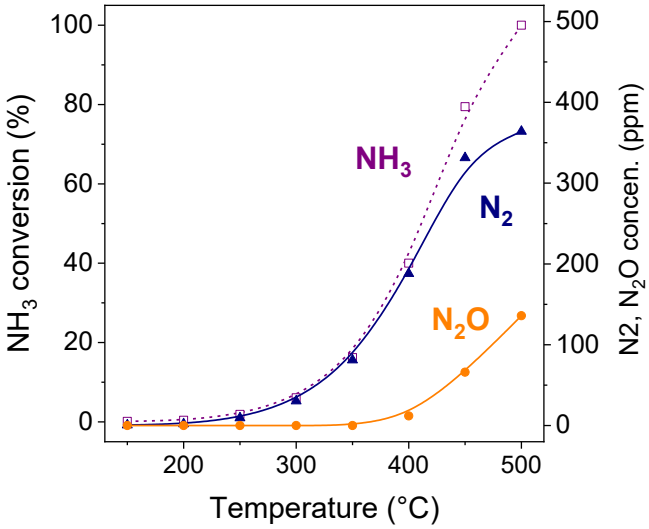

Figure A2. NH_3 conversion and the formation of products from the reaction of 0.1 vol % NH_3, 5 vol % O_2/He on commercial V_2O_5-WO_3/TiO_2 (1 wt. % V, 6 wt. % W) catalyst

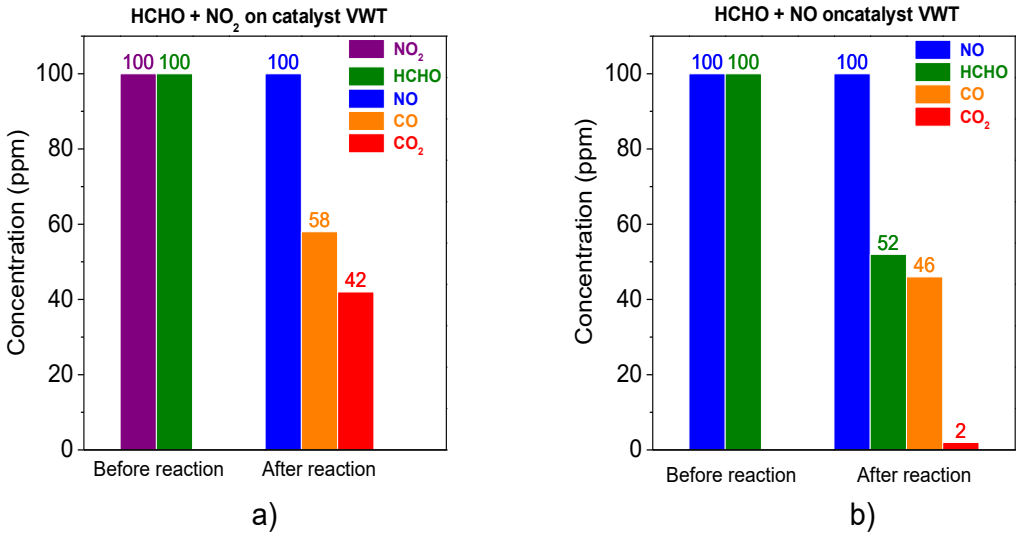

Figure A3. Reaction at 150 °C on commercial V_2O_5-WO_3/TiO_2 catalyst of a) 100 ppm HCHO, 100 ppm NO_2, 0.1 % O_2/He, and b) 100 ppm HCHO, 100 ppm NO/He. Reproduced from ref. Ngo et al.[2]

(the commercial NO_2 bottle contained 1 % O_2 added to stabilize NO_2, which corresponding to 0.1% O_2 in the total feed)

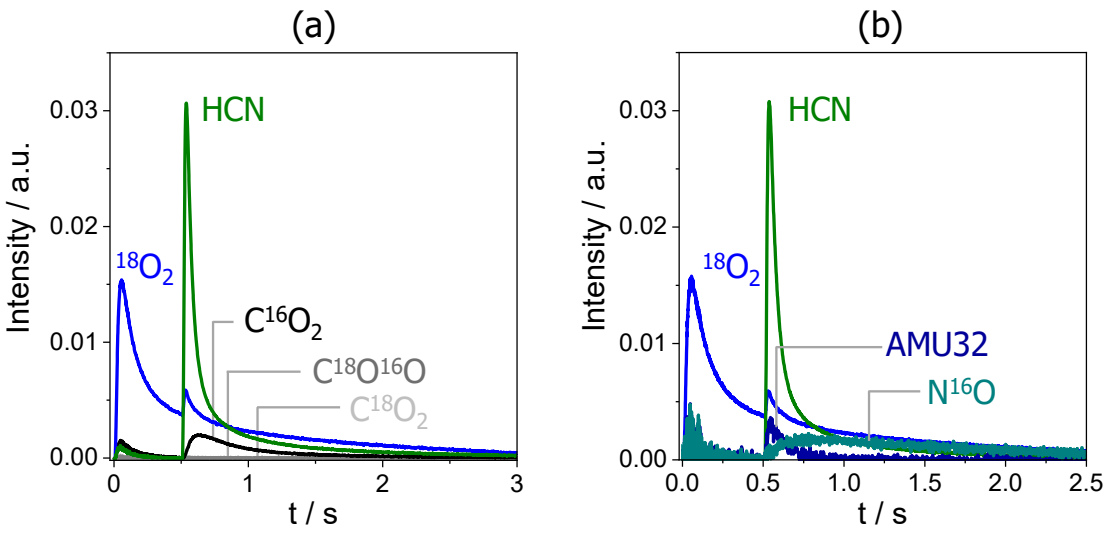

Figure A4. Transient signal obtained after the pulsing of $^{18}O_2$ and 10 vol % HCN/N_2 over the commercial V_2O_5-WO_3/TiO_2 catalyst at 500°C: (a) $^{18}O_2$, HCN, and differently labeled CO_2, (b) $^{18}O_2$, HCN, $N^{16}O$, and AMU32. Reproduced from ref. Ngo et al.[2]

A signal at an atomic mass unit of 32 (AMU32) can be assigned to $^{16}O_2$ or $N^{18}O$. However, it should belong to $^{16}O_2$ as the same signal in the feed of 10 vol % HCN/N_2, i.e., impurity oxygen. If this signal belongs to $N^{18}O$, the shape should be like $N^{16}O$ due to the strong adsorption of nitrates on the surface of the catalyst.

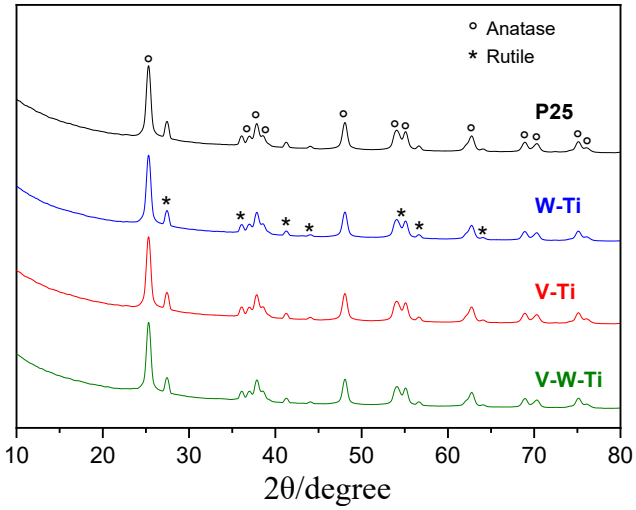

Figure A5. The X-ray diffuse reflection spectra of vanadium tungsten supported catalysts

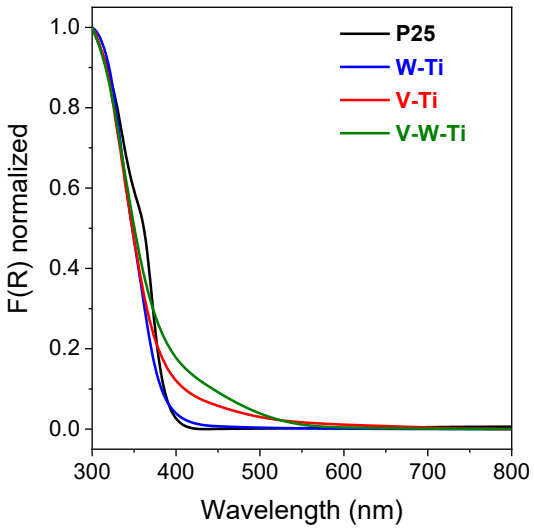

Figure A6. The UV-Vis DRS spectra of vanadium-tungsten supported catalysts and the bare support TiO_2 P25 at room temperature after removing surface water with pretreatment at 300 °C by a flow of 5 vol % O_2/He in 1 h

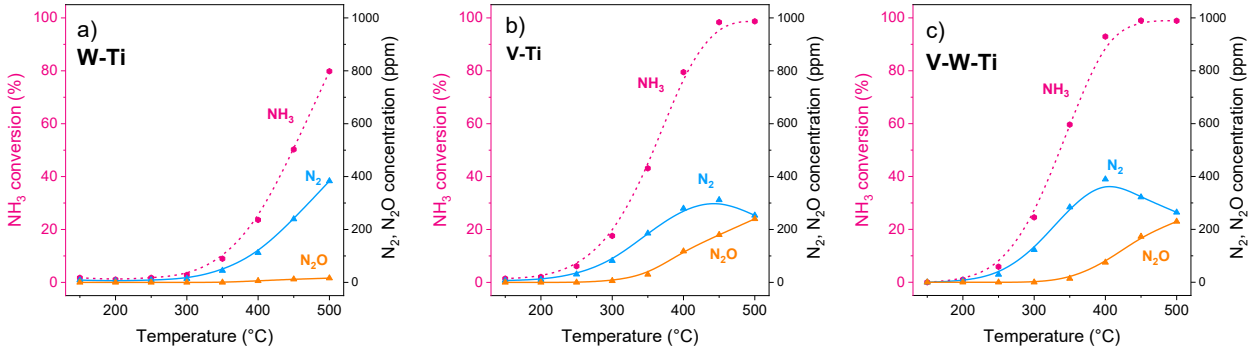

Figure A7. NH_3 conversion and the formation of N_2 and N_2O from NH_3 oxidation of 0.1 vol % NH_3, 5 vol % O_2/He on W-Ti, V-Ti and V-W-Ti catalysts

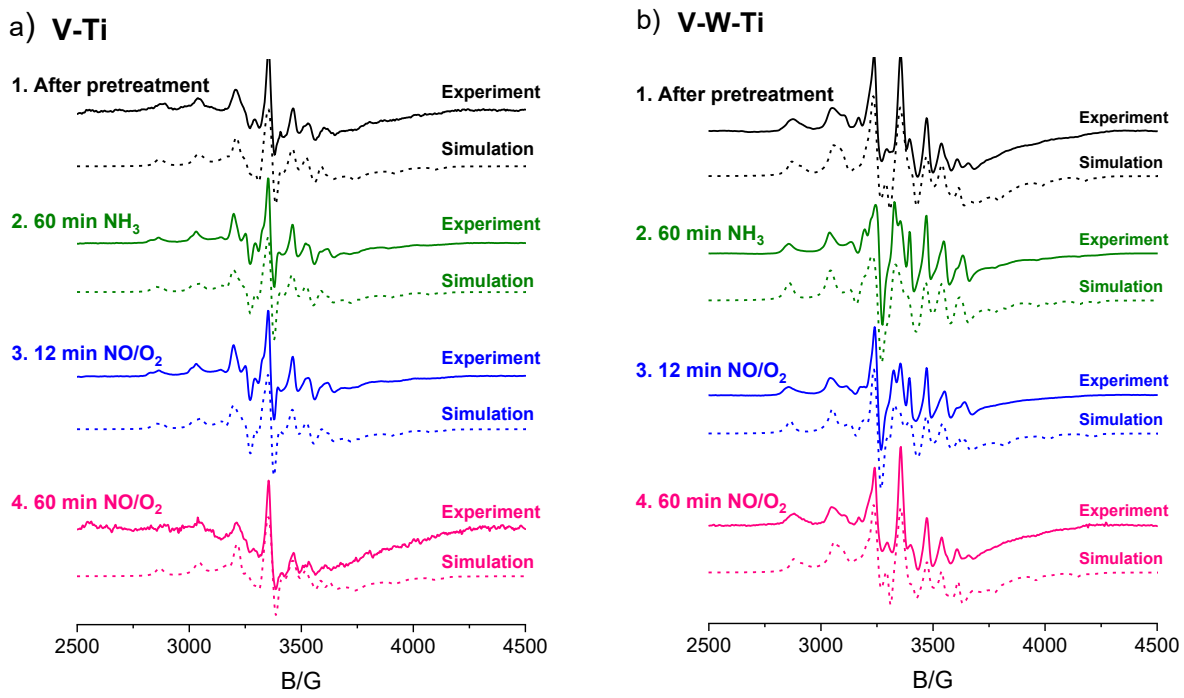

Figure A8. The corresponding simulated EPR normalized spectra, and the original EPR normalized spectra of a) V-Ti and b) V-W-Ti catalyst following by the pretreatment at 300 °C by 5 vol % O_2/He, 60 min pre-adsorption with 0.2 vol % NH_3/He, 30 min flushing He and 60 min exposure with 0.2 vol % NO, 5 vol % O_2/He at 150 °C

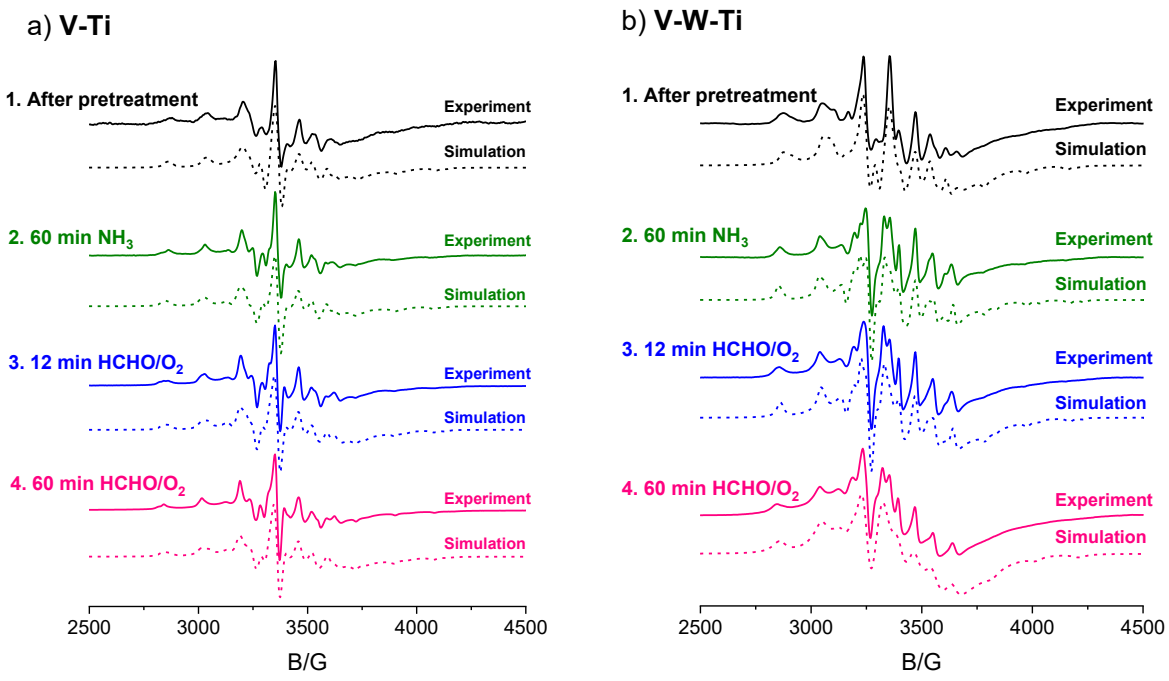

Figure A9. The corresponding simulated EPR normalized spectra, and the original EPR normalized spectra of a) V-Ti and b) V-W-Ti catalyst following by the pretreatment at 300 °C by 5 vol % O_2/He, 60 min pre-adsorption with 0.2 vol % NH_3/He, 30 min flushing He and 60 min exposure with 400 ppm HCHO, 5 vol % O_2/He at 150 °C

Table A1. Simulated parameters of the EPR spectra of V-Ti catalyst (cf. Figure 46a) and parameters calculated thereof. g and A values, the relative intensities (I_{rel} %) $\Delta g_{\parallel}/\Delta g_{\perp}$ (axial distortion of VO^{2+} site) and delocalization coefficient $\beta_2{}^{*2}$

	V species	$g_{\parallel}$	$g_{\perp}$	$A_{\parallel}/G$	$A_{\perp}/G$	$\Delta g_{\parallel}/\Delta g_{\perp}$	$\beta^*{}_2{}^2$	I_{rel} %
After pretreatment	VO^{2+} (I)	1.937	1.970	169.6	52.7	2.02	0.676	30.4
	VO^{2+} (II)	1.916	1.979	173.4	68.7	3.70	0.570	8.8
	Singlet	1.963		-		-	-	60.8
60 min NH_3	VO^{2+} (I)	1.945	1.969	170.8	52.3	1.72	0.696	32.2
	VO^{2+} (II)	1.922	1.979	173.6	65.0	3.44	0.603	21.7
	Singlet	1.963		-		-	-	46.2
12 min NO/O_2	VO^{2+} (I)	1.945	1.969	170.8	52.8	1.75	0.692	28.0
	VO^{2+} (II)	1.922	1.979	177.8	65.2	3.43	0.625	22.2
	Singlet	1.962						49.9
60 min NO/O_2	VO^{2+} (I)	1.935	1.969	171.6	53.1	2.02	0.685	20.5
	VO^{2+} (II)	1.917	1.976	172.2	72.0	3.24	0.545	4.5
	Singlet	1.964						74.6

Table A2. Simulated parameters of the EPR spectra of V-W-Ti catalyst (cf. Figure 46b) and parameters calculated thereof. g and A values, the relative intensities (I_{rel} %) $\Delta g_{\parallel}/\Delta g_{\perp}$ (axial distortion of VO^{2+} site) and delocalization coefficient $\beta_2{}^{*2}$

	V species	$g_{\parallel}$	$g_{\perp}$	$A_{\parallel}/G$	$A_{\perp}/G$	$\Delta g_{\parallel}/\Delta g_{\perp}$	$\beta^*{}_2{}^2$	I_{rel} %
After pretreatment	VO^{2+} (I)	1.914	1.966	177.2	55.7	2.43	0.680	16.9
	VO^{2+} (II)	1.880	1.979	182.5	75.8	5.24	0.541	17.8
	Singlet	1.963		-		-	-	65.3
60 min NH_3	VO^{2+} (I)	1.918	1.970	181.5	60.8	2.61	0.678	28.0
	VO^{2+} (II)	1.890	1.974	186.3	69.0	3.97	0.622	25.3
	Singlet	1.963		-		-	-	46.6
12 min NO/O_2	VO^{2+} (I)	1.918	1.967	179.6	57.2	2.39	0.690	16.3
	VO^{2+} (II)	1.892	1.974	188.4	70.2	3.90	0.630	33.1
	Singlet	1.972						50.7
60 min NO/O_2	VO^{2+} (I)	1.916	1.966	175.5	55.5	2.38	0.674	17.9
	VO^{2+} (II)	1.884	1.973	184.1	74.7	4.04	0.566	16.1
	Singlet	1.977						67.0

Table A3. Simulated parameters of the EPR spectra of V-Ti catalyst (cf. Figure 47a) and parameters calculated thereof. g and A values, the relative intensities (I_{rel} %) $\Delta g_{\parallel}/\Delta g_{\perp}$ (axial distortion of VO^{2+} site) and delocalization coefficient $\beta_2{}^{*2}$

	V species	$g_{\parallel}$	$g_{\perp}$	$A_{\parallel}/G$	$A_{\perp}/G$	$\Delta g_{\parallel}/\Delta g_{\perp}$	$\beta^*{}_2{}^2$	I_{rel} %
After pretreatment	VO^{2+} (I)	1.940	1.970	172.4	52.8	1.93	0.697	27.5
	VO^{2+} (II)	1.916	1.981	175.9	68.6	4.05	0.587	11.0
	Singlet	1.963		-		-	-	61.5
60 min NH_3	VO^{2+} (I)	1.945	1.970	169.4	51.9	1.77	0.690	35.1
	VO^{2+} (II)	1.918	1.979	177.2	65.6	3.62	0.617	20.8
	Singlet	1.963		-		-	-	44.1
5 min $HCHO/O_2$	VO^{2+} (I)	1.947	1.971	173.0	52.2	1.77	0.712	25.6
	VO^{2+} (II)	1.921	1.980	177.9	66.6	3.65	0.618	21.4
	Singlet	1.963		-		-	-	53.0
60 min $HCHO/O_2$	VO^{2+} (I)	1.946	1.972	173.0	53.8	1.86	0.701	27.8
	VO^{2+} (II)	1.922	1.981	174.3	68.5	3.77	0.584	12.2
	Singlet	1.963		-		-	-	60.0

Table A4. Simulated parameters of the EPR spectra of V-W-Ti catalyst (cf. Figure 47b) and parameters calculated thereof. g and A values, the relative intensities (I_{rel} %) $\Delta g_{\parallel}/\Delta g_{\perp}$ (axial distortion of VO^{2+} site) and delocalization coefficient $\beta_2{}^{*2}$

	V species	$g_{\parallel}$	$g_{\perp}$	$A_{\parallel}/G$	$A_{\perp}/G$	$\Delta g_{\parallel}/\Delta g_{\perp}$	$\beta^*{}_2{}^2$	I_{rel} %
After pretreatment	VO^{2+} (I)	1.915	1.966	179.7	56.4	2.43	0.693	16.9
	VO^{2+} (II)	1.890	1.975	186.3	72.1	5.25	0.602	17.8
	Singlet	1.963						65.3
60 min NH_3	VO^{2+} (I)	1.914	1.967	181.5	55.8	2.49	0.765	24.2
	VO^{2+} (II)	1.904	1.978	183.9	71.9	4.00	0.651	20.2
	Singlet	1.963						55.6
5 min $HCHO/O_2$	VO^{2+} (I)	1.922	1.968	182.7	57.0	2.64	0.715	10.7
	VO^{2+} (II)	1.908	1.974	184.1	66.2	3.76	0.647	17.9
	Singlet	1.963						71.4
60 min $HCHO/O_2$	VO^{2+} (I)	1.920	1.972	181.7	61.6	2.19	0.676	4.9
	VO^{2+} (II)	1.898	1.975	183.9	66.7	3.75	0.631	11.4
	Singlet	1.963						83.8

Scientific publications

Journal articles fully related to this work:

1. A. B. Ngo, T. H. Vuong, H. Atia, U. Bentrup, V. A. Kondratenko, E. V. Kondratenko, J. Rabeah, U. Armbruster, and A. Brückner*, Effects of Formaldehyde in Selective Catalytic Reduction of NO_x by Ammonia (NH_3-SCR) on a Commercial V_2O_5-WO_3/TiO_2 Catalyst under Model Conditions, *Environ. Sci. Technol.*, **2020**, 54, 19, 11753-11761.
2. A. B. Ngo, T. H. Vuong, H. Atia, U. Bentrup, J. Weiß, J. Rabeah, U. Armbruster, and A. Brückner*, In situ Studies on the Effect of Formaldehyde in NH_3-SCR on different V_2O_5-WO_3/TiO_2 catalysts, *manuscript prepared.*

Additional articles:

1. A. B. Ngo, H. L. Nguyen, D. Hollmann, Criticial Assessment of the Photocatalytic Reduction of Cr(VI) over Au/TiO_2, *Catalysts*, **2018**, 8(12), 606.

Contribution in conference:

Oral presentations

1. Impact of HCHO in NH_3-SCR of NO_x on a commercial catalyst V_2O_5-WO_3/TiO_2, *14th European Congress on Catalysis, EuropaCat* **2019**, Aachen, Germany
2. Role of HCHO in NH_3-SCR of NO_x on a commercial catalyst V_2O_5-WO_3/TiO_2 under Model Conditions, *3nd RoHan DAAD SDG Summerschool* **2019,** Hanoi, Vietnam
3. Impact of HCHO in NH_3-SCR of NO_x on a commercial catalyst V_2O_5-WO_3/TiO_2 under Model Conditions, *22. Norddeutschen Doktorandenkolloquiums*, **2019**, Oldenburg, Germany
4. Effect of Formaldehyde in NH_3-SCR on different V_2O_5-WO_3/TiO_2 catalysts, *Summer School of the European Federation of Catalysis Societies*, **2020**, Portorose, Slovenia
5. In situ Studies on the Effect of Formaldehyde in NH_3-SCR on different V_2O_5-WO_3/TiO_2 catalysts, *Virtual RoHan DAAD SDG Winterschool* **2020**

Poster Presentations

1. Role of formaldehyde in NH_3-SCR of NO_x on a commercial V_2O_5/WO_3-TiO_2 catalyst, *21. Norddeutschen Doktorandenkolloquiums*, **2018**, Braunschweig, Germany
2. Impact of formaldehyde in NH_3-SCR of NO_x on a commercial V_2O_5/WO_3-TiO_2 catalyst under model conditions, *11th International Congress on Catalysis and Automotive Pollution Control* **2018**, Brüssel, Belgium

Full name: **Anh Binh Ngo**

Date of birth: 12.08.1993 Sex: Male

Nationality: Vietnam Place of birth: Nghe An, Vietnam

Education:

❖ High School for Gifted Student

- Phan Boi Chau Gifted High School, Vinh, Vietnam | 2008 – 2011
- Studying in Gifted Class of Chemistry

❖ Engineer in Chemical Engineering

- Hanoi University of Science and Technology, Hanoi, Vietnam | 2011 – 2016
- Studying in Petrochemical and Organic Technology, GPA 3.31/4.00

❖ Master of Science

- Hanoi University of Science and Technology, Hanoi, Vietnam | 2016 – 2018
- Studying in Chemical Engineering, GPA 3.88/4.00

❖ Doctor of Philosophy

- Leibniz Institute for Catalysis, University of Rostock, Rostock, Germany | 2018 – present
- PhD Student in Department of Catalytic in situ Studies

Award:

- Second Prize in National Excellent Student of Chemistry 2011
- First Prize in National Olympiad of Chemistry 2014
- Honored by Hanoi University of Science and Technology for Excellent Student in Studying and Social Activities

Rostock, 08.02.2021

Anh Binh Ngo